The volcanic source of the Paleocene-Eocene Harwich ash layer in South-East England.

Master Thesis

E.A.M. van de Lisdonk
UNIVERSITY UTRECHT

The initiation process of the PETM (Paleocene Eocene thermal maximum) is still under debate. A possible mechanism is volcanic activity of the NAIP (North Atlantic Igneous Province). Ashes occurring in Denmark, Germany and the North Sea Basin were linked with the volcanic activity in the NAIP. Ashes occurring in Harwich, SE England, were found by Elliott (1971). These ashes are thought to be the distal representative of the Danish ashes and therefore also a product of the volcanic activity of the NAIP. The aim of this study was to characterize the petrology and geochemistry of the ash layers from Harwich to make a correlation with the Danish and German ashes. Additionally the location of the magmatic source can be identified using the chemical composition of the ash-layer. If possible the volcanic activity was linked to the PETM. This was done by studying the Harwich samples as hand specimens and thin sections. Light microscopy, table top SEM and electron microprobe analysis were used to study the chemical composition of the ash layers. The chemical compositions of the Harwich ashes do not correlate with the ashes from Denmark and Germany. This can be explained by mixing of magmas, fractionation, multiple volcanic sources or alteration. The most likely process is alteration of basaltic glass to palagonite. This alteration took place during eruption when the temperatures under elevated temperature conditions resulting in fast alteration. Water-magma interaction was needed during eruption to form the palagonite. As a result of alteration of the Harwich ashes, the major elements cannot be correlated with any of the former studies. The grainsize and thickness distribution throughout Northern Europe indicates a source area in the North Atlantic Ocean. The travel distance of the ash will be 1100 to 1600 km from the NAIP to northern Europe, a water-magma interaction during the eruption is needed to reach this travel distance. Water-magma interaction is also expected because of the palagonite grains.

Content

1. Introduction

The Paleocene Eocene Thermal Maximum (PETM) started approximately 56 Ma and lasted for 170 kyr (Frieling et al., 2016). A major mass extinction of benthic foraminifera occurred during the PETM (Saunders, 2016). During the PETM a negative excursion in $\delta^{13}C$ and $\delta^{18}O$ and an average rise of global temperatures of approximately 5°C occurred (Wieczorek et al., 2013). It has been suggested that a rapid injection of a large mass of isotopically light carbon into the ocean-atmosphere system was linked to the PETM (Saunders 2016). The mechanisms proposed to cause such a rapid injection of a large mass of isotopically light carbon are: Volcanism in the NAIP (North Atlantic Igneous Province), dissociation of gas hydrates and organic matter oxidation (from permafrost thawing) (Frieling et al., 2016). Wieczorek et el. (2013) and Saunders (2016) showed that volcanic activity occurred at the onset of the PETM but could not conclusively show that the PETM was a result of volcanic activity. Volcanic activity caused mantle outgassing of CO_2, this is thought to be one of the reasons of the long term warming trend (Thomas and Bralower, 2005). Caldeira and Rampino (1991) and Eldholm and Thomas (1993) showed the first major NAIP activity could have contributed 10^{20} g of CO_2 in the ocean-atmosphere reservoirs. This may have led to the Paleogene warming trend. Paleocene-Eocene ash layers correlating to NAIP activity were found in Denmark, the Netherlands, Germany and the North Sea basin (Morton and Knox, 1990; Larsen et al., 2003; Obst et al., 2015). The Danish Mo-clay, containing Paleocene-Eocene ash layers, is of lower Eocene age (Knox and Ellison, 1979), and varies in composition. The ash layers in the Danish Mo-clays are composed of alkali basalts, strongly alkaline to peralkaline rocks, contaminated trachytes or dacites, alkali basalts, basalts and peraluminous rhyolites (Larsen et al., 2003). These ash layers are thought to be a distal representative of the Harwich ash layers. Time correlation of the Danish and the Harwich ash was confirmed by Knox and Harland (1979), by studying dinoflagellate cyst assemblages. Ash layers occurring at the base of the London Clay (Knox and Harland,1979) were discovered by Elliott (1971) in Harwich (Fig. 1.1), SE England. The lowest London Clay layers are sandy or pebbly and volcanic ash is only present in scattered patches. Ash layers higher in the stratigraphy are relatively thin and interbedded with silty or sandy clay (Knox and Harland, 1979). Different studies (e.g. Pedersen et al., 1975; Morton and Evans, 1988; Morton and Knox, 1990; Larsen et al., 2003; Obst et al., 2015) have investigated the source area of the Paleocene – Eocene ashes throughout northern Europe. Three possible eruptive centres have been proposed; the North Atlantic Igneous Province (NAIP), where the continental breakup of Europe and Greenland in combination with a mantle plume caused volcanic activity, the Skagerrak volcanism linked with the tectonic movement of the Thornquist Zone (Fig. 3.2) or the Eifel volcanism a result of rifting and subsidence of the European Cenozoic rift system (Fig. 3.3). Alternatively a multi-source hypothesis could be a serious consideration (Morton and Knox, 1990).

The aim of this study was to characterize the petrology and geochemistry of the ash layers from Harwich and the Netherlands. The geochemistry was used to show a correlation with the Danish and German ashes. Additionally the location of the magmatic source can be identified using the chemical composition of the ash-layer. If possible the volcanic activity was linked to the PETM.

Samples found on the beach in Harwich (England) were available at Utrecht University. Drill cores, from the drill core facility of TNO, were investigated to identify related Dutch ash layers. The samples were studied as hand specimens and thin sections. Light microscopy, tabletop SEM and electron microprobe analysis were used to study the chemical composition of the ash layers. The grainsize and thickness of the ash layers were used to estimate the travel distance of the ash particles. The major element compositions obtained by microprobe analysis and trace element data obtained by laser ablation ICP-MS were used to correlate the ashes from Harwich and the Netherlands with the Danish and German ashes. The source area was determined using the chemical composition.

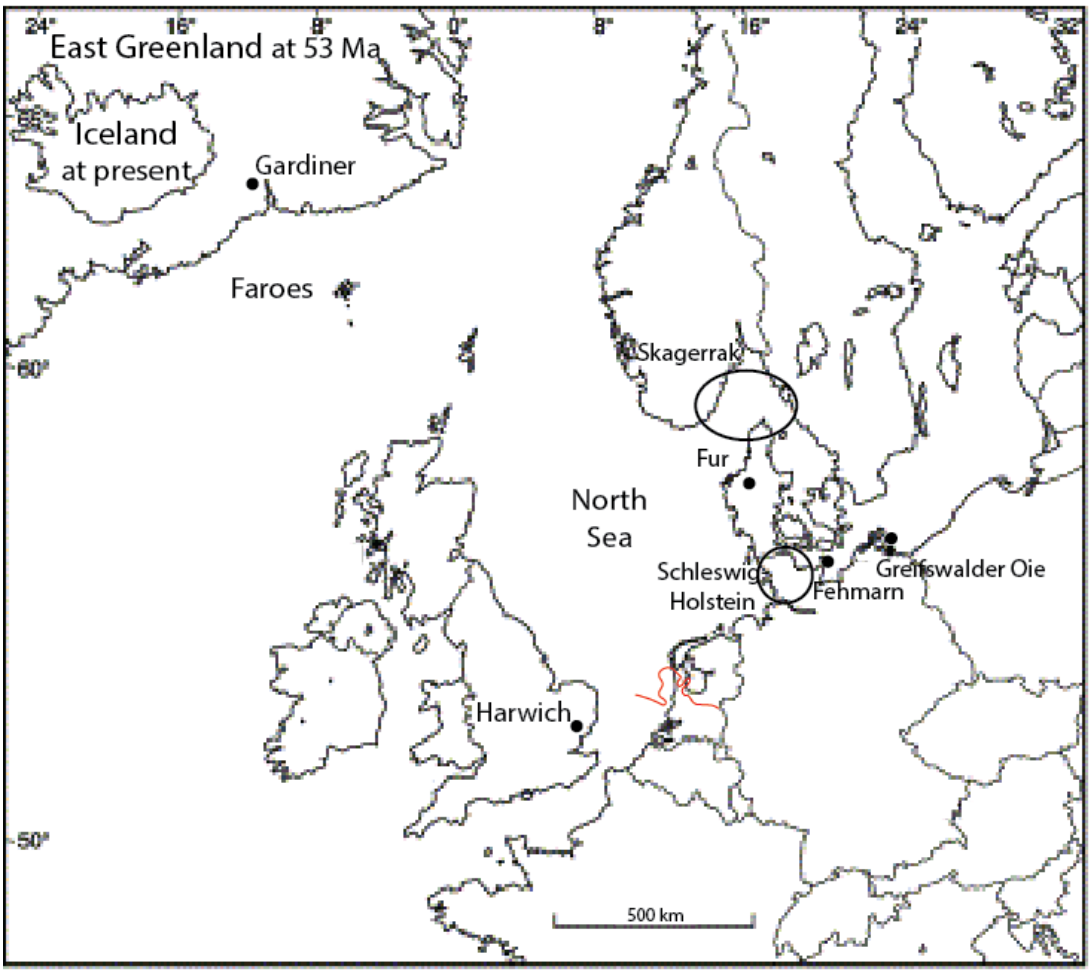

Figure 1.1: Map of the North Atlantic and northern Europe. The position of Greenland at 53 Ma. (Larsen et al., 2003). The red line through the Netherlands indicates the erosional southern boundary of the Basal Dongen Tuffite (Van Bergen and Sissingh, 2007).

2. Geological setting

The ash layers close to the Paleocene-Eocene boundary were deposited in offshore and onshore settings as seen in stratigraphic records from South East England, the Netherlands, North Sea, Germany and Denmark (Van Bergen and Sissingh, 2007). Major occurrences from around the North Sea basin are outlined below:

North sea basin

The ash layers from the North Sea basin have been found in drill cores (Morton and Knox, 1990). There are over 200 ash layers found, with a thickness of 1mm to 18 cm (Morton and Knox, 1990). The ashes are normally graded, except for some which are bottom-current reworked. The lowest tuff formation found in the North sea basin, the Sele formation, contains isolated tuffs. The Balder formation, a unit with abundant tuff occurrence, is present on top of the Sele formation (Morton and Knox 1990). The Sele and balder formation have an age of approximately 56.0 – 51.9 Ma (Obst et al., 2015).

South East England

The presence of ash layers in Harwich (South East England Fig. 1.1) was discovered by Elliott (1971). The ash layer was discovered at the bottom of the London Clay, laterally the ash content varies, in the less ashy portions fossil traces are common (Elliott, 1971). Over 40 ash layers are present in the

London Clay of the Harwich area (Knox and Harland, 1979). The lowest ash beds are present as scattered patches, the ash layers stratigraphically higher are relatively thin (0.5-0.8 cm thick).

The Netherlands

The ash layers in the Netherlands were defined as the Basal Dongen Tuffite. The southern boundary of the ash layer is indicated in Figure 1.1. The Dongen Tuffite layer is a member of the Lower North Sea Group. This group is divided in the Landen and Dongen formations, and is of Thanetian to Bartonian age (59.2-37.8 Ma; Wong et al., 2007). The Dongen formation was deposited conformably on the Landen formation. The Dongen formation consists of sandy deposits in the south, and grade northward into marls and silty clays (Wong et al., 2007). In the north the Dongen Tuffite forms a distinct marker. The stratigraphic logs of the drill cores present at the TNO drill core facility, described these ashes as scattered patches.

Denmark

200 layers of volcanic ash were discovered in the mo-clay on the island of Fur, Denmark (Fig. 1.1; Pedersen et al, 1975; Morton and Evans., 1988; Larsen et al., 2003) the age of these layers range from 55.39 ± 0.12 Ma to 54.04 ± 0.14 Ma (Obst et al., 2015). The thickness of these layers vary from a few mm to 19 cm. The grain sizes vary from 100-200 µm to 500µm, and is carbonate cemented. The ash layers are divided in negative and positive series. The negative series is the lower part of the ash layers and the positive series the upper part, the zero level was chosen based on visual appearances (Larsen et al., 2003). The negative series consist of widely spaced, light coloured, thin ash layers. The upper part contains closely spaced black basalt ash layers. There are two exceptions in the upper part layer +13 and +19 are grey rhyolitic (Larsen et al., 2003). The total ash thickness of the negative series is 0.6 m and of the positive series 3.5 m (Larsen et al., 2003)

Germany

The study of the Greifswalder Oie (Fig. 1.1) started in 1885 by BornHöft, who reported solid blocks of black limestone with fine lamination from beaches of the Greifswalder Oie. The similarities with the Danish ash-bearing cementstone was discovered by Gottsche in 1901 (Obst et al., 2015). The ash-bearing cementstone in northern Germany can be divided in three groups based on different macroscopic features (Obst et al., 2015). The western group (distributed in Schleswig-Holstein) is characterised by distinct ash layers in light-coloured cement stones (Grönwall, 1903; Obst et al., 2015), while the eastern group (distributed on Greifswalder Oie) contains non-regular layers of rather homogeneous ashes (Grönwall, 1903; Obst et al., 2015). The third group was described by Andersen (1938) as a group that links the two other groups, it is called the Fehmarn type which has varying features of ash layers. Two types of cement stones on Greifswalder Oie were distinguished by Obst and Ansorge (2010) based on colour, mineralogical compositions and facies. The first type are erratic boulders in glacial tills exposed at the south-eastern cliff of the island or as beach boulders at the cliff foot (Obst et al., 2015). Type two cement stones occur as ellipsoidal concretions in glacial rafts of early Eocene grey-greenish clay (Obst et al., 2015). The ash layers reached thicknesses between 12 and 50 cm (Obst et al., 2015).

3. Possible eruptive centres

Different studies (Pedersen et al., 1975; Morton and Evans, 1988; Morton and Knox, 1990; Larsen et al., 2003; Obst et al., 2015; and more) investigated the source area of the Paleocene – Eocene ashes throughout Northern Europe. Three possible eruptive centres are proposed to be the source area.

North Atlantic Igneous Province

During the Late Cretaceous, until Early Campanian time (80 Ma) the Eurasian and Greenland plate moved to the NNE (Mjelde et al., 2008). At 61 Ma a mantle plume formed and reached the base of the Greenland lithosphere (Saunders, 2016). This caused minor uplift and continental flood basalt magmatism (Saunders, 2016) resulting in a change in movement of the Greenland and Eurasian plate to NW with limited continental rifting (Smallwood and White, 2002; Mjelde et al., 2008).

Sea floor spreading initiated between 53-56 Ma (Smallwood and White, 2002) marked by a NE-directed kink in the motion of the Eurasian plate (Mjelde et al., 2008). Around 35 Ma the Greenland plate moved along with the North American plate, allowing the Atlantic to open further northwards. The opening of the North Atlantic ocean resulted in the North Atlantic Igneous Province (NAIP). The NAIP extends from Eastern Canada to the British Isles (Saunders et al., 1997). The NAIP had two main phases of volcanism. The initial phase, during the pre-break up (61 Ma), produced a volume of around 175000 km^3 of lava, which spread over an area of 2000 km in width (Saunders et al., 1997; Saunders, 2016). The second phase was more voluminous and associated with the break-up of Greenland and Eurasia (56 Ma). The second phase produced around $6.6x10^6$ km^3 of lava and concentrated along the lines of plate separation (Eldholm and Grue, 1994; Saunders et al., 1997). Figure 3.1 illustrates the area of volcanism. If the NAIP is the source area of the ashes throughout Northern Europe, the transport distance to would have been 1200-1600 km to England and Greifswalder Oie and 1100 km to Denmark

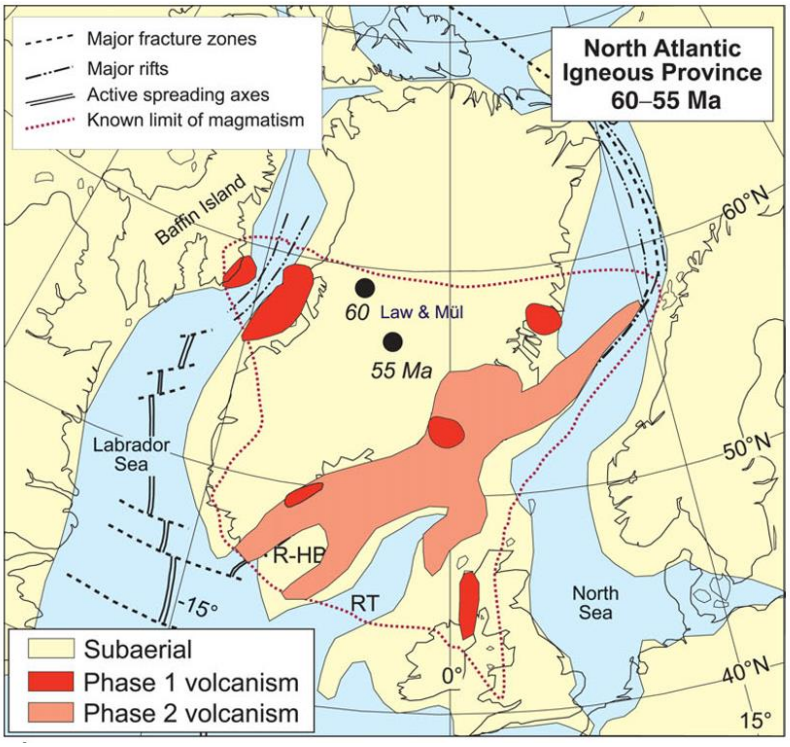

Figure 3.1: Map of the North Atlantic igneous province at 55-60 Ma, prior to full separation of the North American and Eurasian plates. Law Mül 55, 60 Ma refer to proposed locations of the axis of the Iceland plume at 55 and 60 Ma. (Saunders, 2016).

Skagerrak volcanism

Sharma (1970) and Pedersen (1975) showed geophysical evidence for a volcanic centre in the Skagerrak area. The volcano is buried below 250 m marine sediments. The Skagerrak volcanism was probably linked with the tectonic movements of the Tornquist Zone (Fig. 3.2; Malm et al., 1984). The Thornquist Zone is a dextral strike-slip system located in Southernmost Sweden, Bornholm and the surrounding Baltic Sea (Fig. 3.2; Erlström et al., 1996). The Thornquist Zone has been active since Carboniferous time and stayed active into at least early Tertiary (Pegrum and Ljones, 1983; Erlström et al., 1996). Paleozoic volcanism in Norwegian-Danish sectors was linked to the movements of the Tornquist Zone (Malm et al., 1984; Erslström et al., 1996). This zone was tectonically active into the early Tertiary, therefore the Skagerrak volcanism might also be linked with the Tornquist Zone. If the Skagerrak area is the source area of the ashes throughout Northern Europe, the transport distance to would have been 900 km to England, 500 km to Greifswalder Oie and 100 km to Denmark

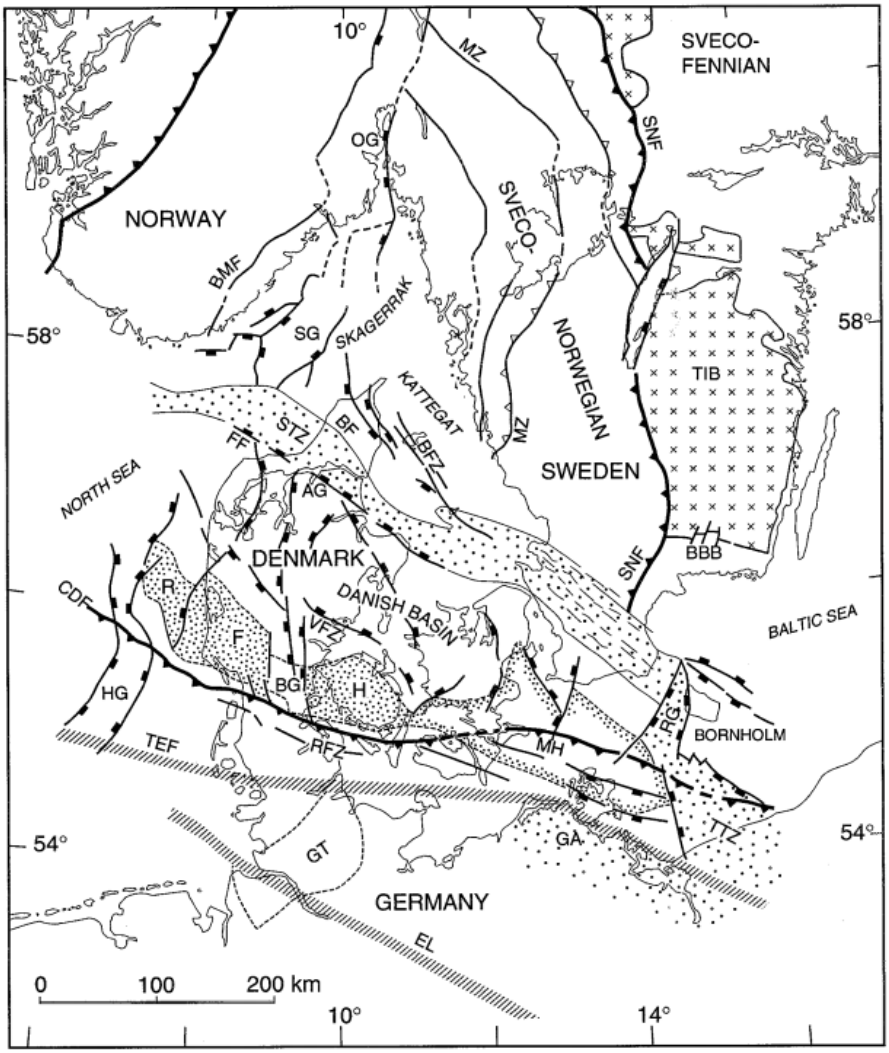

Figure 3.2: Geological map of the Tornquist fan (Thybo, 1997). AG: Ålborg Graben; BBB: Blekinge Bornholm Block; BF: Børglum Fault, BFZ – Border Fault Zone; BG: Brande Graben; BMF: Bamble Fault; CDF: Caledonian Deformation Front; EL: Elbe Lineament; FF: Fjerritslev Fault; GA: Grimmen Axis; GT: Glückstadt Trough; HG: Horn Graben; MH: Møn High; MZ: Mylonite Zone; OG: Oslo Graben; RFH: Ringkøbing-Fyn High; RFZ: Rømø Fault Zone; RG: Rønne Graben; SG: Skagerrak Graben; SNF: Sveconorwegian Front; STZ: SorgenfreiTornquist Zone; TEF: Trans-European Fault; TIB: TransScandinavian Igneous Belt; TTZ: Teisseyre-Tornquist Zone; VFZ: Vinding Fault Zone.

Eifel volcanism

The Eifel volcanic centre is situated close to the Rhine Graben (Fekiacova et al., 2007). The Eifel had different volcanic phases. The Upper Rhine Graben was active from 59 to 47 Ma, the Hocheifel during 44 to 39 Ma and 37 to 35 Ma (Fekiacova et al., 2007) and the West and East Eifel volcanic field were active less than 700 ka (Schminke, 2007). The activity of the Upper Rhine Graben occurred during the deposition of the Harwich ashes. It activated as a result of the European Cenozoic rift system, extending from the North Sea to the Mediterranean (Fig. 3.3; Schumacher, 2002). If the Eifel area is the source area of the ashes throughout Northern Europe, the transport distance to would have been 590 km to England, 620 km to Greifswalder Oie and 740 km to Denmark.

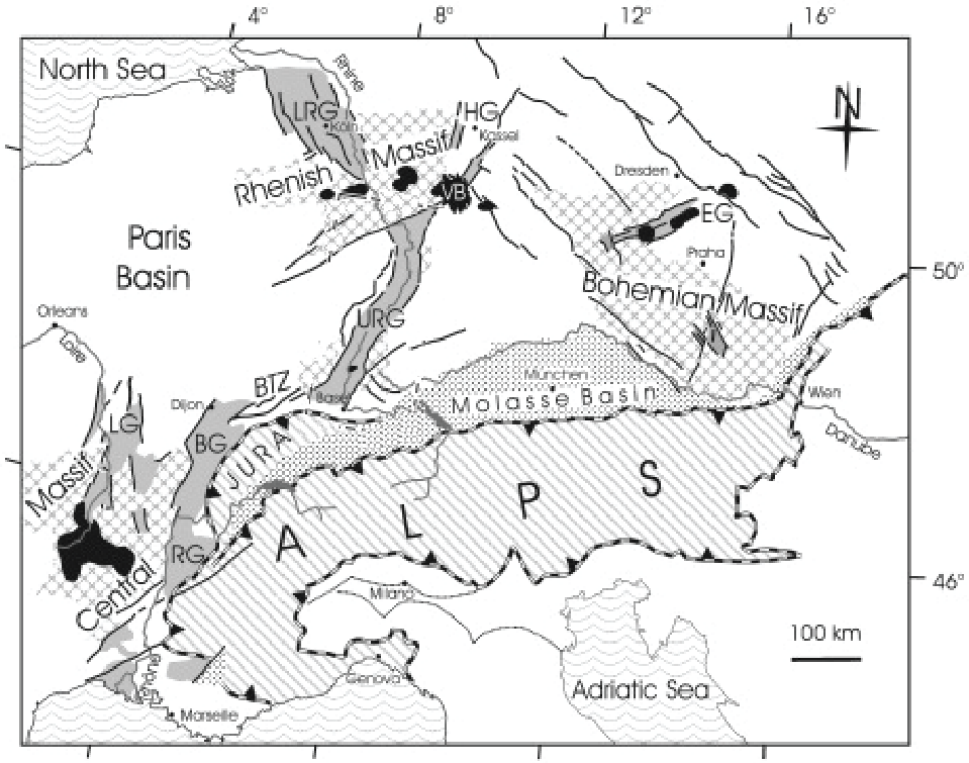

Figure 3.3: European Cenozoic rift system. Cross hatched: Variscan basement outcrops on the European platform; shaded: Cenozoic rift deposits; dotted: Alpine Molasse; dark: Cenozoic volcanics. BG: Bresse Graben; BTZ: Burgundy Transform Zone; EG: Eger Graben; HG: Hessian Grabens; LG: Limagne Graben; LRG: Lower Rhine Graben (Roer Valley Graben); RG: Rhône Graben; URG: Upper Rhine Graben; VB: Vogelsberg volcano. Schumacher, 2002.

4. Method

The Harwich samples were cut in half and polished, to improve the visibility of structural characteristics of the ash. Thin sections of 30 µm were made from these samples (Fig. 4.1). These thin sections were carbon coated and used for light microscopy, Table top Scanning Electron Microscopy (SEM) and Electron Microprobe analysis. Light microscopy and SEM were used to identify the mineralogy of the ash layers, and to identify the glass grains for further investigation. The Electron Microprobe was used to analyse the major element compositions of the glass grains. Thin sections were made from the black patches present on the Dutch drill core samples. Light microscopy was used to investigate whether the black patches were volcanic ash.

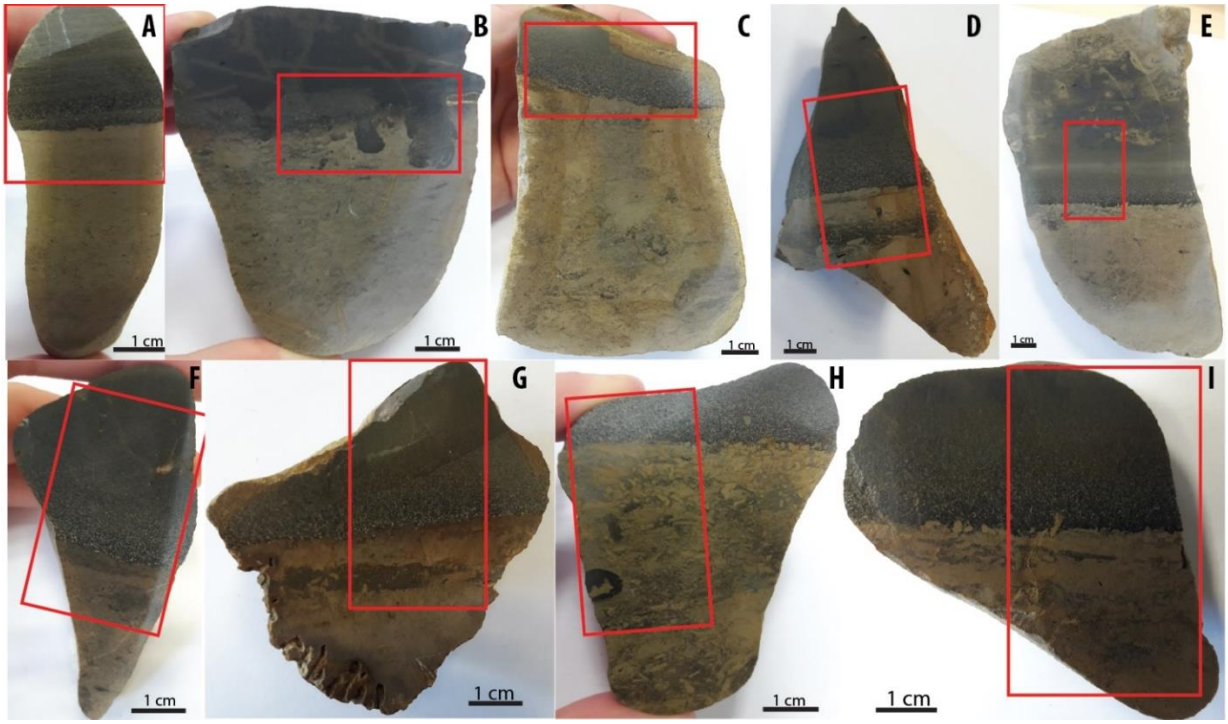

Figure 4.1: The red boxes in the samples show the area of the thin section. A: HW-S1; B: HW-S2; C: HW-S3; D: HW-S4; E: HW-S5; F:HW-S6; G:HW-S7; H: HW-S8; I: HW-S15.

5. Results

Description of ash layers occurring on top of limestone substrate

Sample	Brief sample description
HW-S1	Crossbedded, alternation of coarse and fine grained ash.
HW-S2	Normally graded and partly bioturbated.
HW-S3	Normally graded and partly bioturbated.
HW-S4	Normally graded. A second smaller ash layer occurs below the first.
HW-S5	Normally graded. A dark grey fossil rich layer occurs on top of the ash layer.
HW-S6	Normally graded.
HW-S7	Normally graded. In the limestone layer another smaller ash layer is visible. A vein is formed perpendicular on the ash layer.
HW-S8	Normally graded. A tubular ash is present in the limestone.
HW-S9	Normally graded.
HW-S10	Normally graded.
HW-S11	Normally graded.
HW-S12	Normally graded.
HW-S13	Normally graded.
HW-S14	Normally graded.
HW-S15	Normally graded.
HW-S16	Normally graded.

Appendix 10.1 contains a more detailed description of the samples.

Ash layer thickness and grainsize of the glass

Samples HW-S1 and HW-S2 do not show the original thickness of the ash layer, HW-S1 shows crossbedding and HW-S2 is bioturbated. Only a part of the original thickness of the cemented section is preserved in samples HW-S3, 4, 6-15. The ash layer thickness of these samples varies between 1.5 and 4 cm. Sample HW-S5 is the only sample showing a realistic ash layer thickness. A layer consisting of many fossils is situated on top of the ash layer. The ash layer thickness is 4 cm.

All samples except for HW-S1 show normal grading, HW-S2 also shows normal grading where it was not reworked by bioturbation. The grainsize of the volcanic glass is not graded, these grains are approximately 100 µm with some exceptions between 25 and 200 µm. While other grains ranging from 200 µm at the base of the ash layer to 40 µm at the top.

Light microscopy and SEM

Light microscopy and the SEM were used to identify the mineralogy of the ash layers. The ash layers consist of glass grains, feldspar, igneous crystallized grains, clay minerals and pyrite. These grains have a matrix of calcium carbonate. The glass grains are yellow or dark brown and are sideromelane or palagonite. Palagonite is a general term for any hydrous, altered, basaltic glass (Fisher and Schmincke, 1984). These glass grains were analysed by electron microprobe analysis. The igneous crystallized grains are tachylites full of smaller crystallized grains (Fig. 10.2.2A). Figure 5.1 shows an element map of one of the tachylite grains in sample HW-S5. This element map shows the smaller crystallized grains in the tachylite have different compositions, SEM analysis showed the same chemical variations (Table 5.1). Feldspar has a higher calcium content than sodium indicating a mafic magma (Table 5.1; Marshak, 2011). Iron-oxides, characteristic for tachylites, are identified as small accumulations of iron in the element map (Fig. 5.1; Fisher and Schmincke, 1984). Appendix 10.2 contains a more detailed description of the mineralogy present in the thin sections.

Light microscopy study of the Dutch samples showed no glass was present in the samples, the black patches are not ash. This will not be discussed further in this thesis.

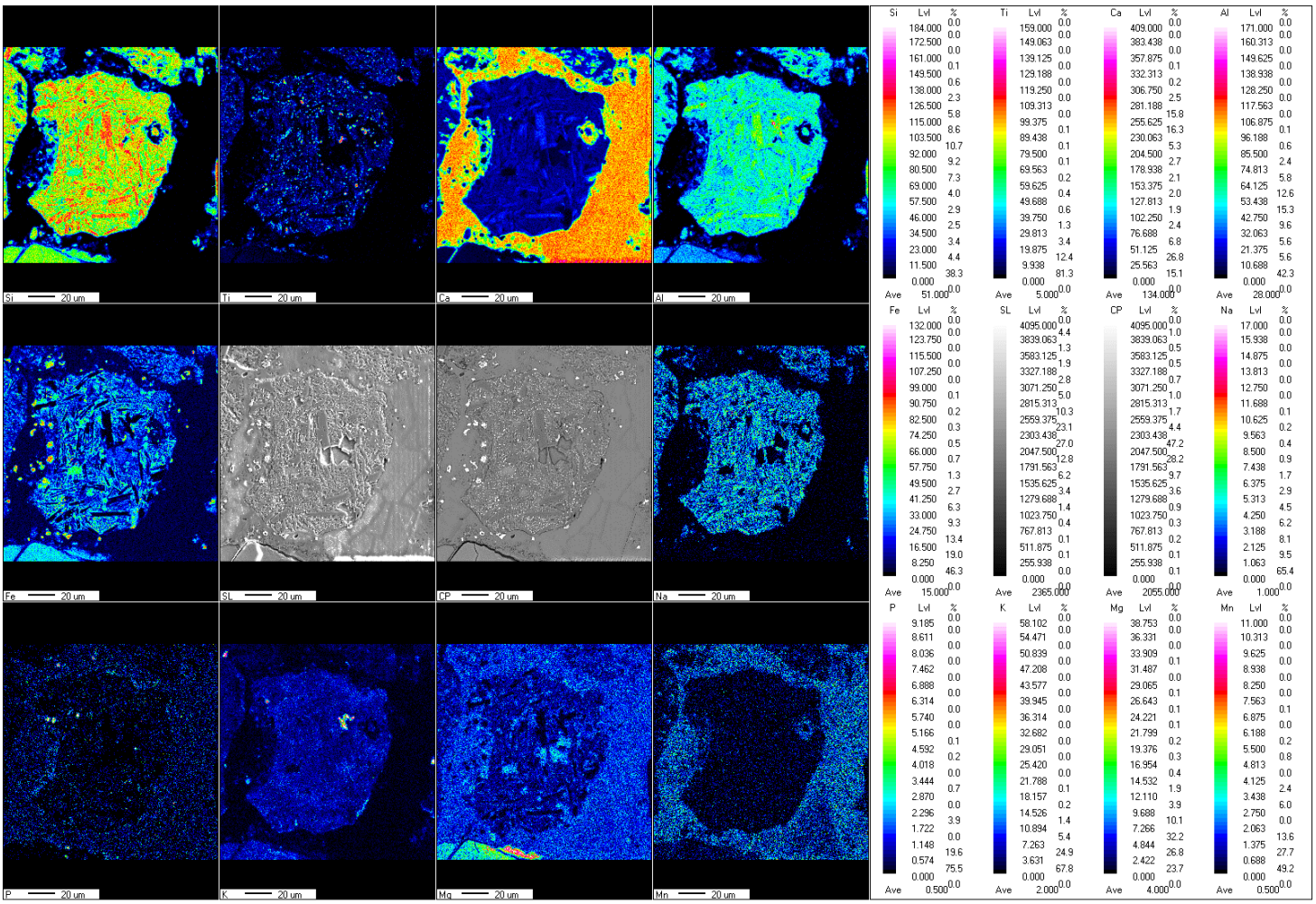

Figure 5.1 : Element map of a tachylite grain in HW-S5.

SAMPLE	HW-S1,27 *	HW-S1,28	HW-S1,29	HW-S1,30	HW-S1,31 *	HW-S1,32	HW-S1,38	HW-S1,39	HW-S1,40 *	HW-S1,41 *	HW-S1,47	HW-S1,48	HW-S1,49	HW-S5,06 *	HW-S5,07	HW-S5,08
SIO2 (WT%)	53.69	41.3	31.92	32.67	55.18	47.57	50.57	56.27	53.95	51.08	37.46	49.11	47.31	50.49	50.45	53.53
NA2O (WT%)	4.53	0.54	b.d.	1.9	4.93	b.d.	b.d.	5.73	4.8	6.16	b.d.	b.d.	3.85	4.31	0.18	4.87
TIO2 (WT%)	b.d.	1.85	b.d.	10.55	b.d.	1.58	b.d.	b.d.	1.73	2.61	b.d.	b.d.	b.d.	b.d.	0.56	1.28
CAO (WT%)	11.67	3.57	1.24	1.75	10.9	2.29	1.86	9.67	11.28	7.69	1.21	2.68	4.22	18.59	2.33	10.06
K2O (WT%)	b.d.	0.86	b.d.	0.44	b.d.	1.41	1.16	b.d.	b.d.	b.d.	b.d.	b.d.	b.d.	b.d.	0.74	0.28
MGO (WT%)	b.d.	3.44	5.41	3.88	b.d.	3.43	6.03	b.d.	b.d.	b.d.	5.77	1.95	2.06	b.d.	3.11	0.45
AL2O3 (WT%)	27.58	20.37	16.13	15.57	27.69	17.28	18.62	26.96	28.24	23.09	19.66	36.45	25.91	25.14	26.27	27.48
FEO (WT%)	2.54	28.07	45.3	33.23	1.29	26.44	21.77	1.36	b.d.	9.37	35.92	9.81	16.65	1.47	16.36	2.04
TOTAL (WT%)	100.01	100	100	99.99	99.99	100	100.01	99.99	100	100	100.02	100	100	100	100	99.99

*Table 5.1: SEM results. The samples with a *, are interpreted as feldspar grains. b.d.= below detection limits*

	HW-S5.1	HW-S5.2	HW-S5.3	HW-S5.4A	HW-S5.4B	HW-S5.6A	HW-S5.6B	HW-S5.6C	HW-S5.6D	HW-S5.7	HW-S5.8A	HW-S5.8B	HW-S5.8C	HW-S5.9	HW-S5.10A	HW-S5.10B	HW-S4.1	HW-S4.2	HW-S4.3
SIO2 WT%	37.43	36.82	36.11	43.16	42.84	25.24	37.39	47.71	38.98	38.64	38.02	42.16	42.87	40.90	38.10	40.91	31.42	49.73	37.61
NA2O WT%	0.15	0.12	0.16	3.36	3.18	0.34	0.18	4.13	0.18	0.12	0.08	0.09	0.05	0.10	0.24	0.23	0.27	3.06	0.13
P2O5 WT%	0.06	0.01	0.92	0.24	0.23	0.04	0.61	0.46	0.02	0.03	0.39	0.93	0.05	0.03	0.05	0.02	4.60	0.19	0.02
TIO2 WT%	9.57	2.82	1.61	2.82	2.78	10.32	1.03	2.94	0.73	1.01	2.45	1.57	4.78	1.37	6.62	0.52	1.33	2.14	3.04
CAO WT%	2.30	2.08	3.06	3.75	3.69	1.31	2.61	4.87	1.68	2.02	2.74	3.52	2.24	2.22	2.18	2.40	8.65	3.89	2.01
K2O WT%	0.19	0.25	0.83	3.47	3.23	0.26	1.47	3.37	1.55	1.07	0.33	0.37	0.36	0.36	0.44	1.12	0.26	4.16	0.34
MGO WT%	2.88	3.08	5.05	0.11	0.21	1.66	3.84	0.05	6.59	4.74	2.79	2.79	2.81	2.74	2.06	4.33	5.62	0.05	2.83
AL2O3 WT%	17.48	17.13	14.92	16.11	15.97	13.88	14.23	17.91	13.31	15.50	19.41	19.57	21.07	22.14	20.60	16.02	11.84	17.74	19.04
FEO WT%	13.39	22.24	21.98	8.98	9.86	15.88	22.69	6.58	21.21	22.02	19.61	16.65	13.55	16.24	16.95	20.27	18.61	4.34	16.41
FE2O3 WT%	2.63	4.36	4.31	1.76	1.93	3.12	4.45	1.29	4.16	4.32	3.85	3.27	2.66	3.19	3.32	3.98	3.65	0.85	3.22
MNO WT%	0.08	0.09	0.16	0.03	0.02	0.05	0.14	b.d.	0.20	0.15	0.15	0.10	0.12	0.09	0.13	0.11	0.22	0.10	0.30
TOTAL	86.17	89.01	89.11	83.79	83.95	72.11	88.63	89.32	88.61	89.62	89.82	91.00	90.56	89.37	90.69	89.92	86.48	86.25	84.94
VOLATILE WT%	13.83	10.99	10.89	16.21	16.05	27.89	11.37	10.68	11.39	10.38	10.18	9.00	9.44	10.63	9.31	10.08	13.52	13.75	15.06

	HW-S4.4A	HW-S4.4B	HW-S4.4C	HW-S4.5A	HW-S4.5B	HW-S4.6	HW-S4.7	HW-S4.8	HW-S4.9	HW-S7.1	HW-S7.2	HW-S7.3A	HW-S7.3B	HW-S7.4	HW-S7.5A	HW-S7.5B	HW-S7.5C	HW-S7.6	HW-S7.7
SIO2 WT%	40.20	41.91	40.31	16.65	3.09	41.42	47.25	37.48	36.23	40.01	44.58	39.99	43.58	42.50	41.40	41.72	42.41	38.02	41.57
NA2O WT%	0.11	0.11	0.13	0.52	0.67	0.24	3.62	0.31	0.12	0.26	0.14	0.20	0.12	0.39	0.09	0.13	0.16	0.12	0.24
P2O5 WT%	0.08	0.03	0.03	18.70	26.90	0.06	0.42	2.00	0.02	0.06	0.47	0.02	0.06	1.13	0.02	0.01	0.04	0.04	0.03
TIO2 WT%	2.36	0.69	1.06	2.14	7.84	2.37	3.15	3.94	1.32	4.08	1.32	3.63	4.81	1.57	1.04	1.84	1.70	4.15	1.48
CAO WT%	2.21	2.46	2.20	29.57	41.41	1.99	4.20	4.81	1.97	2.12	3.09	2.39	2.40	3.47	2.63	2.40	2.61	2.54	2.45
K2O WT%	0.55	0.73	0.85	0.53	0.04	0.28	3.97	1.25	0.58	0.30	0.27	0.32	0.73	3.02	0.33	0.67	1.35	0.88	1.61
MGO WT%	5.37	4.19	3.99	1.26	0.17	2.08	0.04	3.44	5.99	1.31	2.34	2.40	3.56	4.49	3.44	5.11	3.88	4.57	4.25
AL2O3 WT%	15.27	16.52	16.42	7.13	1.66	25.89	17.28	14.85	13.94	27.68	25.63	20.79	19.69	13.16	17.23	15.80	16.15	13.94	13.88
FEO WT%	19.27	19.46	20.53	9.83	4.17	13.92	6.15	18.32	24.40	12.39	11.16	17.68	13.43	17.06	19.57	18.72	17.90	21.32	21.47
FE2O3 WT%	3.78	3.82	4.03	1.93	0.82	2.73	1.21	3.59	4.79	2.43	2.19	3.47	2.63	3.35	3.84	3.67	3.51	4.18	4.21
MNO WT%	0.19	0.19	0.17	0.18	0.17	0.20	0.11	0.16	0.27	0.16	0.12	0.14	0.11	0.20	0.12	0.13	0.13	0.22	0.17
TOTAL	89.39	90.11	89.72	88.42	86.94	91.17	87.40	90.16	89.64	90.81	91.32	91.02	91.13	90.34	89.69	90.20	89.84	89.97	91.36
VOLATILE WT%	10.61	9.89	10.28	11.58	13.06	8.83	12.60	9.84	10.36	9.19	8.68	8.98	8.87	9.66	10.31	9.80	10.16	10.03	8.64

*Table 5.**Fout! Geen tekst met de opgegeven stijl in het document.**2: Electron microprobe results. Assumed is a Fe2O3/FeO ratio of 0.15 (Brooks, 1976). b.d. = below detection limits*

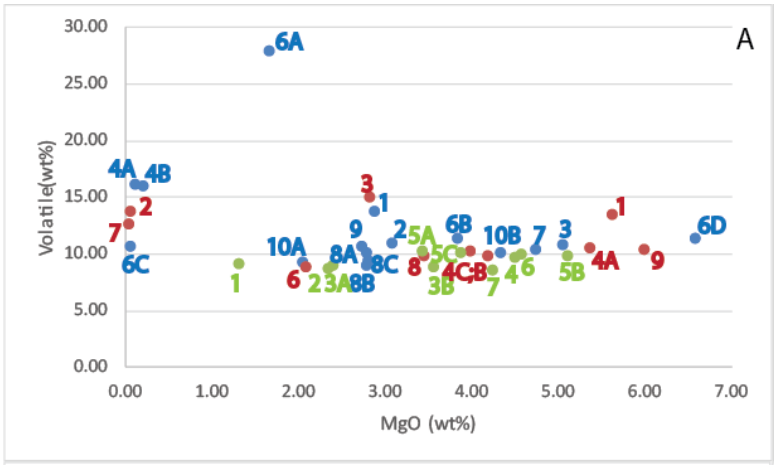
A
Volatile(wt%)
MgO (wt%)

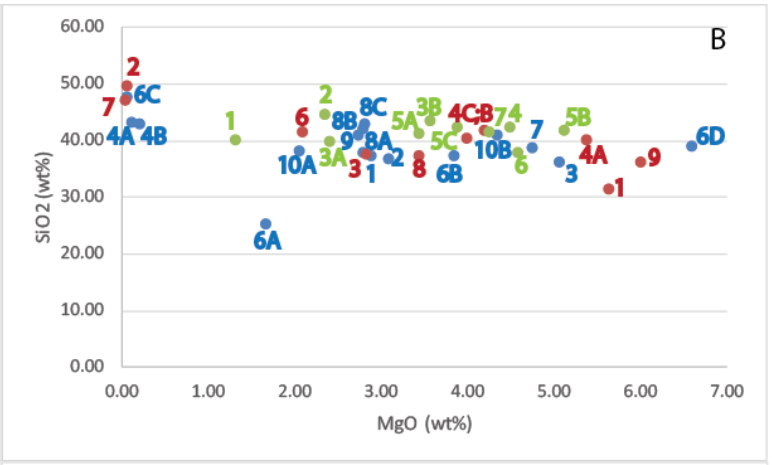
B
SiO2 (wt%)
MgO (wt%)

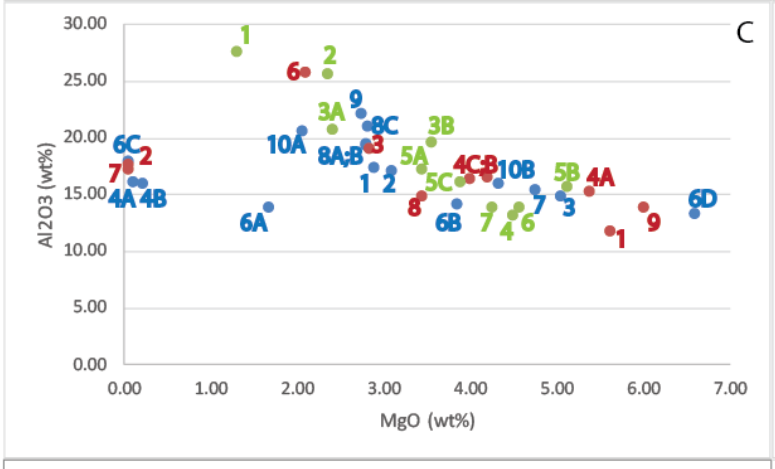
C
Al2O3 (wt%)
MgO (wt%)

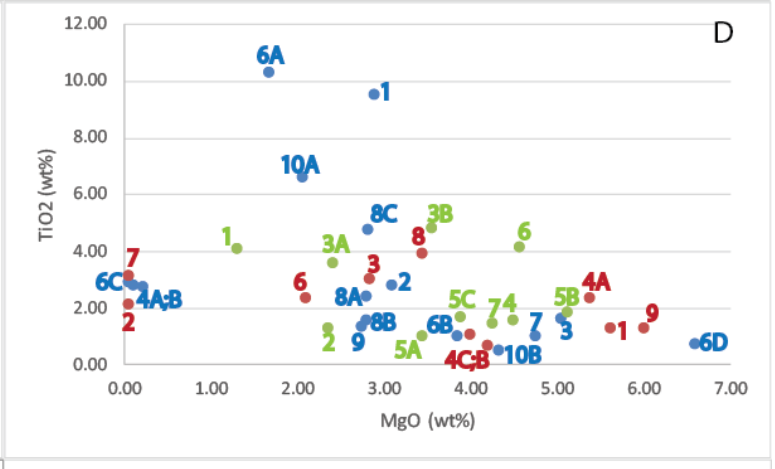
D
TiO2 (wt%)
MgO (wt%)

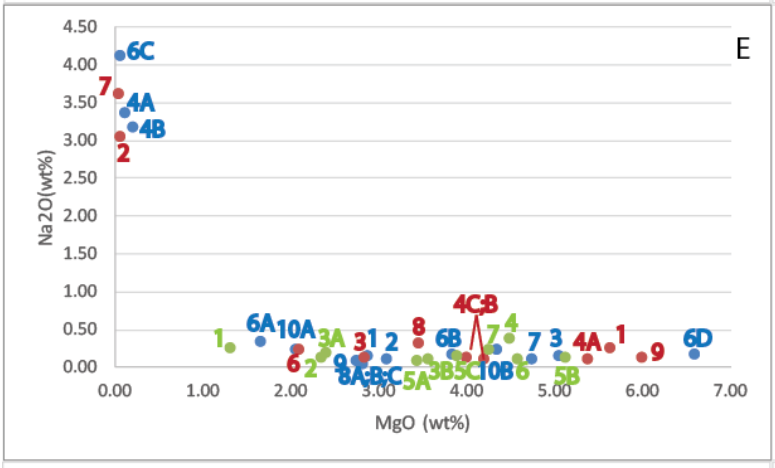
E
Na2O(wt%)
MgO (wt%)

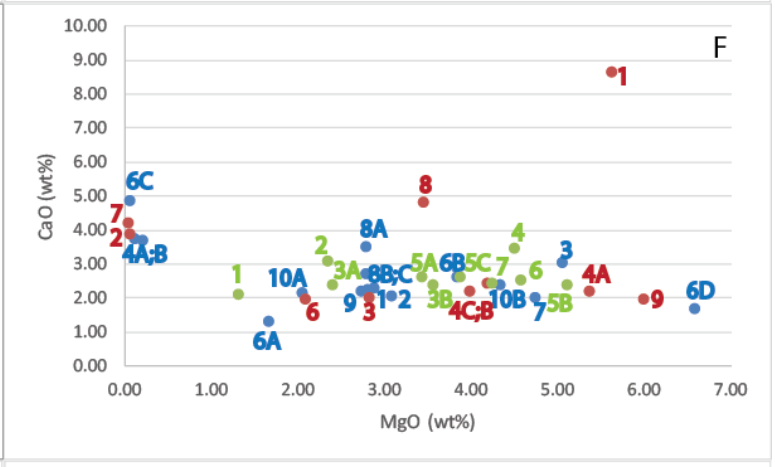
F
CaO (wt%)
MgO (wt%)

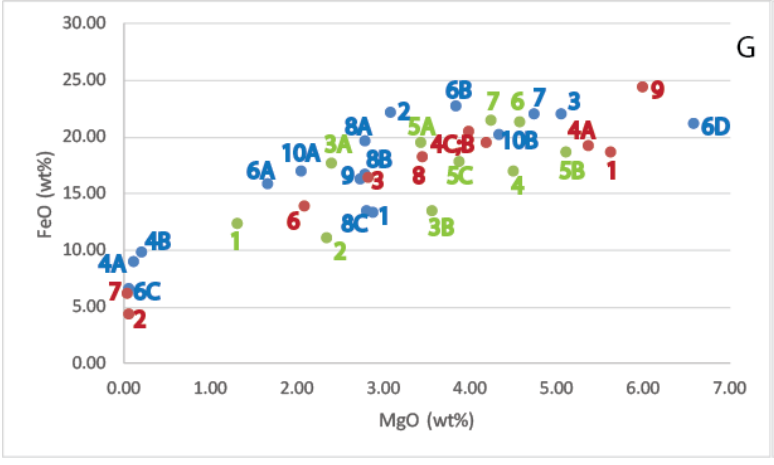
G
FeO (wt%)
MgO (wt%)

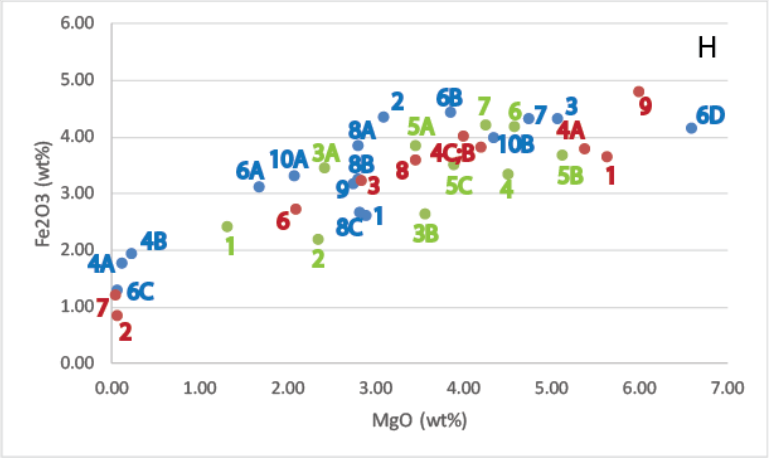
H
Fe2O3 (wt%)
MgO (wt%)

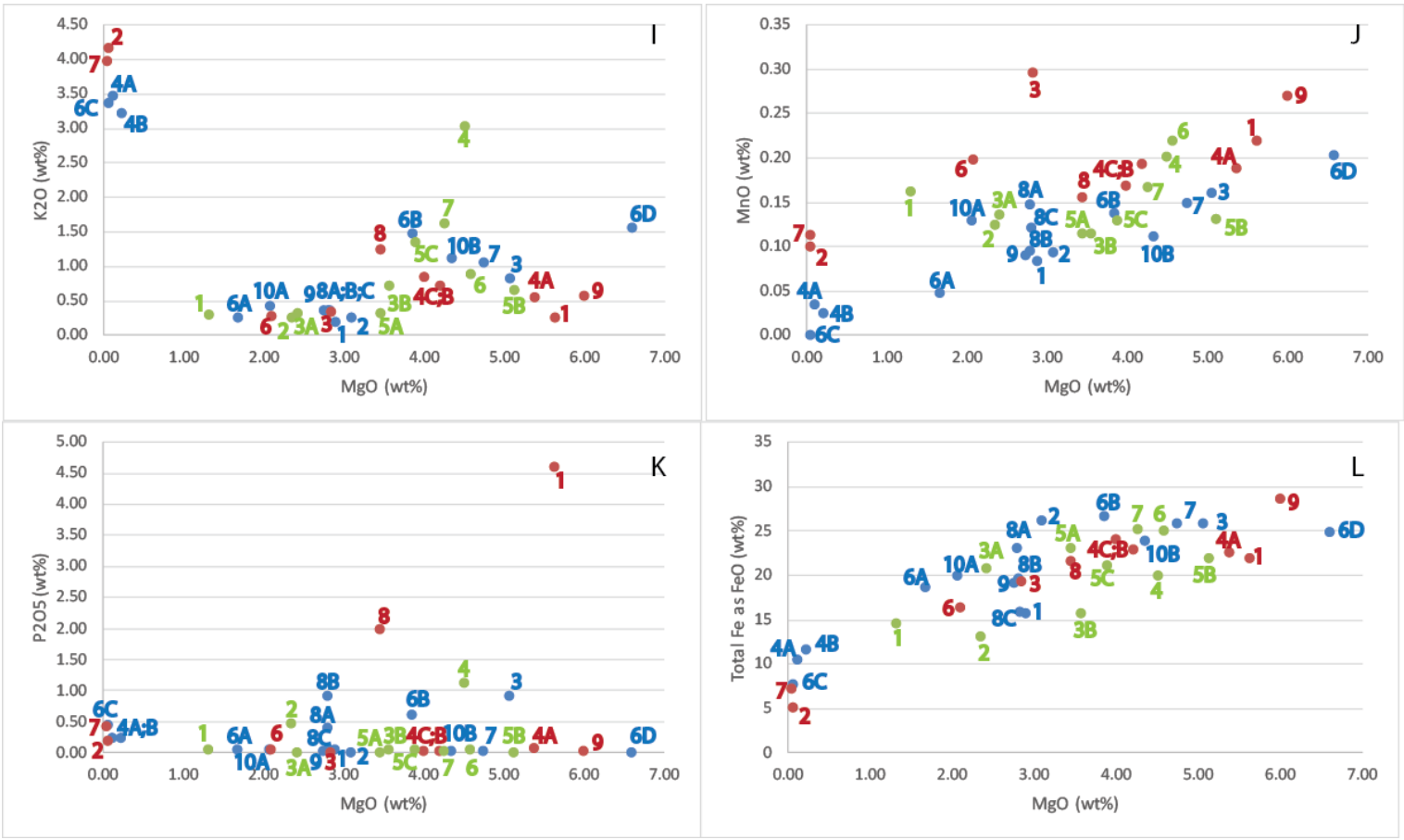

Figure 5.2: Bivariate plots of major elements versus MgO. Blue is sample HW-S5; Red is sample HW-S4; Green is sample HW-S7.

Electron microprobe

Both dark brown and yellow glass grains were investigated. Chemically there is not a clear difference between them. The different rims of glass grains 5.8, 4.4 and 4.5 were analysed (Appendix 10.3). The rims of grains 5.8 and 4.4 do not have large chemical variations, while the rims of 4.5 have chemical variations and is a hydroxyapatite instead of a glass grain.

Major element results are presented in bivariate plots versus MgO used as fractionation index (Fig. 5.2). Samples HW-S4.5A and B were removed from the graphs, this because the SiO_2, P_2O_5, CaO and the Al_2O_3 concentrations are too different from the other results. These grains are hydroxyapatite instead of volcanic glass.

All samples showed low totals during EMPA analysis, most likely due to a high volatile content between 8.6 and 16 wt%, and in extreme cases up to 27.89 wt% (sample HW S5.6A). The SiO_2 contents varies between 30 and 50 wt%, and sample HW-S5.6A has a low SiO_2 content of 25.24 wt%. The MgO content varies up to 6.59 wt%. The TiO_2 concentrations varies up to 10 wt% and the aluminium concentrations varies between 11.84 and 27.68 wt%. CaO concentrations varies between 1-5 wt%, with the exception of sample HW-S4.1 with a CaO concentration of 8.65 wt%. Na_2O concentrations varies up to 0.5 wt%, with the exception of samples HW-S5.4A and B, HW-S5.6C, HW-S4.2 and HW-S4.7 with a Na_2O concentration of 3.36, 3.18, 4.13, 3.06 and 3.62 wt% respectively. The iron concentrations are divided across FeO and Fe_2O_3 (the microprobe only measures FeO, these results are shown in Appendix 10.3), this is done by assuming the Fe_2O_3/FeO ratio is 0.15. This ratio is assumed to be close to the original value in nature for basalts especially tholeiites (Brooks, 1976). The FeO concentrations are between 5 and 25 %, and the concentrations of Fe2O3 varies between 1 and 5 wt%. Both of the iron versus magnesium plots show a positive slope. Potassium has varying

concentrations between 0.19 and 1.61 wt%, the exceptions are samples HW-S5.4A and B, HW-S5.6C, HW-S4.2, HW-S4.7 and HW-S7.4 which have a K_2O concentration of 3.47, 3.23, 3.37, 4.16, 3.97 and 3.02 respectively. P_2O_5 content varies up to 1.13 wt%, samples HW-S4.1 and HW-S4.8 have a concentration of 4.60 and 2.00 respectively. The MnO content varies up to 0.3 wt%. Measurements were grouped by ash layer to determine the chemical trends within one ash layer. No clear trends are present (scattered chemical compositions).

Samples contain altered rims or fractures (Appendix 10.3), but the areas studied in the glass grains appear to be fresh. The high volatile content indicate the glass grains are not fresh but were altered. Trace element chemistry is often heavily influenced by alteration and was not further investigated.

6. Discussion

Morton and Knox (1990) studied early Eocene ashes from the North Sea Basin. The ashes in the basin are divided into two formations, the Balder and the Sele formations. The Sele formation contains isolated and thin tephras with varying compositions. They are composed of, tholeiite, alkali basalt, trachyte and trachyandesite (Morton and Knox, 1990). The ash layers have a heterogeneous feldpar assemblage, which can be divided in five assemblages. The ash layers in the balder formation are closely spaced and are thick tephras. The phenocrysts identified in the Balder formation are homogeneous feldspars, consisting of labradorite-bytownite. The data obtained in the study of Morton and Knox (1990) showed a significant degree of hydration. Thin sections and X-ray diffraction analysis prove that hydration was the result of alteration of vitric material to smectite. In this case major elements could not be used to determine the source area. Immobile trace elements were used for geochemical identification of magma type, these results showed the majority of Balder formation tephras are Fe-Ti tholeiitic. The tephras near the top of the Balder formation have a rhyolitic composition, and the ones near the base a dacitic or trachytic composition.

Danish ashes (Mo-clay) were studied by Pedersen et al. (1975) and Larsen et al. (2003). The Danish ashes were divided into positive series and negative series. The positive series can be correlated with the Balder formation and the negative series with the Sele formation (Morton and Knox, 1990).
The positive series has a volatile content between 0.5-4 wt.% (Pedersen et al., 1975; Larsen et al., 2003). The phenocrysts in the ash layers are plagioclase and Fe-Ti oxides (Pedersen et al., 1975). The chemical composition of the glass grains indicate the magma type to be an evolved Fe-Ti rich tholeiitic basalt, with two rhyolitic layers (Larsen et al., 2003). This chemical composition of magma is common in Iceland and rare in the Faroes and East Greenland, therefore the source of the ash from the positive series is thought to be the mantle plume beneath proto-Iceland (Larsen et al., 2003). The negative series has a high volatile content of 6-14 wt.%. This high volatile content is the result of alteration, this makes it difficult to determine the source area. Larsen et al. (2003) used multi-element plots to find consistent patterns which reflect igneous processes. The elements which were not scattered (TiO_2, Nb and Zr) indicate a number of strongly different magma types (Larsen et al., 2003). These are: Alkali basalts, strongly alkaline to peralkaline rocks, contaminated trachytes or dacites, alkali basalts, basalts and peraluminous rhyolites. The difference in chemistry of the magmas indicate the existence of several central volcanoes (Pedersen et al., 1975).

Ashes from Germany, Greifswalder Oie, were studied by Obst et al. (2015). They divided the ashes in two groups. The first type was found exclusively as erratic boulders in glacial tills, exposed at the south-eastern cliff of the island, or as beach boulders at the cliff foot (Obst et al., 2015). This type has a volatile content of 1-2 wt.%. The chemical composition is typical for moderately evolved basaltic rocks (Obst et al., 2015). The geochemical data from type one, obtained by Obst et al. (2015), correlates with the tholeiitic basalts of the Danish positive series and the Balder formation. The source of these ashes are supposed to be the proto-Iceland plume. Type two of the Greifswalder Oie ashes are cement stones which occur as ellipsoidal concretions in glacial rafts of early Eocene greenish-grey clay. The volatile content of this type varies between 12.5 and 14.3 wt.% (Obst et al.,

2015). The chemical composition (when calculated volatile free) falls into the field of andesite. The high volatile content, unusual high TiO_2 concentrations, low MgO concentrations, unusual low REE concentrations and a very distinct positive Eu anomaly was interpreted as leaching of the glass shards, therefore the source area of these ashes cannot be determined (Obst et al., 2015).

Pedersen et al. (1975), Pedersen and Jørgensen (1981) and Larsen et al. (2003) suggested 4 volcanic stages based on the chemical composition of the glass grains (Fig. 6.1). The first stage is represented by basalts and rhyolites, produced from centres on NW European shelf (Obst et al., 2015). The ash layers from the second stage are trachytes and rhyolites, which were produced by centres on NW European shelf. The strongly alkaline layers originate from the Gardiner Complex in East Greenland. This represents continental rift zone volcanism (Pedersen and Jørgensen, 1981). The alkali basalts from the third stage were products of a failed or propagating part of the opening oceanic rift (Obst et al., 2015). The last stage consists of tholeiitic basalts, sourced from the proto-Iceland plume. The first three stages were based on the chemical composition of the Danish negative series. Both of the studies showed results in which the ash layers are hydrated. Therefore the conclusion of the first three stages have to be made with caution, as the hydration could have caused alteration. The last stage includes only layers from the Danish positive series. The hydration of these ash layers was not significant so the source area determined is reliable. The visual appearances of the Danish positive and negative series are different (Larsen et al., 2003), the difference in source area seems to be correct.

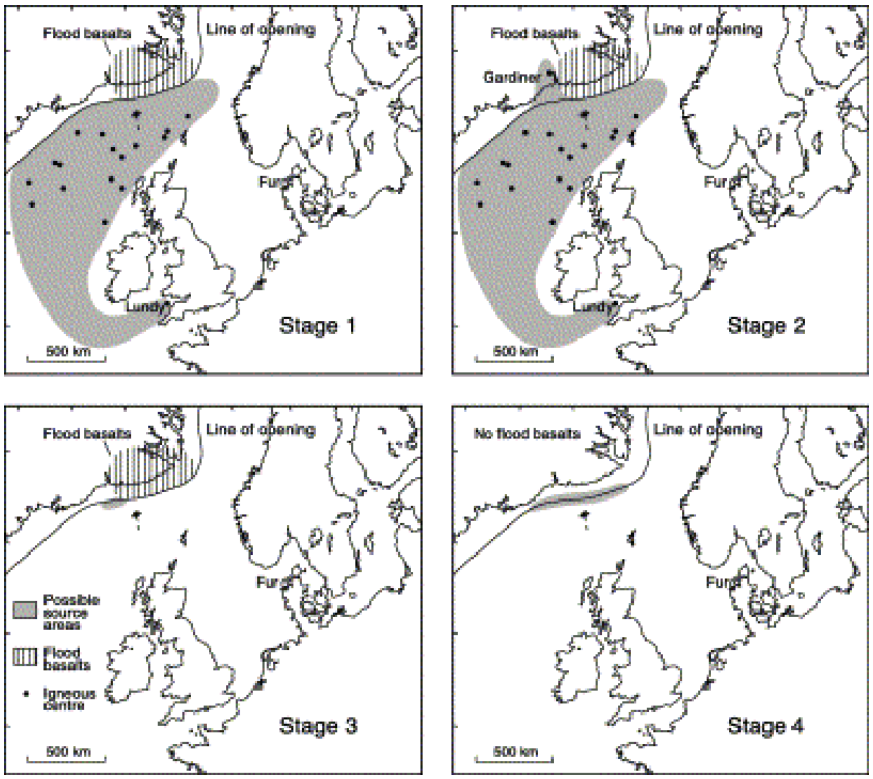

Figure 6.1: Possible source areas for the ashes for each stage (Larsen et al., 2003).

Knox and Harland (1979) showed that the age of the Harwich ashes can be correlated with the age of the Danish ashes. Morton and Knox (1990) suggested the Harwich member is equivalent to the Balder formation, subsequently it is also equivalent to the Danish positive series and type 1 ashes from the Greifswalder Oie. The data of all these ash layers are compared using bivariate plots versus MgO in Figure 6.2. Only electron microprobe data was used for the following correlations, as chemical composition measured by SEM is normalized to 100 wt% while the loss on ignition by microprobe analysis is assumed to be volatiles. As a result of alteration, major elements of the Balder formation were not used to correlate the ash layer. Subsequently the Harwich ashes cannot be

correlated with the Balder formation. Correlating the Harwich ashes with the remaining data shows that the chemical composition of the Harwich ashes contains a lower SiO_2, Na_2O, CaO and MnO content and a higher Al_2O_3, FeO and Fe_2O_3 content. TiO_2 and MgO are more variable than the Danish positive series and the Greifswalder Oie type 1. Compared with the Danish negative series and the Greifswalder Oie type 2, the Harwich ashes have a lower SiO_2 and Na_2O content and a higher CaO, Al_2O_3, MnO and FeO content. Not all papers used the Fe2O3/FeO = 0.15 ratio to determine the FeO or Fe2O3 content. Therefore another plot is made in which all iron is taken as FeO (Fig. 6.2L). This plot shows the Harwich ashes have a higher iron content than the ashes from the North Sea basin, Denmark or Germany. Apart from these differences, the oxides SiO_2, Al_2O_3, FeO, Fe_2O_3, K_2O and MnO show similar chemical trends. The differences in oxides between the Harwich ashes and the Danish and German ashes can be explained by mixing of magmas, fractionation, multiple volcanic sources or alteration. Mixing of magmas was found by Tomlinson et al. (2012) in the volcanic glass grains from the Katla volcano, Iceland. The chemical compositions vary (Fig. 6.2) and the data lies on a linear trend between mafic basaltic and rhyolite composition, indicating mixing of magmas. There is no linear trend in the chemical composition of the Harwich ashes (Fig. 6.2) therefore magma mixing is unlikely. Phenocrysts were found in small amounts in the samples (feldspar and apatite). Fractionation of these phenocrysts is not enough to explain all the differences in major element content between these samples and the samples from Larsen et al. (2013), Morton and Knox (1990), Pedersen et al. (1975) and Obst et al. (2015). Fractionation in the magma chamber would cause the magma to be more felsic (Tomlinson et al., 2012; Lucic et al., 2016). The low silica content shows this is not the case for the Harwich ashes. Fractionation is also unlikely to be the cause of the difference in chemical content. This work investigates 3 separate ash layers. Assuming an ash layer originated from one volcanic centre, the chemical composition is expected to cluster. This is the case for the Danish positive series and the Greifswalder type 1. The high variability of especially magnesium and titanium indicates the ash layers were altered or an ash layer originated from different volcanic centres. Figure 5.2 shows the chemical composition of the glass grains in individual layers are scattered (e.g. in analysis HW-S5.6 four glass grains surrounding each other were analysed, the chemical composition varies significantly) and the trend occurring in the total Fe – MgO plot (Fig. 5.2L) cannot be explained by magma derived from multiple volcanic sources. Furnes (1978) and Fisher and Schmincke (1984) suggested the alteration of basaltic glass to palagonite (palagonitization) involves addition of H_2O, and Fe_2O_3 and loss of other major elements (Furnes, 1978; Fisher and Schmincke, 1984). Palagonitization is accompanied by formation of clay minerals, which were identified by SEM data of the samples (Appendix 10.2). Palagonite was formed in the entire glass grain, there are no rims with different chemical content. Palagonitization occurs at low temperatures as a slow process, as a result palagonitization of entire volcanic glass grains may have taken place at elevated temperatures. This most likely occurred during eruption and cooling of the lava (Bonatti, 1965). As a result there has to be magma-water interaction during eruption to form the palagonite. The part of the magma directly interacting with water was hydrated during cooling and formed palagonite. The parts not directly interacting with water cooled slower and formed tachylite. A better understanding of this process is needed to prove this last assumption of entire grain palagonitization. There has been one stage of alteration, which occurred during eruption. As a result of the arguments described above it is most likely the volcanic glass in the Harwich ash layer is altered during eruption. This means the major elements cannot be correlated with any of the former studies.

Chemical data of the Katla eruption 11,100 yr B.P. the 2010 eruption of the Eyjafjallajökull are presented in Figure 6.2 (Tomlinson et al., 2012; Cioni et al., 2014). The Danish positive series and the Greifswalder Oie type 1 are on the same linear trend as the data of the Katla eruption. The Katla eruption data is a trend instead of a clustered position as a result of magma mixing (Tomlinson et al., 2012). The Harwich ashes cannot correlate to the younger eruptions, this means it is most likely the Harwich ashes were altered.

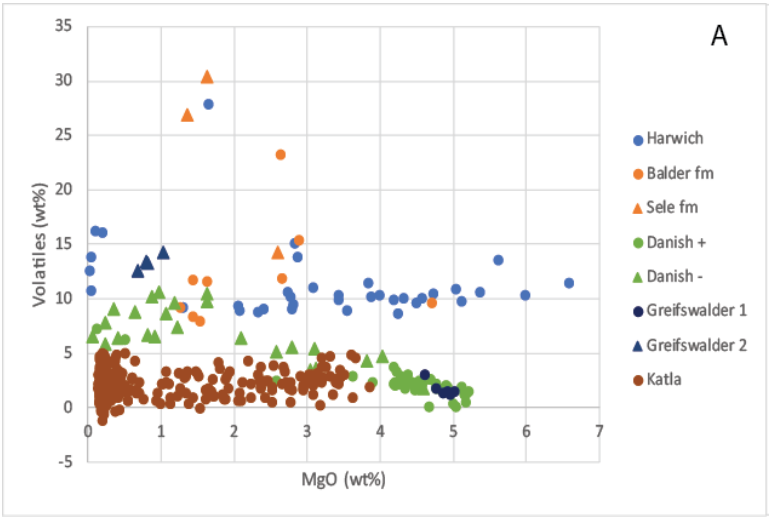
A
Volatiles (wt%)
MgO (wt%)
Harwich
Balder fm
Sele fm
Danish +
Danish -
Greifswalder 1
Greifswalder 2
Katla

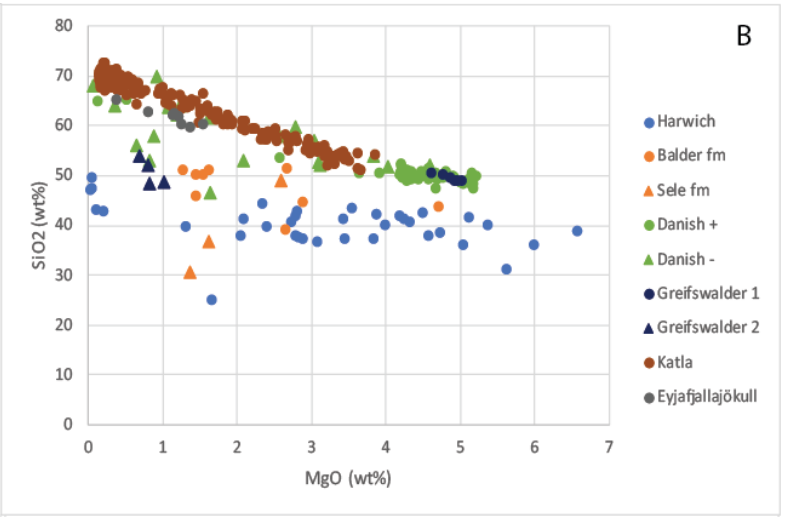
B
SiO2 (wt%)
MgO (wt%)
Harwich
Balder fm
Sele fm
Danish +
Danish -
Greifswalder 1
Greifswalder 2
Katla
Eyjafjallajökull

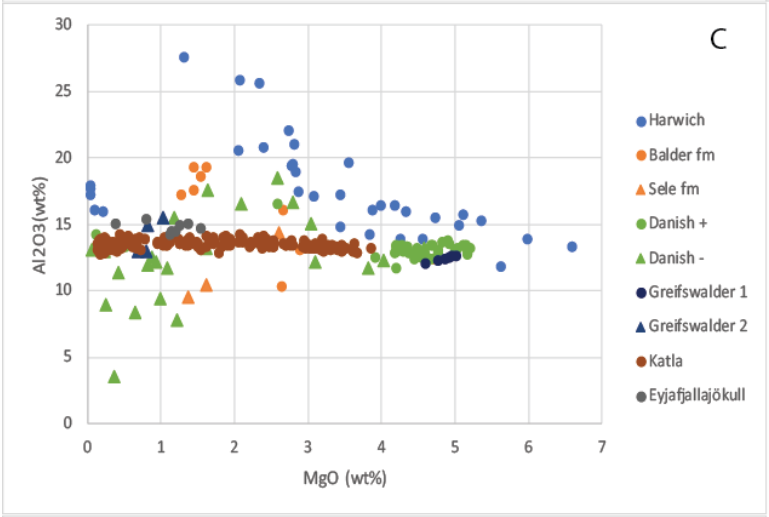
C
Al2O3(wt%)
MgO (wt%)
Harwich
Balder fm
Sele fm
Danish +
Danish -
Greifswalder 1
Greifswalder 2
Katla
Eyjafjallajökull

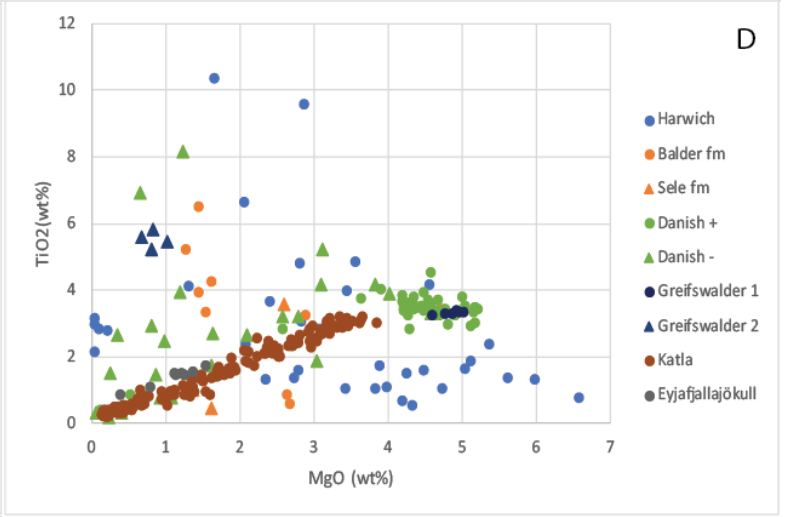
D
TiO2(wt%)
MgO (wt%)
Harwich
Balder fm
Sele fm
Danish +
Danish -
Greifswalder 1
Greifswalder 2
Katla
Eyjafjallajökull

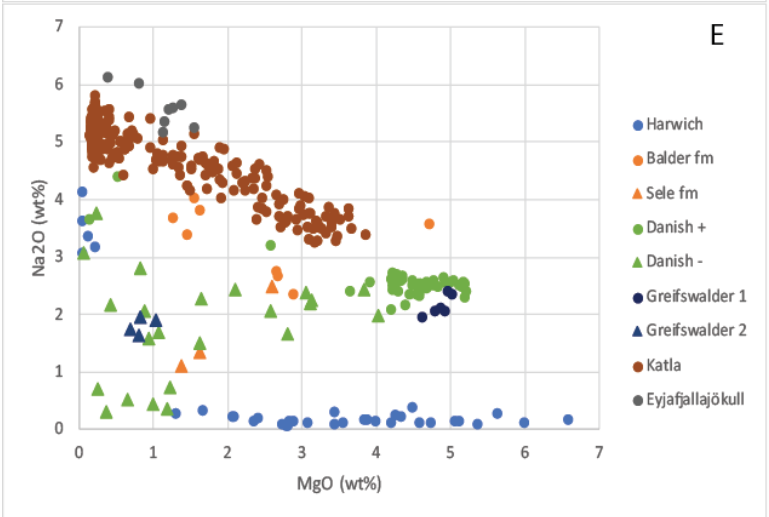
E
Na2O (wt%)
MgO (wt%)
Harwich
Balder fm
Sele fm
Danish +
Danish -
Greifswalder 1
Greifswalder 2
Katla
Eyjafjallajökull

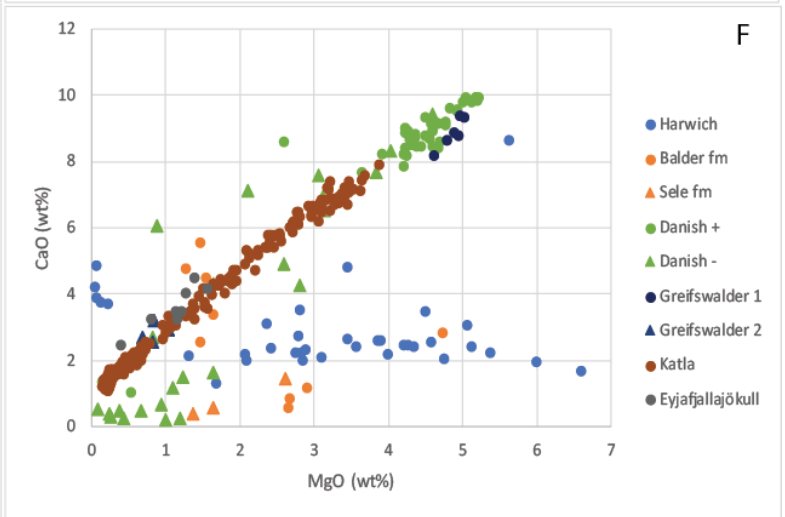
F
CaO (wt%)
MgO (wt%)
Harwich
Balder fm
Sele fm
Danish +
Danish -
Greifswalder 1
Greifswalder 2
Katla
Eyjafjallajökull

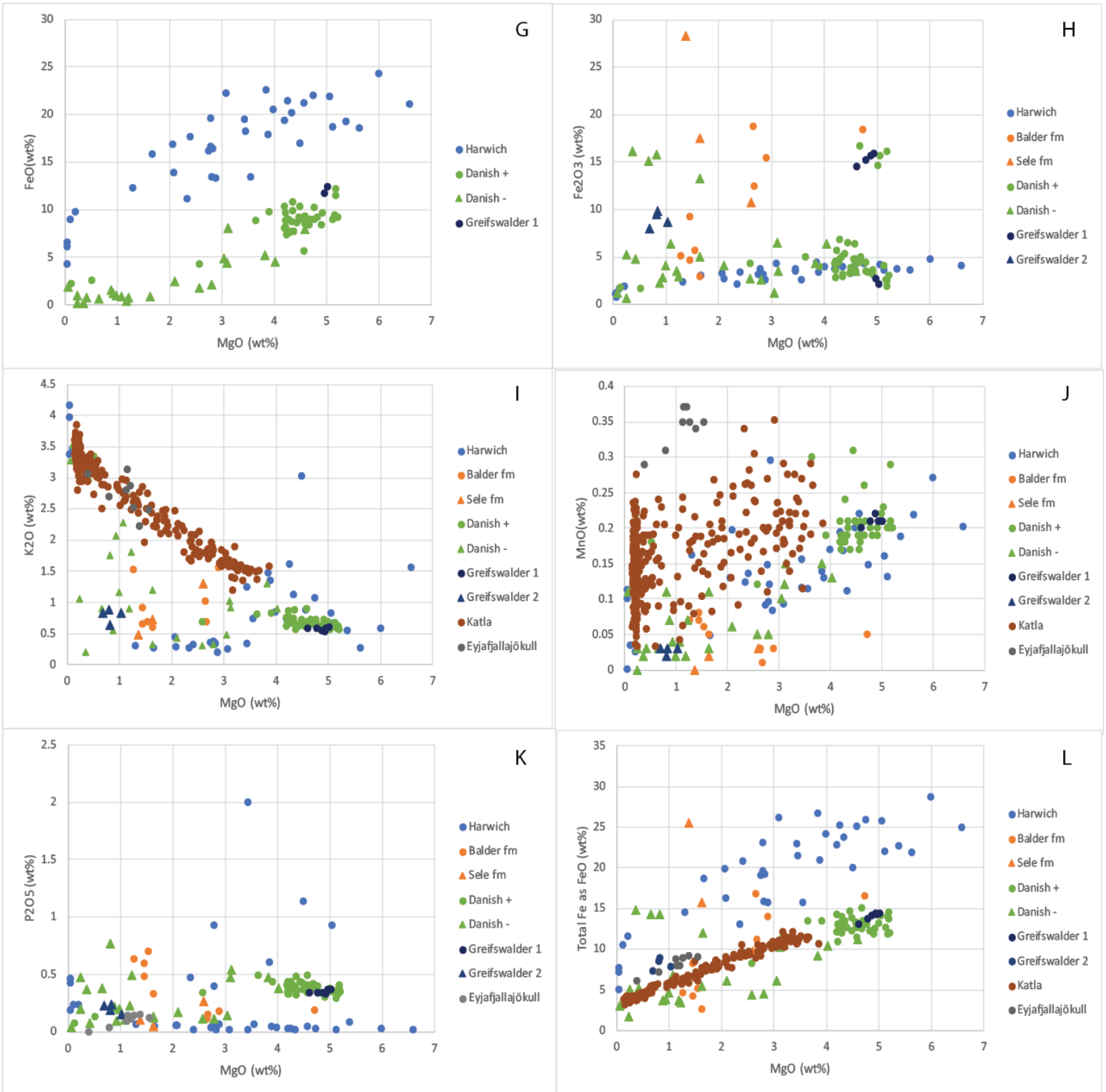

Figure 6.2: Bivariate plots of major elements versus MgO. The results from the Balder and Sele formation are from Morton and Knox (1990); Danish positive and negative series from Larsen et al. (2003); Greifswalder type 1 and 2 from Obst et al. (2015); Katla from Tomlinson et al. (2012); Eyjafjallajökull form Cioni et al. (2014). FeO was not reported in all papers so all Fe2O3 was calculated as FeO in Figure L.

Some studies proposed other techniques to identify the fresh glass composition. Morton and Knox (1990) found inclusions of unaltered volcanic glass in phenocrysts, which were sufficiently large for microprobe analysis. The feldspar phenocrysts in the Harwich samples do not contain inclusions of volcanic glass, but tachylite consist of many small crystals, including some glass crystals. These grains are interpreted not to be hydrated, as a result these glass grains might show the original composition of the magma. Microprobe analysis of the phenocrysts may also help in the correlation with the NAIP (Knox and Morton, 1988; Obst et al., 2015).

Grains size vs travel distance

The grainsize (up to 0.5 mm) and the thickness (varying from a few mm to approximately 15 cm) of the Danish and German ash layers suggest the eruption site to be at most a few hundred kilometres away (Norin, 1940; Pedersen et al., 1975). Calculating the travel distance using stokes' law gives a distance of 160 km (Norin, 1940). The variation throughout Denmark suggests the source to be NW of Denmark. Pedersen et al. (1975) therefore suggested the source area was located in the region between Skagerrak and the North Sea. Later studies (Knox and Ellison, 1979; Morton and Evans, 1988) suggested the source area is located in the NE Atlantic, as a result of the extension of the ash layers into northern Germany, NW Netherlands, SE England, NE Atlantic and westward and north westward of the entire North Sea Basin. Also the increase in ash thickness in a north westward direction indicates the Skagerrak and the Eifel were not the source areas.

The samples from Harwich have a grainsize ranging from 0.04 mm to 0.2 mm with a mean glass thickness of 0.1 mm and thickness of the ash layers of approximately 4 cm. Figure 6.3 indicates the glass grainsize of 0.1 mm has an approximate distance from the volcanic source of 345 km. This does not correlate with the distance to the suggested volcanic sources. Assuming the Harwich ash can be correlated with the other north European ashes, the distribution of the ashes throughout northern Europe indicates the source of the Harwich ash is in the NE Atlantic.

The ash distribution and the chemical content of the ash indicates the volcanic source to be the proto-Iceland plume (Larsen et al., 2003; Obst et al., 2015). This would infer the transport distances to England and northern Germany must be at least 1200-1600 km and 1100 to Denmark (Larsen et al., 2003). To achieve this travel distance, the eruptions must have been highly explosive. Basaltic magmas normally erupt as low viscosity lava flows with minor explosive activity (Knox, 1997). The necessary explosivity needed for this type of eruption usually results from water-magma interaction. Water-magma interaction was possible within the NAIP, as subsidence and extrusion continue and the sequence remained close to sea level (Brooks and Nielsen, 1982). Tephra morphology indicated that the ashes of the Danish positive series were erupted into shallow water by surtseyan eruptions (Pedersen and Jørgensen, 1981; Morton and Evans, 1988; Larsen et al., 2003). The presence of palagonite grains also indicates water-magma interaction (Fisher and Schmincke, 1984) as described above.

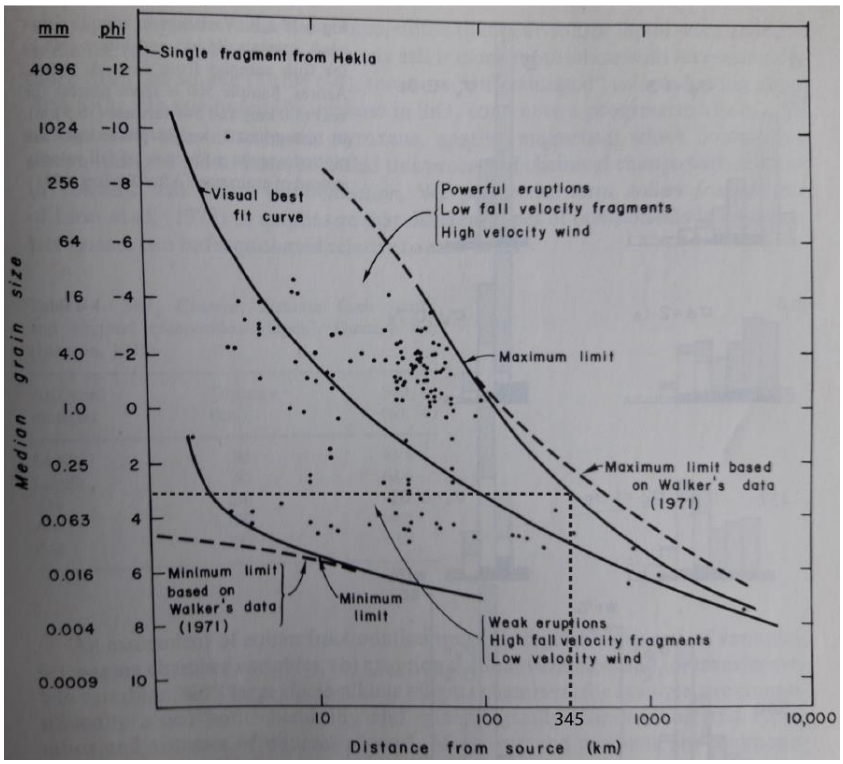

Figure 6.3: Median diameter plotted against distance from source (Fisher and Schmincke, 1984).

7. Conclusion

The Harwich ashes contain a lower SiO_2, Na_2O, CaO and MnO content and a higher Al_2O_3, Fe (FeO + Fe_2O_3) content. TiO_2 and MgO are more variable than the Danish positive series and the Greifswalder Oie type 1. Compared with the Danish negative series and the Greifswalder Oie type 2, the Harwich ashes have a lower SiO_2 and Na_2O content and a higher CaO, Al_2O_3, MnO and Fe (FeO + Fe_2O_3) content. Apart from these differences, the oxides SiO_2, Al_2O_3, FeO, Fe_2O_3, K_2O and MnO show similar chemical trends. The differences in oxides between the Harwich ashes and the Danish and German ashes can be explained by mixing of magmas, fractionation, multiple volcanic sources or alteration. Mixing of magmas shows a linear chemical trend between the oxides, this is not the case for the Harwich ashes. Mixing of magma is unlikely to have caused the chemical differences within the Harwich ashes. Fractionation of the small amount of phenocrysts in the Harwich ashes is not enough to explain all the differences in major element content between these samples and the samples from Denmark and Germany. A more felsic magma is expected by fractionation in the magma chamber. The Harwich ashes are mafic, as a result fractionation is unlikely to be the cause of the difference in chemical content. The chemical compositions of the glass grains in individual layers are scattered and the trend occurring in the total Fe – MgO plot cannot be explained by magma derived from multiple volcanic sources. Addition of H_2O and Fe_2O_3 and the loss of other major elements suggest alteration of basaltic glass to palagonite. This alteration took place during eruption, under elevated temperature conditions resulting in a fast alteration process. Water-magma interaction was needed during eruption to form the palagonite. The Harwich ashes were most likely altered. This means the major elements cannot be correlated with any of the former studies.

The grainsize of the Harwich ash layers is between 0.2 to 0.04 mm and the thickness of the layers is 4 cm, this would suggest the source area to be approximately 345 km away. But the grainsize and thickness distribution throughout Northern Europe indicates a source area in the North Atlantic Ocean. The travel distance of the ash will be 1100 to 1600 km from the NAIP to northern Europe, a water-magma interaction during the eruption is needed to reach this travel distance. Water-magma interaction is also expected because of the palagonite grains.

8. Acknowlegdement

I would like to thank Martyn Drury and Paul Mason for their guidance during this project. Tilly Bouten and Serguei Matveev are thanked for their assistance during the electron microprobe analysis. I would like to thank Leonard Bik for preparing the thin sections, and Jan Willem Weegink and Alex Klomp for their help with selecting the right drill cores from the TNO drill core facility.

9. References

Andersen, S. A. (1938). Die verbreitung der eozänen vulkanischen ascheschichten in Da¨nemark und nordwestdeutschland. Z Geschiebeforsch Flachlandgeol, 14, 179-207.

Bonatti, E. (1965). Palagonite, hyaloclastites and alteration of volcanic glass in the ocean. Bulletin of Volcanology, 28(1), 257-269.

Bornhöft, E. (1885). Der greifswalder bodden, seine morphologie geologische zusammensetzung und entwicklungsgeschiechte. Abel, , 1-72.

Bowen, G. J., Beerling, D. J., Koch, P. L., Zachos, J. C., & Quattlebaum, T. (2004). A humid climate state during the Palaeocene/Eocene thermal maximum. Nature, 432, 495-499.

Brooks, C. K. (1976). The Fe2O3/FeO ratio of basalt analyses: An appeal for a standardized procedure. Bull. Geol. Soc. Denmark, 25, 117-120.

Brooks, C. K., & Nielsen, T. F. D. (1982). The E greenland continental margin: A transition between oceanic and continental magmatism. Journal of the Geological Society, 139, 265-275.

Caldeira, K., & Rampino, M. R. (1991). The mid-cretaceous super plume, carbon dioxide, and global warming. Geophysical Research Letters, 18(6), 987-990.

Cioni, R., Pistolesi, M., Bertagnini, A., Bonadonna, C., Hoskuldsson, A., & Scateni, B. (2014). Insights into the dynamics and evolution of the 2010 eyjafjallajökull summit eruption (iceland) provided by volcanic ash textures. Earth and Planetary Science Letters, 394, 111-123.

Eldholm, O., & Grue, K. (1994). North atlantic volcanic margins: Dimensions and production rates. Journal of Geophysical Research, 99, 2955-2968.

Eldholm, O., & Thomas, E. (1993). Environmental impact of volcanic margin formation. Earth and Planetary Science Letters, 117, 319-329.

Elliott, G. F. (1971). Eocene volcanics in south-east england. Nature Physical Science, 230, 9.

Erlström, M., Thomas, S. A., Deeks, N., & Sivhed, U. (1997). Structure and tectonic evolution of the tornquist zone and adjacent sedimentary basins in scania and the southern baltic sea area. Tectonophysics, 271(3), 191-215.

Fekiacova, Z., Mertz, D. F., & Renne, P. R. (2007). Geodynamic setting of the tertiary hocheifel volcanism (germany), part I: 40Ar/39Ar geochronology. In J. R. R. Ritter, & U. R. Christensen (Eds.), Mantle plumes (pp. 185-206) Springer.

Fisher, R. V., & Schmincke, H. U. (1984). Pyroclastic rocks Springer-verlag.

Frieling, J., Svensen, H. H., Planke, S., Cramwinckel, M. J., Selnes, H., & Sluijs, A. (2016). Thermogenic methane release as a cause for the long duration of the PETM. Pnas, 113(43), 12059-12064.

Furnes, H. (1978). Element mobility during palagonitization of a subglacial hyaloclastite in iceland. Elsevier, 22, 249-264.

Grönwall, K. A. (1903). Løse blokke fra nordtyskland af stenarter, der indeholde vulkansk aske. Medd Dan Geol Foren, 9, 13-20.

Heister, L. E., O'Day, P. A., Brooks, C. K., Neuhoff, P. S., & Bird, D. K. (2001). Pyroclastic deposits within the east greenland tertiary flood basalts. Journal of the Geological Society, 158, 269-284.

Knox, R. W. O. (1997). The late paleocene to early eocene ash layers of the danish mo-clay (fur formation): Stratigraphic and tectonic significance. Aarhus Geoscience, 6, 7-11.

Knox, R. W. O., & Ellison, R. A. (1979). A lower eocene ash sequence in SE england. Journal of the Geological Society, 136, 251-253.

Knox, R. W. O., & Harland, R. (1979). Stratigraphical relationships of the early palaeogene ash-series of NW europe. Journal of the Geological Society, 136, 463-470.

Larsen, L. M., Godfrey Fitton, J., & Pedersen, A. K. (2003). Paleogene volcanic ash layers in the danish basin: Compositions and source areas in the north atlantic igneous province. Elsevier, 71, 47-80.
Lucic, G., Berg, A. S., & Stix, J. (2016). Water-rich and volatile-undersaturated magmas at hekla volcano, iceland. Geochemistry, Geophysics, Geosystems, 17(8), 3111-3130.
Malm, O. A., Christensen, O. B., Furnes, H., Løvlie, R., & Ruselåtten, H. (1984). The lower tertiary balder formation: An organogenic and tuffaceous deposit in the north sea region. In A. M. Spenser, & et al (Eds.), Petroleum geology of the north european margin (pp. 149-170) Graham and Trotman Ltd.
Marshak, S. (2011). Earth. portrait of a planet (fourth edition ed.) W.W. Norton & company.
Mjelde, R., Breivik, A. J., Raum, T., Mittelstaedt, E., Ito, G., & Faleide, J. I. (2008). Magmatic and tectonic evolution of the north atlantic. Journal of the Geological Society, 165, 31-42.
Morton, A. C., & Evans, J. A.,. (1988). Geochemistry of basaltic ash beds from the fur formation, island of fur, denmark. Bull. Geol. Soc. Denmark, 37, 1-9.
Morton, A. C., & Knox, R. W. O. (1990). Geochemistry of late paleocene and early eocene tephras from the north sea basin. Journal of the Geological Society, 147, 425-437.
Norin, R. (1940). Problems concerning the volcanic ash layers of the lower tertiary of denmark. Geologiska Föreningen i Stockholm Förhandlingar, 62(1), 31-44.
Obst, K., & Ansorge, J. (2010). Die greifswalder Oie—ein einzigartiges vorkommen von pra¨pleistoza¨nen schollen und geschieben in einer hoch deformierten quarta¨ren abfolge. Eiszeitlandschaften in Mecklenburg-Vorpommern, , 132-158.
Obst, K., Ansorge, J., Matting, S., & Hüneke, H. (2015). Early eocene volcanic ashes on greifswalder oie and their depositional environment, with an overview of coeval ash-bearing deposits in northern germany and denmark. International Journal of Earth Sciences, 104(8), 2179-2212.
Pedersen, A. K., & Jørgensen, K. A. (1981). A textural study of basaltic tephras from lower tertiary diatomites in northern denmark. In S. Self, & S. J. Sparks (Eds.), Tephra studies (pp. 213-218) D. Reidel.
Pedersen, A. K., Engell, J., & Rønsbo, J. G. (1975). Early tertiary volcanism in the skagerrak: New chemical evidence from ash-layers in the mo-clay of northern denmark. Lithos, 8(4), 255-268.
Pegrum, R. M., & Ljones, T. E. (1984). The 15/9 gamma gasfield: A new trap type for the north sea with regional implications. The American Association of Petroleum Geologists, 68(7), 874-902.
Saunders, A. D. (2016). Two LIPs and two earth-system crises: The impact of the north atlantic igneous province and the siberian traps on the earth-surface carbon cycle. Geological Magazine, 153(2), 201-222.
Saunders, A. D., Fitton, J. G., Kerr, A. C., Norry, M. J., & Kent, R. W. (1997). The north atlantic igneous province. In J. J. Mahony, & M. F. Coffin (Eds.), Large igneous provinces, continental, oceanic, and planetary flood volcanism (pp. 45-93) AGU.
Schmincke, H. U. (2007). The quaternary volcanic fields of the east and west eifel (germany). In J. R. R. Ritter, & U. R. Christensen (Eds.), Mantle plumes (pp. 241-322) Springer.
Schumacher, M. E. (2002). Upper rhine graben: Role of preexisting structures during rift evolution. Tectonics, 21(1), 6-1-6-17.
Sharma, P. V. (1970). Geophysical evidence for a buried volcanic mount in the skagerrak. Bull. Geol. Soc. Denmark, 19, 368-377.
Smallwood, J. R., & White, R. S. (2002). Ridge-plume interaction in the north atlantic and its influence on continental breakup and seafloor spreading. Geological Society London, 197, 15-37.
Thomas, D. J., & Bralower, T. J. (2005). Sedimentary trace element constraints on the role of north atlantic igneous province volcanism in late Paleocene–early eocene environmental change. Marine Geology, 217(3-4), 233-254.
Thybo, H. (1997). Geophysical characteristics of the tornquist fan area, northwest trans-european suture zone: Indication of late carboniferous to early permian dextral transtension. Geological Magazine, 134(5), 597-606.

Tomlinson, E. L., Thordarson, T., Lane, C. S., Smith, V. C., Manning, C. J., Müller, W., & Menzies, M. A. (2012). Petrogenesis of the sólheimar ignimbrite (katla, iceland): Implications for tephrostratigraphy. Geochimica Et Cosmochimica Acta, 86, 318-337.

Van Bergen, M. J., & Sissingh, W. (2007). Magmatism in the netherlands: Expression of the north-west european rifting history. In T. E. Wong, D. A. J. Batjes & J. De Jager (Eds.), Geology of the netherlands (pp. 197-221) Royal Netherlands Academy of arts and sciences.

Wieczorek, R., Fantle, M. S., Kump, L. R., & Ravizza, G. (2013). Geochemical evidence for volcanic activity prior to and enhanced terrestrial weathering during the paleocene eocene thermal maximum. Elsevier, 119, 391-410.

Wong, T. E., De Lugt, I. R., Kuhlmann, G., & Overeem, I. (2007). Tertiary. In T. E. Wong, D. A. J. Batjes & J. De Jager (Eds.), Geology of the netherlands (pp. 151-171) Royal Netherlands Academy of arts and sciences.

10. Appendix

Appendix 10.1: Sample description

The Harwich samples were found on the beach. In these samples a clear ash layer is visible.
The samples from the Dutch drill cores were taken from the drill core facility in Zeist. The samples were chosen using the description in the stratigraphic log. Light microscopy was used to find out whether there is ash in the samples.

Harwich-S1

The bottom part of the rock is a light grey/brownish limestone layer. On top of this layer a dark coloured ash layer is situated. This ash shows crossbedding (Fig. 10.1.1B), in which coarse grained and fine grained ash are alternated.

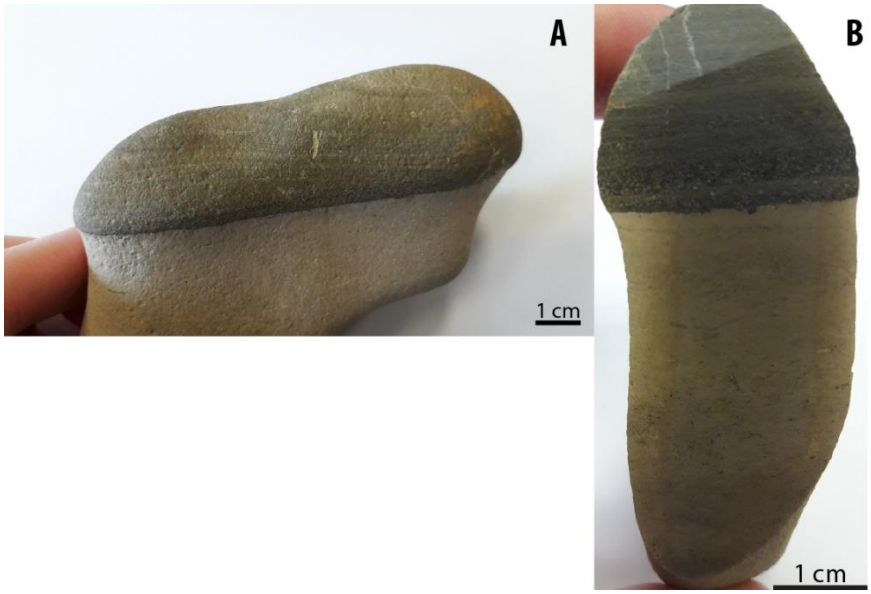

Figure 10.1.1: A: Sideview of sample HW-S1; B: Cross section of sample HW-S1.

Harwich-S2

The bottom part of the rock is a light grey/brownish limestone layer, on top of this layer the dark coloured ash is deposited (Fig. 10.1.2). The ash layer is normally graded, due to bioturbation this grading is not continuous throughout the sample (Fig. 10.1.2B). The base of the ash layer (0.5 cm) is light grey and coarse grained, on top of this a fine grained, dark grey layer is visible.

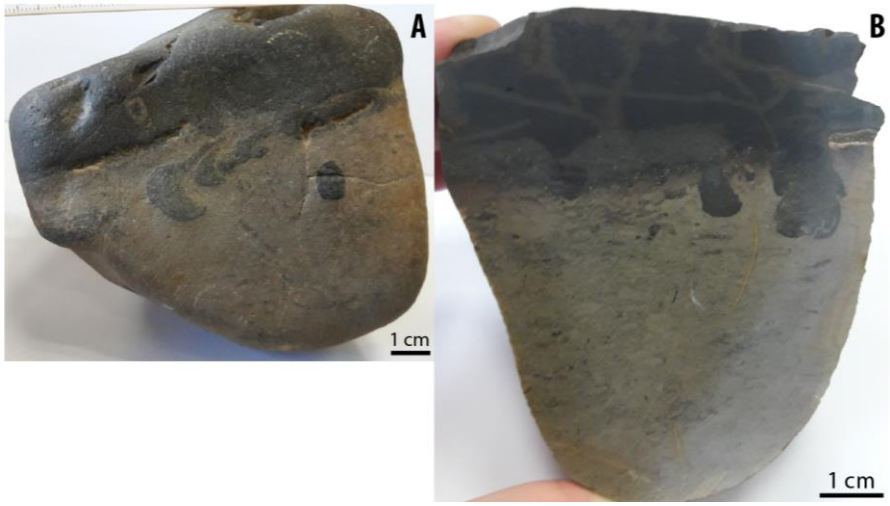

Figure 10.1.2: A: Sideview of sample HW-S2; B: Cross section of sample HW-S2.

Harwich-S3

The bottom part of the rock is a light grey/brownish limestone layer, on top of this layer the dark coloured ash is deposited. The ash layer is normally graded. The coarse grained part is 0.5 – 2 cm thick (Fig. 10.1.3B). One bioturbation structure is visible (Fig. 10.1.3A).

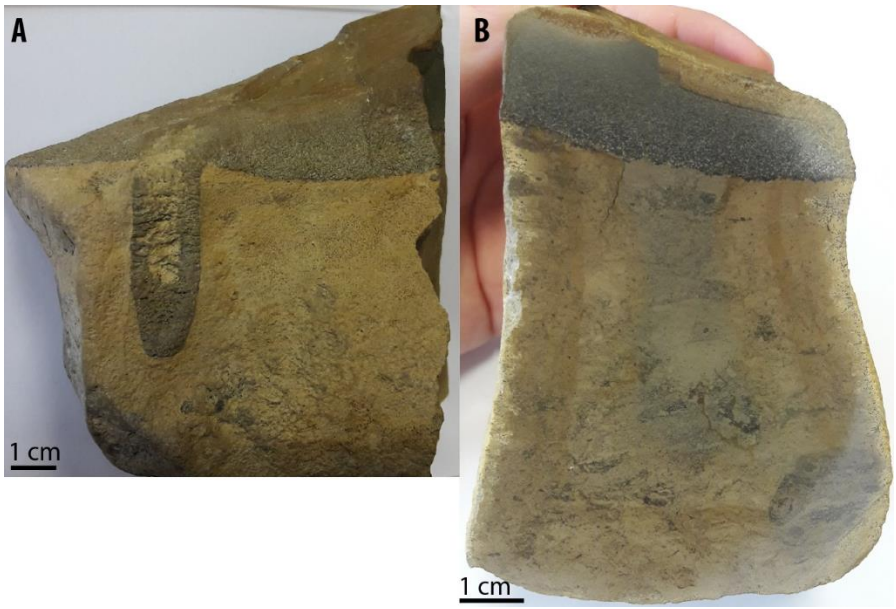

Figure 10.1.3: A: Sideview of sample HW-S3; B: Cross section of sample HW-S3.

Harwich-S4

The bottom part of the rock is a light grey/brownish limestone layer, on top of this layer the dark coloured ash is deposited. The ash layer is normally graded. In the limestone layer another smaller ash layer is visible (Fig. 10.1.4). This ash layer is 0.5 cm thick, including some larger brown grains of 0.3 cm.

Figure 10.1.4: Cross section of sample HW-S4.

Harwich-S5

The bottom part of the rock is a light grey/brownish limestone layer, on top of this layer the dark coloured ash is deposited (Fig. 10.1.5A). The ash layer is normally graded, and is in total approximately 2.5 cm thick (Fig. 10.1.5B). On top of the ash layer a lighter grey layer is present, this layer contains fossils (Fig. 10.1.5C).

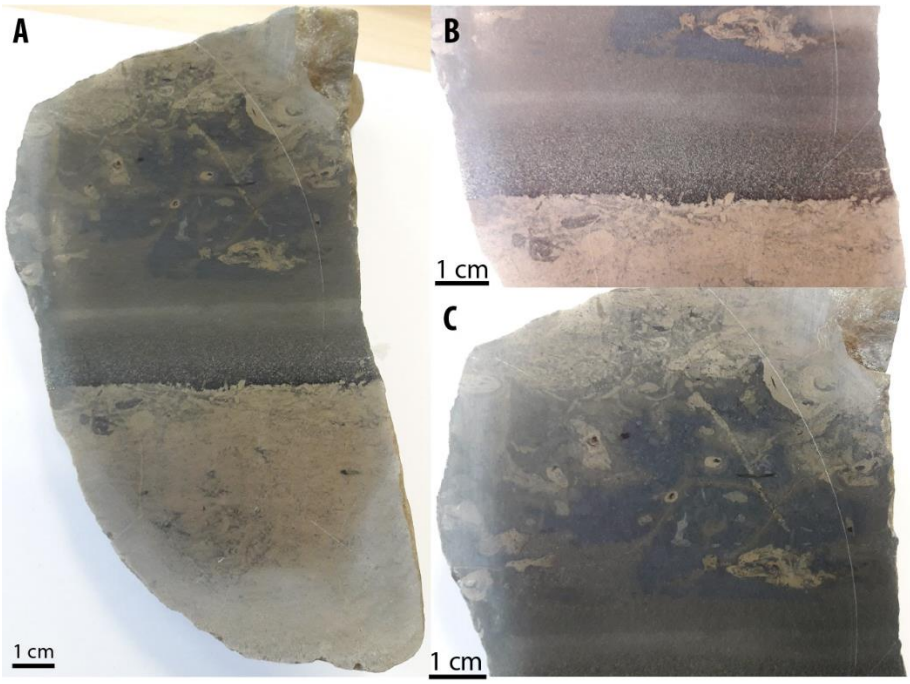

Figure 10.1.5: A: cross section of sample HW-S5; B: Zoomed in image of the ash layer; C: Zoomed in image of the upper layer containing fossils.

Harwich-S6

The bottom part of the rock is a light grey/brownish limestone layer, on top of this layer the dark coloured ash is deposited (Fig. 10.1.6). The ash layer is normally graded.

Figure 10.1.6: Cross section of sample HW-S6.

Harwich-S7

The bottom part of the rock is a light grey/brownish limestone layer, on top of this layer the dark coloured ash is deposited. The ash layer is normally graded. After deposition a vertical fracture is formed, and has been filled (Fig. 10.1.7A).
In the limestone layer another ash layer is visible (Fig. 10.1.7B). This ash layer is 0.5 cm thick and including larger brown grains of 0.2 cm.

Figure 10.1.7: A: Sideview of sample HW-S7; B: Cross section of sample HW-S7.

Harwich-S8

The bottom part of the rock is a light grey/brownish limestone layer, on top of this layer the dark coloured ash is deposited (Fig. 10.1.8). The ash layer is normally graded.
In the limestone layer, some ash patches are visible. One of these patches is a tube of 0.5 cm thick

Figure 10.1.8: Cross section of sample HW-S8.

Harwich-S9

The bottom part of the rock is a light grey/brownish limestone layer, on top of this layer the dark coloured ash is deposited (Fig. 10.1.9). The ash layer is normally graded. In the dark coloured area, some red specks are visible. These can be the result of weathering.

Figure 10.1.9: Sample HW-S9.

Harwich-S10

The bottom part of the rock is a light grey/brownish limestone layer, on top of this layer the dark coloured ash is deposited (Fig. 10.1.10). The ash layer is normally graded.

Figure 10.1.10: Sample HW-S10.

Harwich-S11

The bottom part of the rock is a light grey/brownish limestone layer, on top of this layer the dark coloured ash is deposited (Fig. 10.1.11). The ash layer is normally graded.

Figure 10.1.11: Sample HW-S11.

Harwich-S12

The bottom part of the rock is a light grey/brownish limestone layer, on top of this layer the dark coloured ash is deposited (Fig. 10.1.12). The ash layer is normally graded.

Figure 10.1.12: Sample HW-S12.

Harwich-S13

The bottom part of the rock is a light grey/brownish limestone layer, on top of this layer the dark coloured ash is deposited (Fig. 10.1.13). The ash layer is normally graded.

Figure 10.1.13: Sample HW-S13

Harwich-S14

The bottom part of the rock is a light grey/brownish limestone layer, on top of this layer the dark coloured ash is deposited (Fig. 10.1.14). The ash layer is normally graded. In the limestone some dark coloured ash patches are visible.

Figure 10.1.14: Sample HW-S14.

Harwich-S15

The bottom part of the rock is a light grey/brownish limestone layer, on top of this layer the dark coloured ash is deposited (Fig. 10.1.15). The ash layer is normally graded. In the limestone some ash patches are visible.

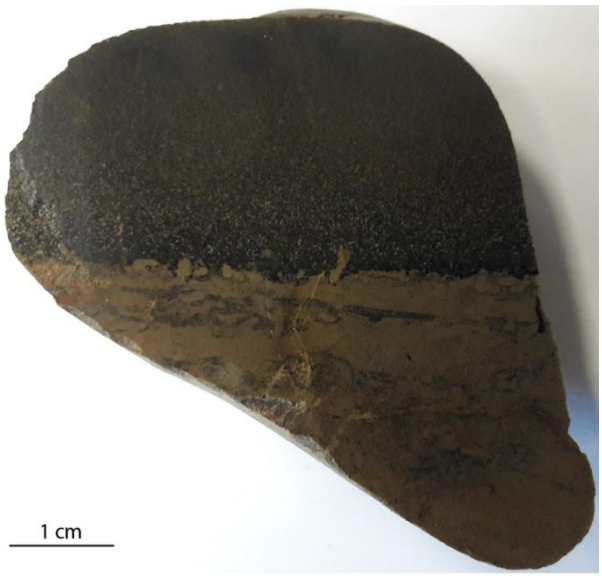

Figure 10.1.15: Cross section of sample HW-S15

Harwich-S16

The bottom part of the rock is a light grey/brownish limestone layer, on top of this layer the dark coloured ash is deposited (Fig. 10.1.16). The ash layer is normally graded. In the limestone some dark coloured ash patches are visible.

Figure 10.1.16: Sample HW-S16.

Raalte-S1, depth: 642-647 m

The stratigraphic log of this drill core described that between a depth of 647.9 and 649.6 m some tuff lenses can be found. The samples taken at approximately the depth are shown in Figure 10.1.17. In these samples some black lenses are visible (red circles) in grey brown claystone.

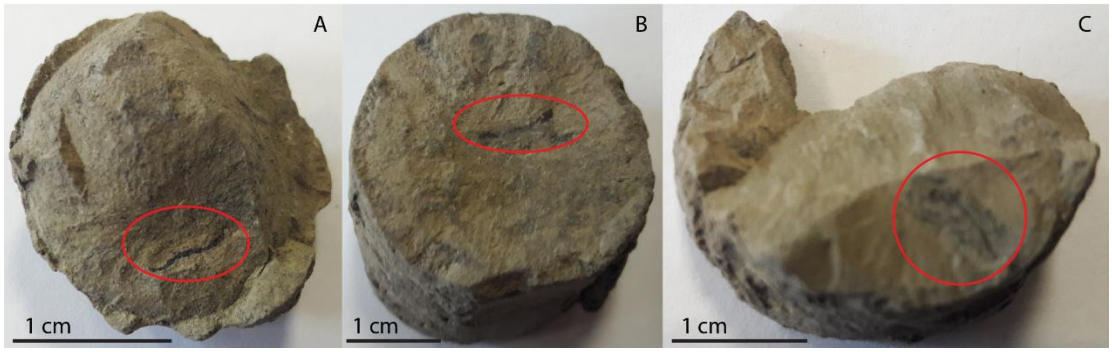

Figure 10.1.17: A, B, C: There were three samples taken. The red circles indicate the black lenses in the samples, which might be ash.

Lommen-S1, depth: 446.2-450.5 m

The stratigraphic log of this drill core described that at a depth of 450.5 m some tuff lenses can be found. The samples taken from this depth are a brown-grey claystone, with black lenses (red circles in Fig. 10.1.18)

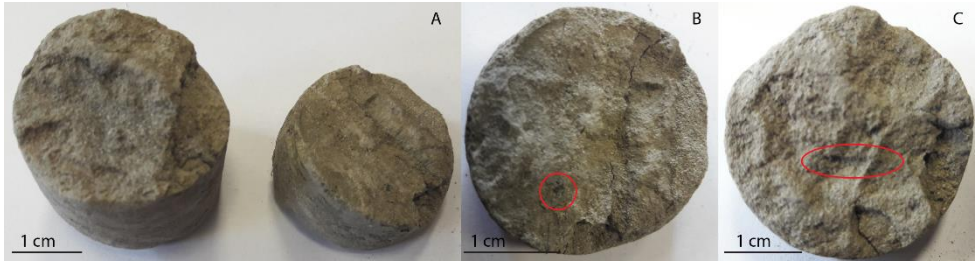

Figure 10.1.18: A: The two samples taken; B, C: The red circles indicate the black lenses in the samples, which might be ash.

Ommen-S1, depth: 615-620 m

The stratigraphic log of this drill core described that at a depth of 612.2 m some tuff lenses can be found. The sample taken from this depth is a brown-grey claystone, with black lenses (red circles in Fig. 10.1.19).

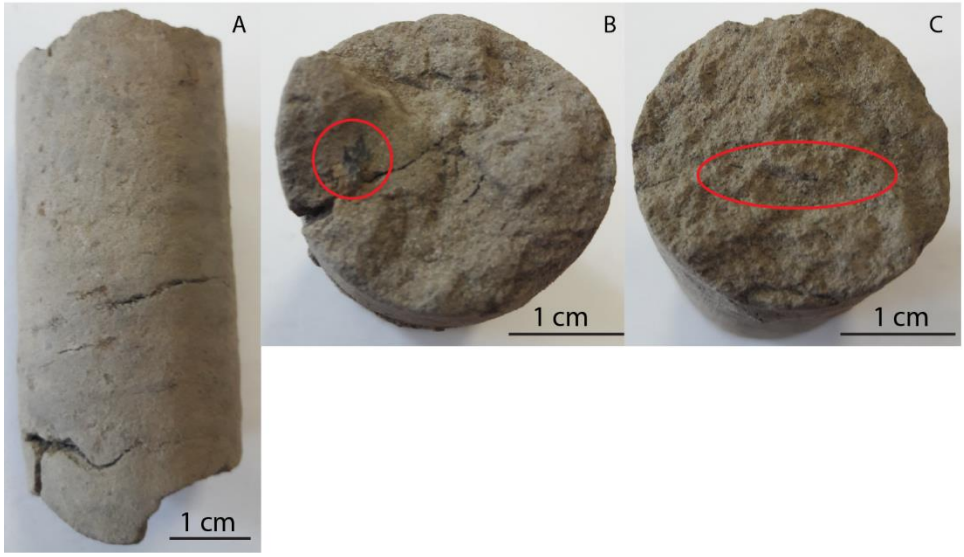

Figure 10.1.19: A: Sideview of the sample; B, C: Top and bottom view of the sample. The red circles indicate the black lenses in the samples, which might be ash.

Schoonebeek-S1, depth: 421-422.7 m

The stratigraphic log of this drill core described that at a depth of 380 m and 417 m some tuff layers can be found. The sample taken from this depth is a brown-grey claystone, with black lenses (red circles in Fig. 10.1.20).

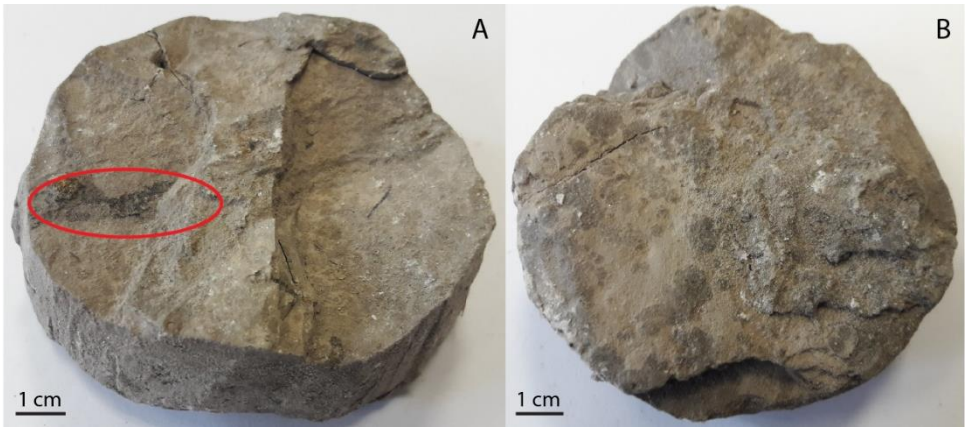

Figure 10.1.20: A, B: Top and bottom view of the sample. The red circle indicates the black lens in the sample, which might be ash.

Coevorden-S1

The stratigraphic log of this drill core described that at a depth of 311 m some tuff layers and tuff lenses can be found. The sample taken from this depth is a brown-grey claystone, with black lenses (red circles in Fig. 10.1.21). This black lens is surrounded with a green/yellow colour.

Figure 10.1.21: The red circle indicates the black lens in the sample, which might be ash.

Coevorden-S2

The stratigraphic log of this drill core described that at a depth of 311 m some tuff layers and tuff lenses can be found. The sample taken from this depth is a brown-grey claystone, with black lenses (red circles in Fig. 10.1.22). This black lens is surrounded with a green/yellow colour.

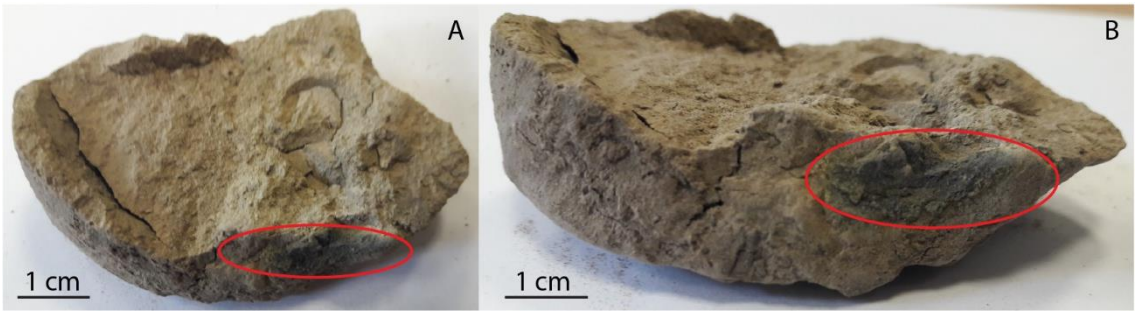

Figure 10.1.22: A, B: Top and side view of the sample. The red circles indicate the black lenses in the samples, which might be ash.

Coevorden-S3

The stratigraphic log of this drill core described that at a depth of 311 m some tuff layers and tuff lenses can be found. The sample taken from this depth is a dark brown claystone, with a black lens (Fig. 10.1.23).

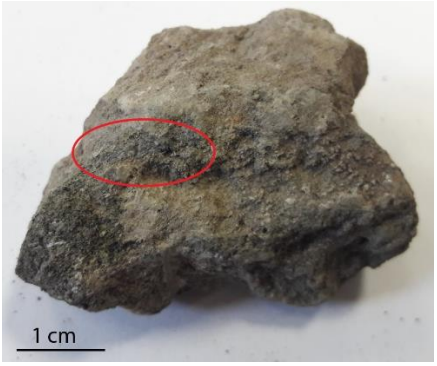

Figure 10.1.23: The red circles indicate the black lenses in the samples, which might be ash.

Appendix 10.2: Light microscopy and SEM

Light microscopy and SEM analysis were used to identify the mineralogy. Below the minerals present in the ash layers were described.

- Calcium carbonate.

Calcium carbonate forms the matrix. In the SEM the grains are visible as a constant light grey colour, indicated by arrows in Figure 10.2.1A. Figures 10.2.1B and 10.2.1C show calcium carbonate grains studied by light microscopy. In plane polarized light $CaC0_3$ is colourless and has a high relief, in crossed polarized light $CaCO_3$ has a 2nd order birefringence.

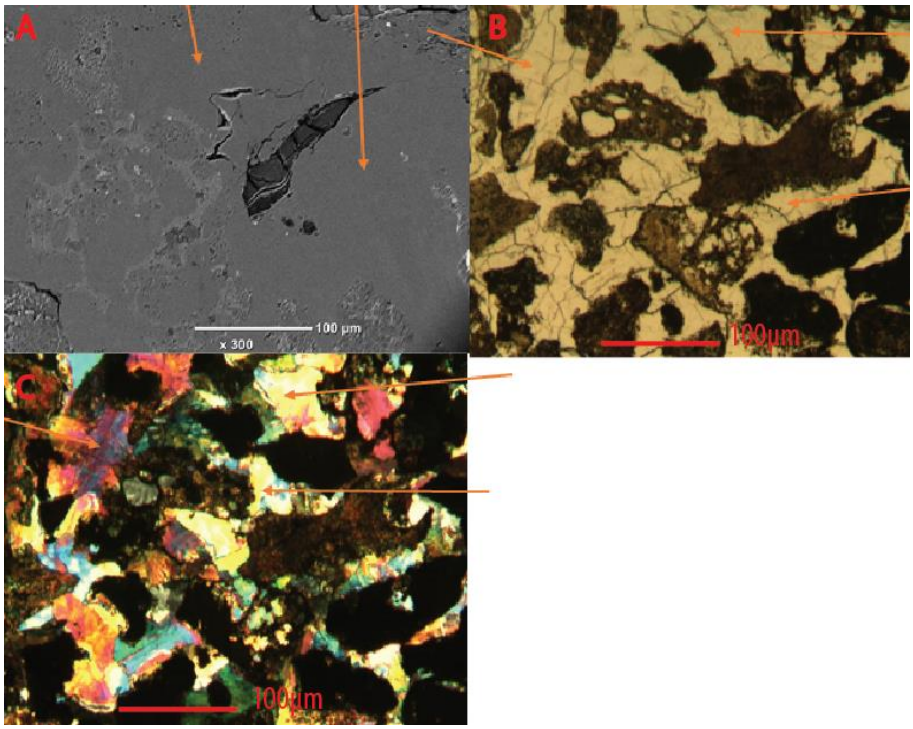

Figure 10.2.1: A: SEM image HW-S5, arrows indicate calcium carbonate; B: Plane polarized light microscope image of HW-S5, arrows indicate CaCO3; C: Crossed polarized light microscope image of HW-S5, arrows indicate CaCO3.

- Tachylite

There are many ‘crystallized igneous grains’ in the samples. These grains consist of smaller crystallized grains (Fig. 10.2.2A), with the compositions of especially glass grains and feldspar. Light microscopy showed these grains are opaque (Fig. 10.2.2B, C), these visual appearances are characteristic for tachylite. Tachylite is one of the two varieties of basaltic glass.

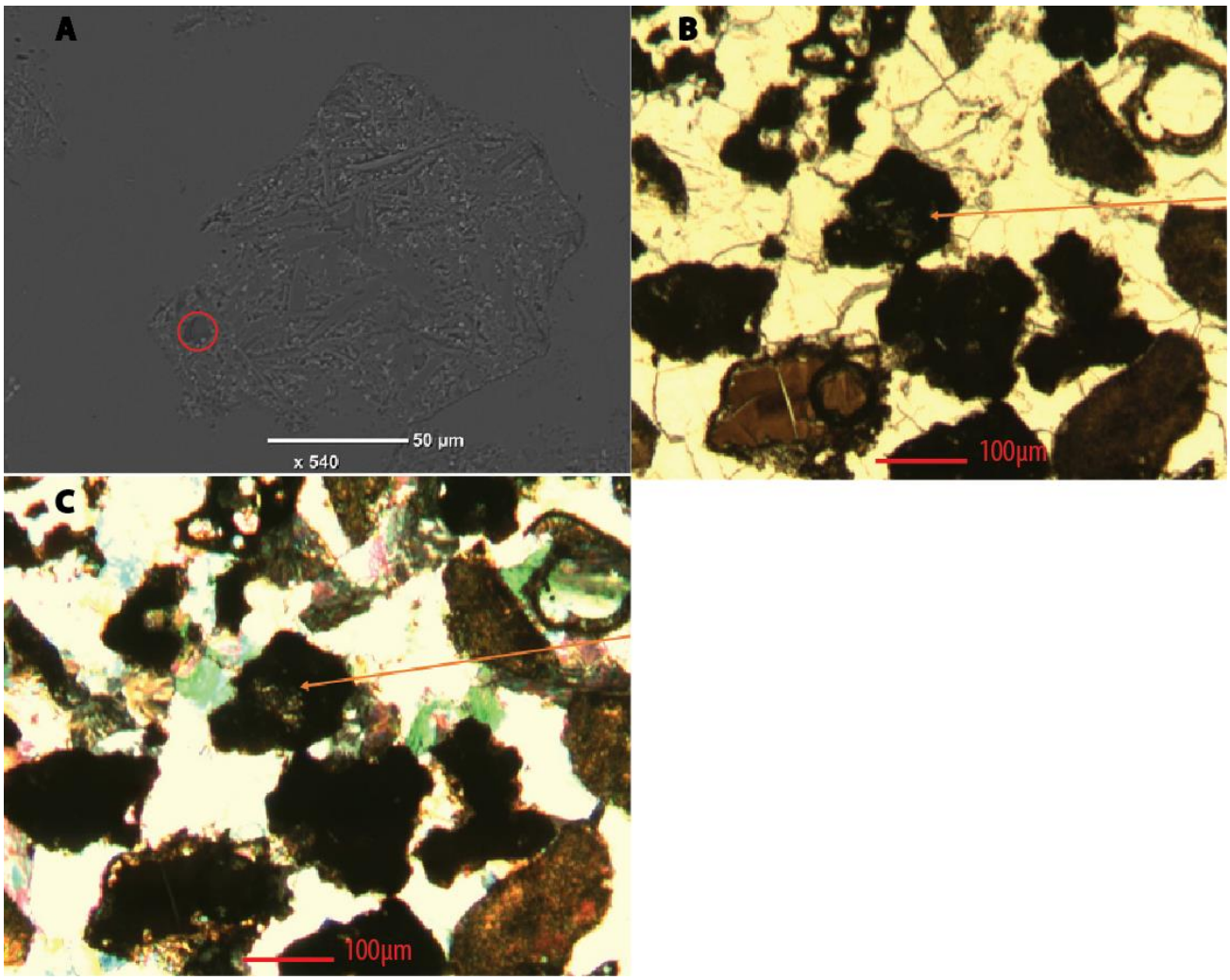

Figure 10.2.2: A: SEM image sample HW-S5, showing tachylyte. The red circle indicates a glass grain; B: Plane polarized light microscope image of HW-S5, arrow indicates tachylite; C: Crossed polarized light microscope image of HW-S5, arrow indicates tachylite.

- Glass grains

Analysing the thin sections using the SEM, some grains have compositions which are not a specific mineral. These are glass grains. Glass was found inside the tachylite and as a single glass grain. The former glass grains are too small to be analysed using the electron microprobe. The larger glass grains are big enough for electron microprobe analysis. These grains can be recognized by the conchoidal fractures. Light microscopy showed the glass grains are yellow to dark brown in plane polarized light (Fig. 10.2.3B). In crossed polarized light the grains are isotropic (Fig. 10.2.3C). The visiual appearances are characteristic for sideromelane or palagonite. Palagonite is a general term for any hydrous, altered, basaltic glass (Fisher and Schmincke, 1984).

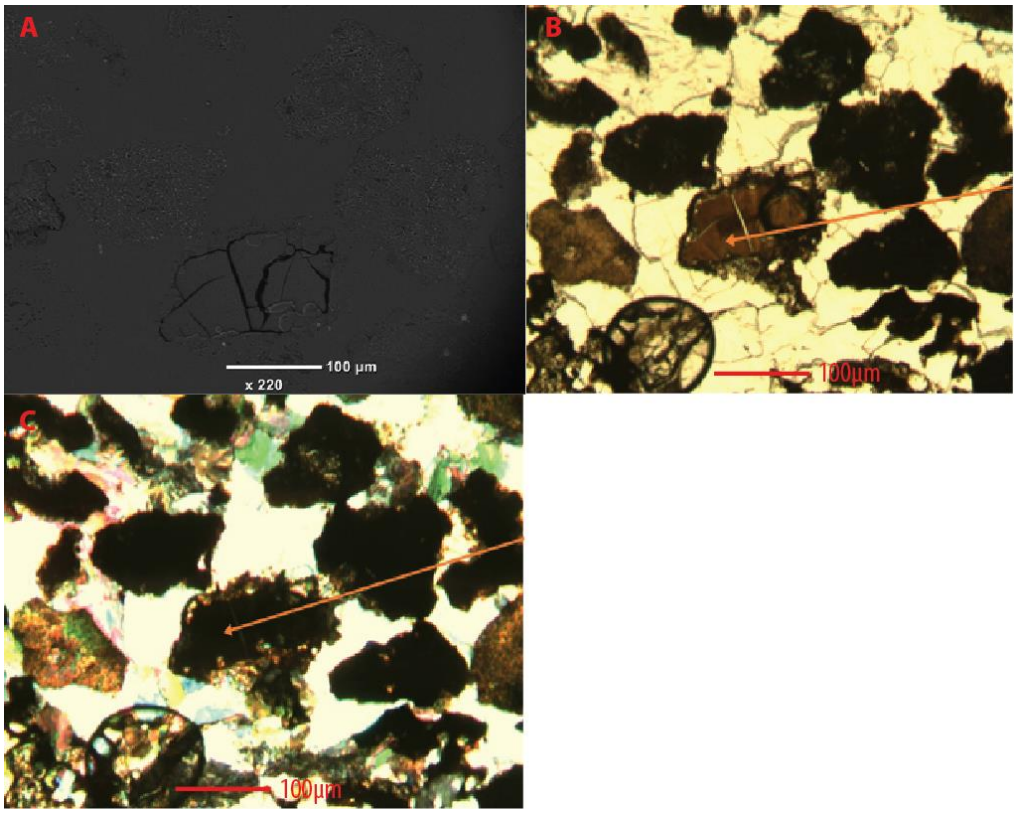

Figure 10.2.3: A: SEM image sample HW-S5, showing a glass grain; B: Plane polarized light microscope image of HW-S5, arrow indicates a glass grain; C: Crossed polarized light microscope image of HW-S5, arrow indicates a glass grain.

- Pyrite

Framboidal pyrite structures were found in sample HW-S1 (Fig. 10.2.4A). Pyrite has also formed rims around grains in this sample (Fig. 10.2.4B). In sample HW-S5 pyrite was formed in sedimentary structures (analysis 27 in Fig. 10.2.4C). The pyrite is sedimentary or caused by alteration, and therefore not originating from the volcano eruption.

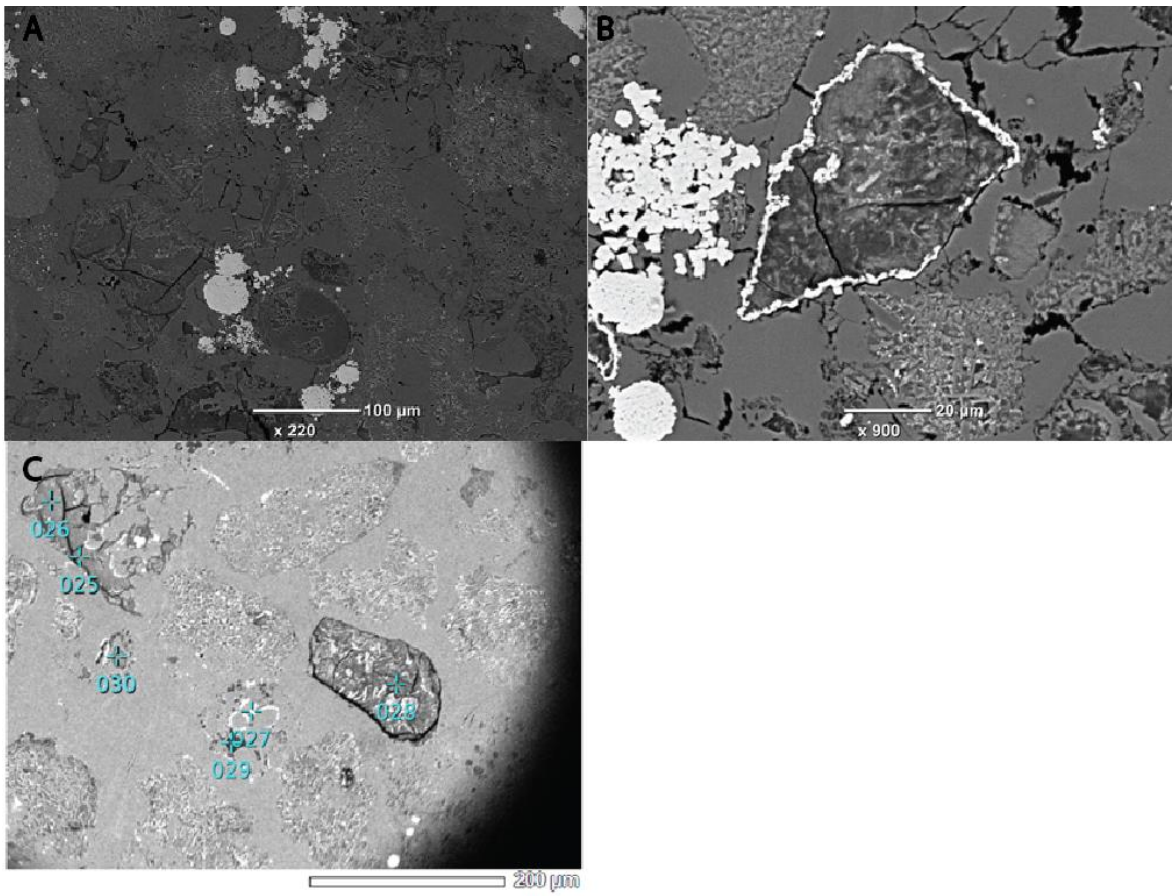

Figure 10.2.4: A: SEM image of sample HW-S1, showing framboidal pyrite; B: SEM image of sample HW-S1, showing a rim of pyrite; C: SEM image of sample HW-S5.

- Feldspar

Feldspar was found as crystallized grains inside a larger igneous grain (Fig. 10.2.5A). Also larger single feldspar grains were found, these are anhedral as in Fig. 10.2.5B or euhedral.

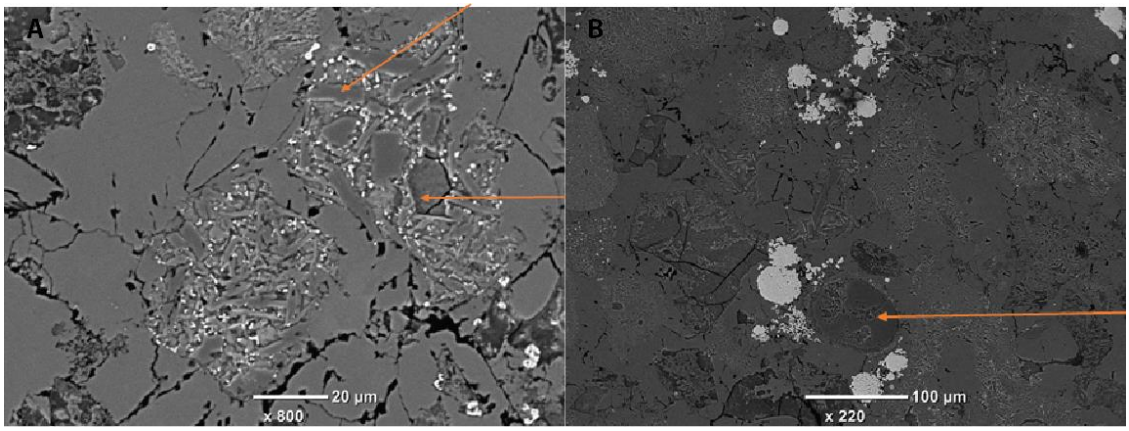

Figure 10.2.5: A: SEM image sampel HW-S1, arrows indicate feldspar crystals; B: SEM image sample HW-S1, arrow indicates a feldspar grain.

- Clay minerals

Clay minerals were interpreted by SEM analysis. The grains are indicated by red circles in Figure 10.2.6, these grains consist of a high aluminium and silica content. Water is not identified by SEM, electron microprobe analysis will indicate the water content which proves, the grains indicated, are clay minerals. The clay grains present in Figure 10.2.6B appears to be pore filling, which is characteristic for clay minerals.

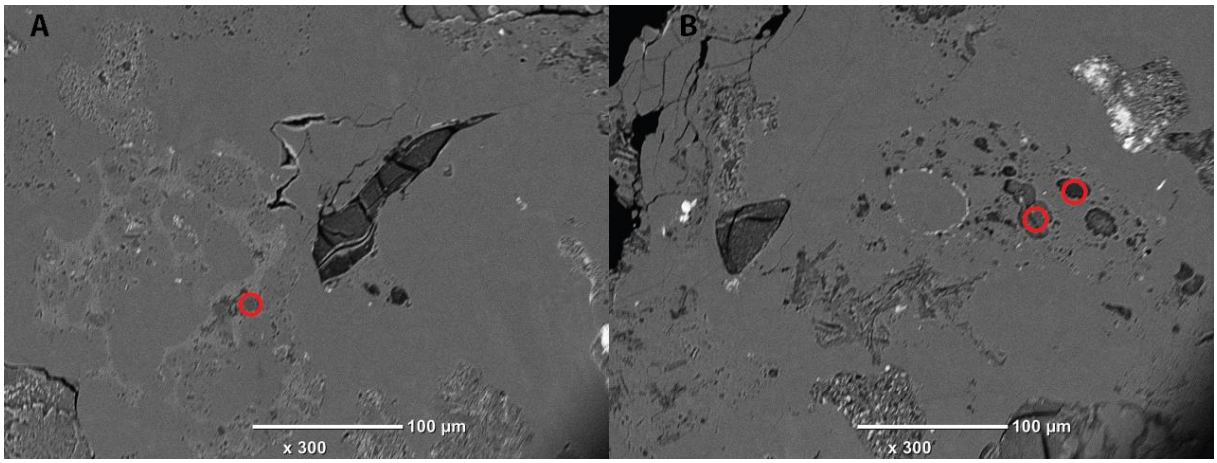

Figure 10.2.6: A and B: SEM analysis. The grains indicated by the red circles are interpreted as clay minerals.

Appendix 10.3: Electron microprobe

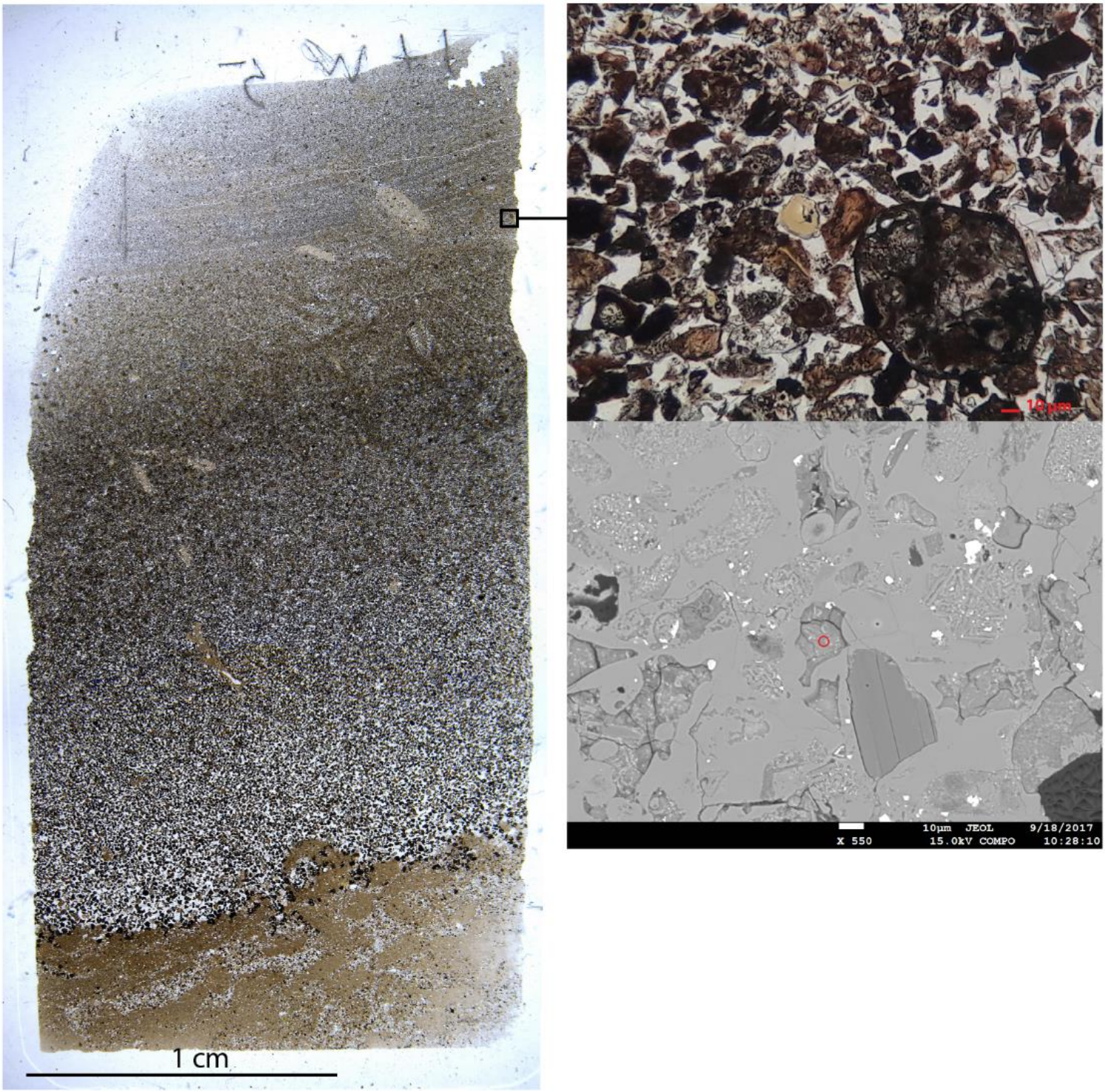

Figure 10.3.1: Analysis 5.1.

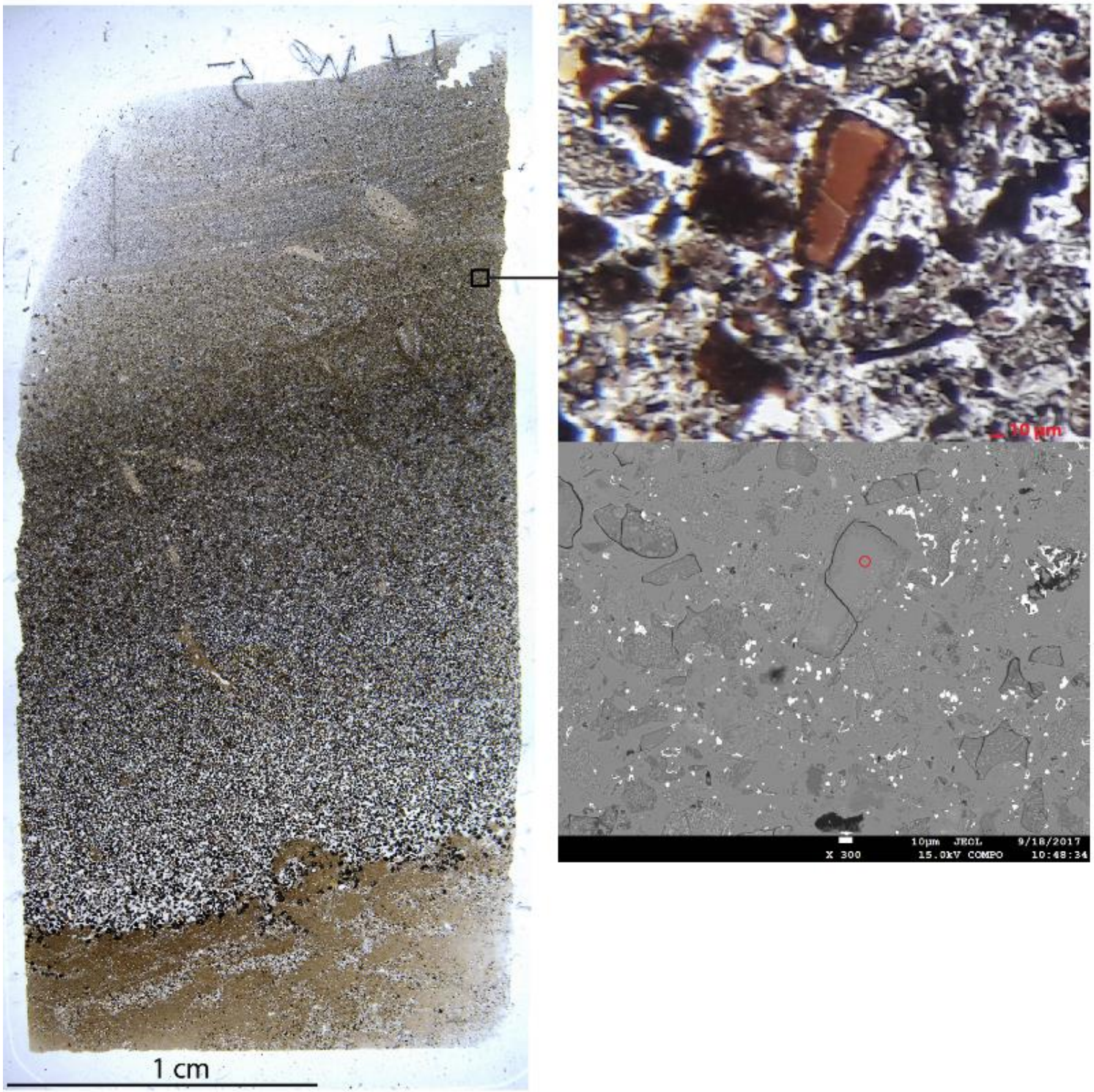

Figure 10.3.2: Analysis 5.2.

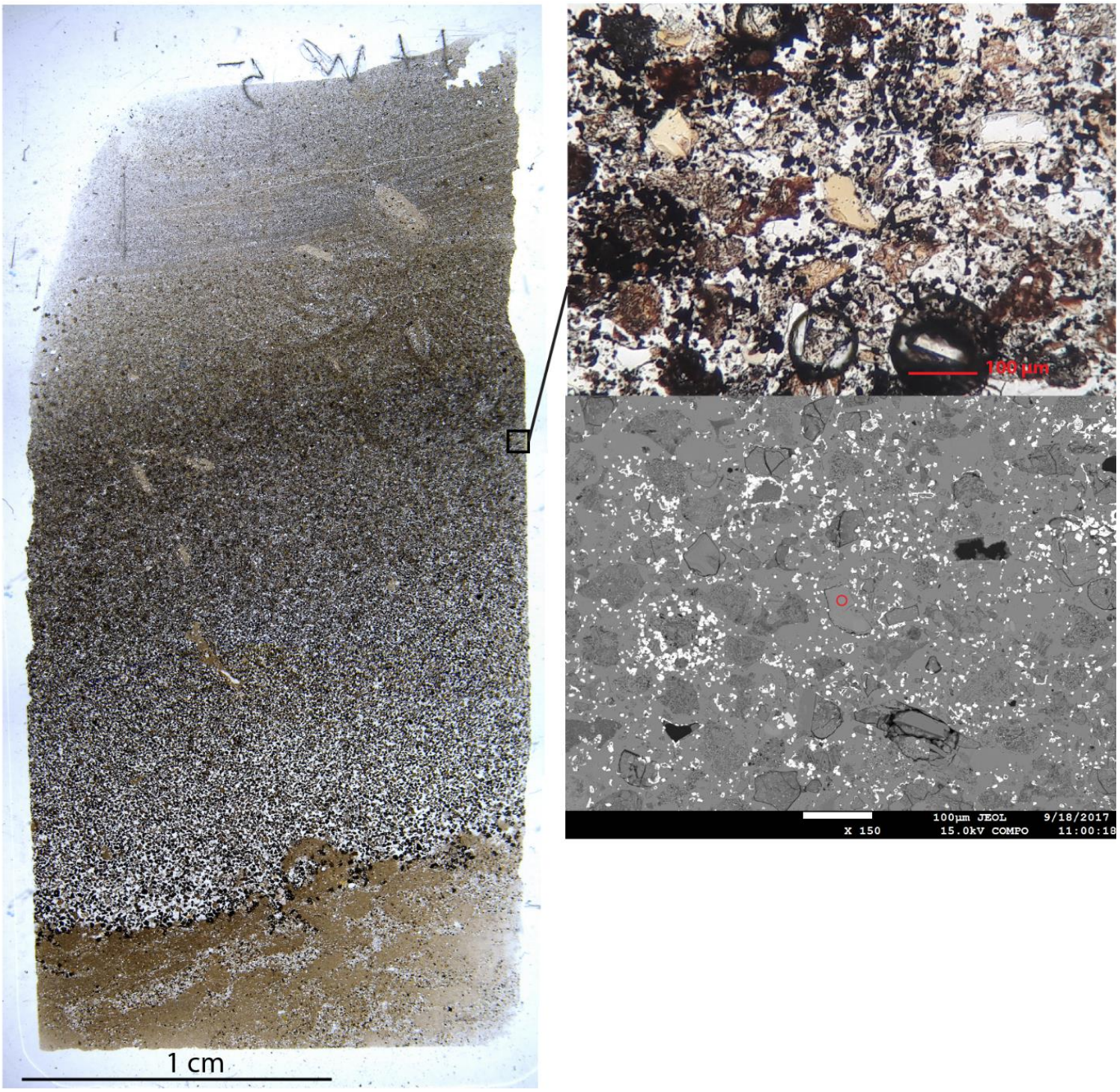

Figure 10.3.3: Analysis 5.3.

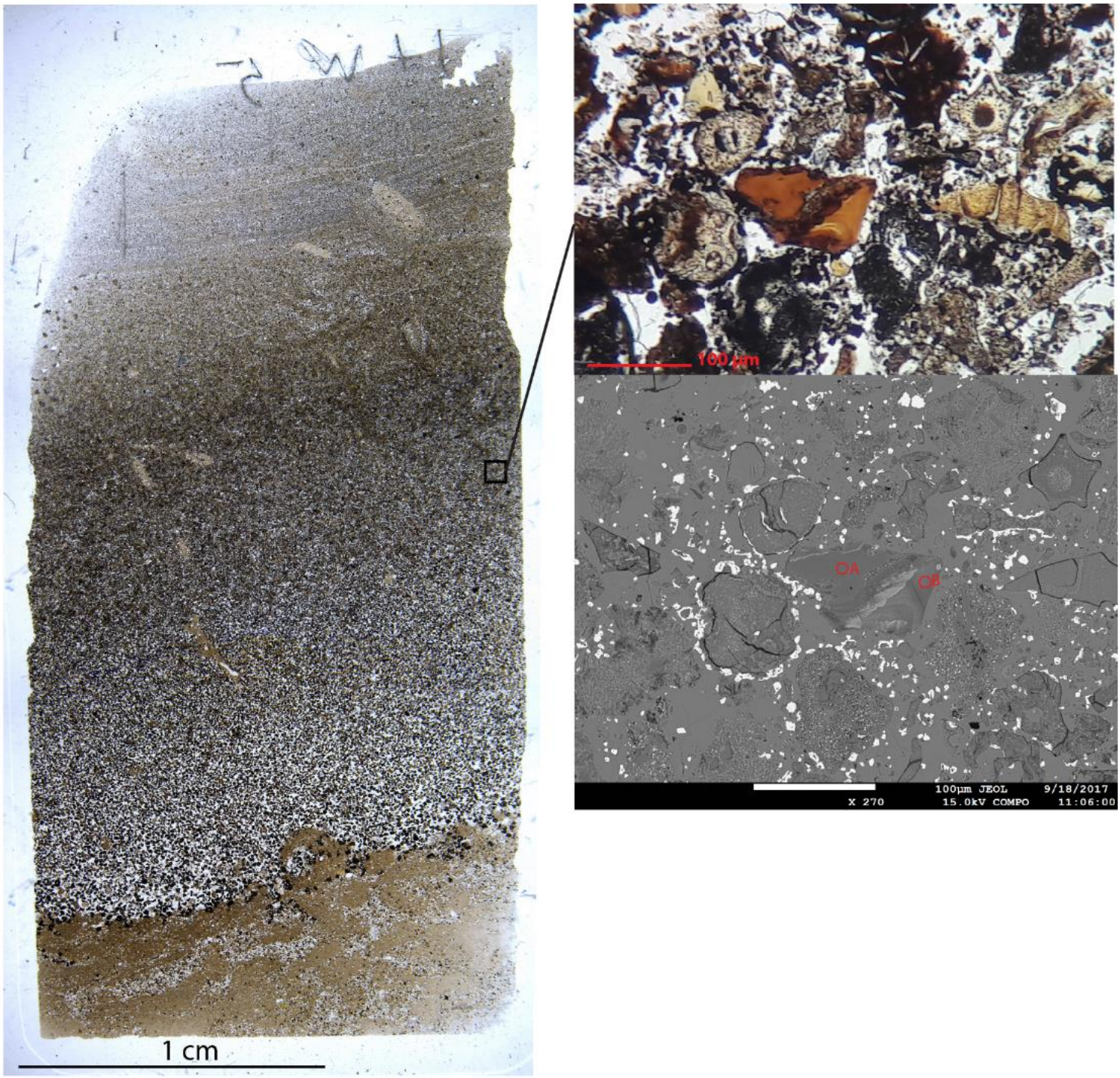

Figure 10.3.4: Analysis 5.4.

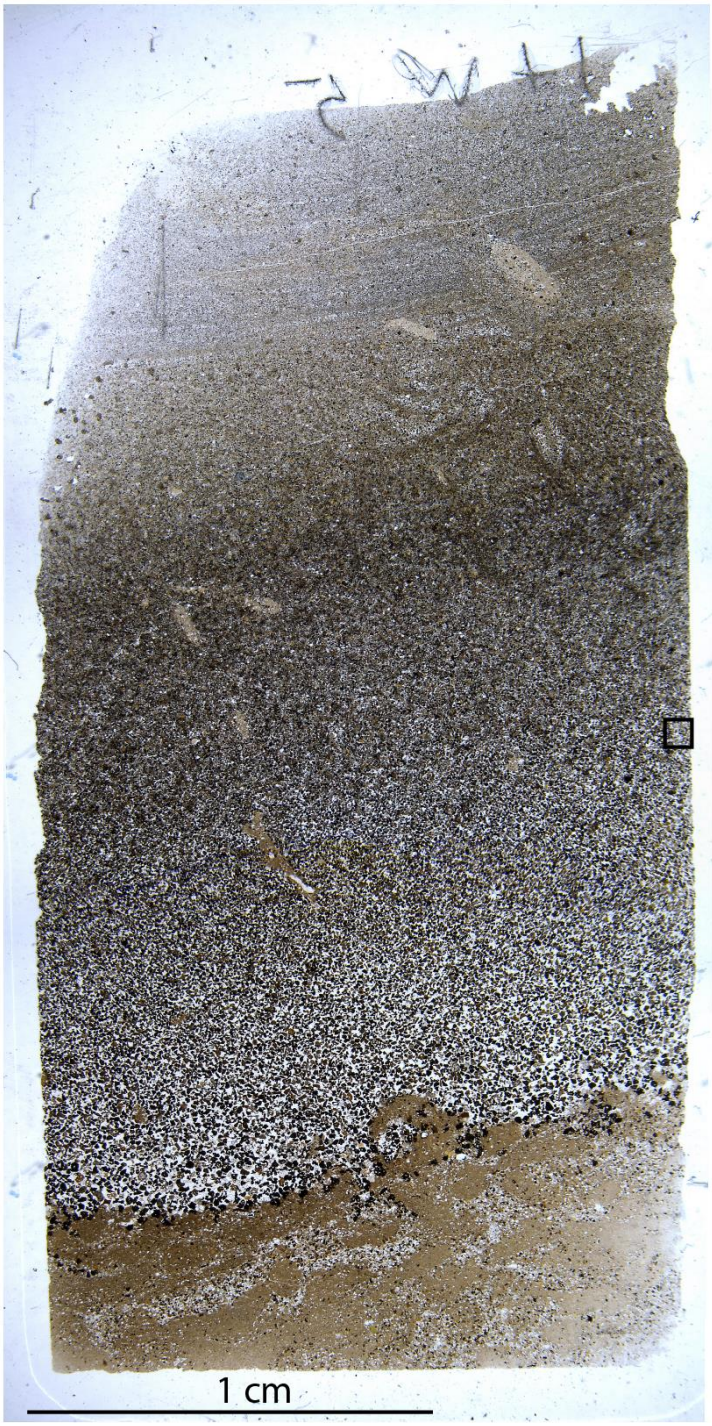

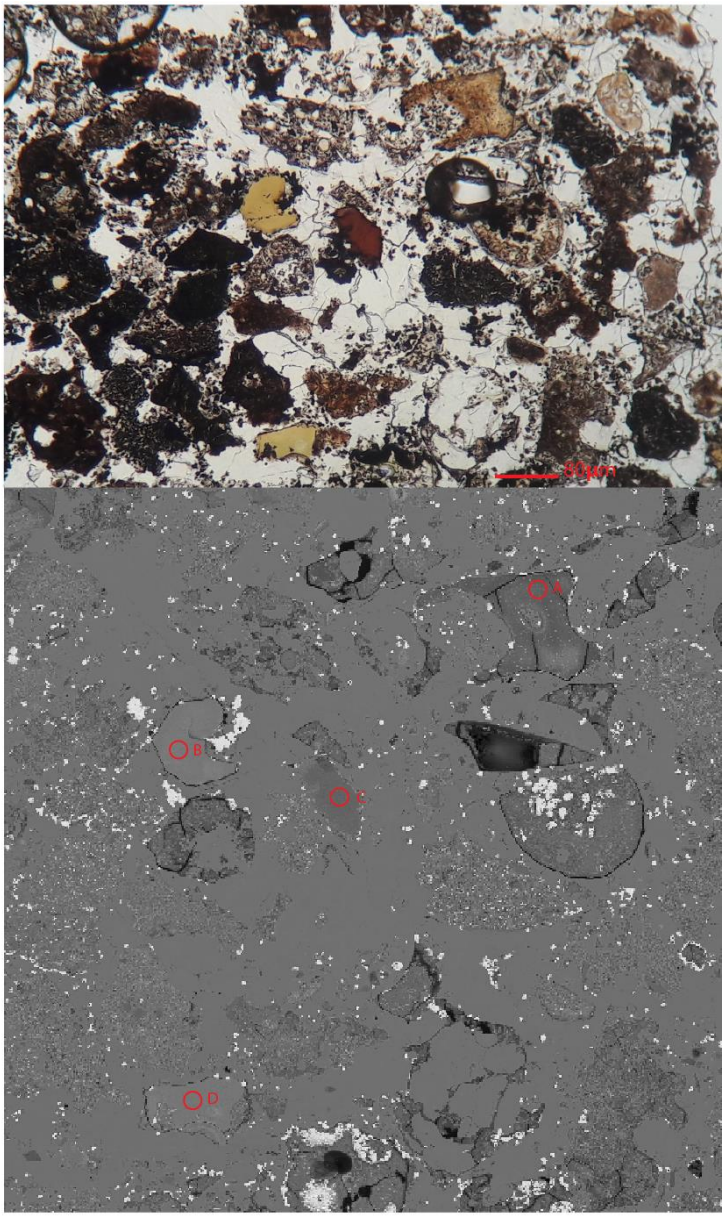

Figure 10.3.5: Analysis 5.6.

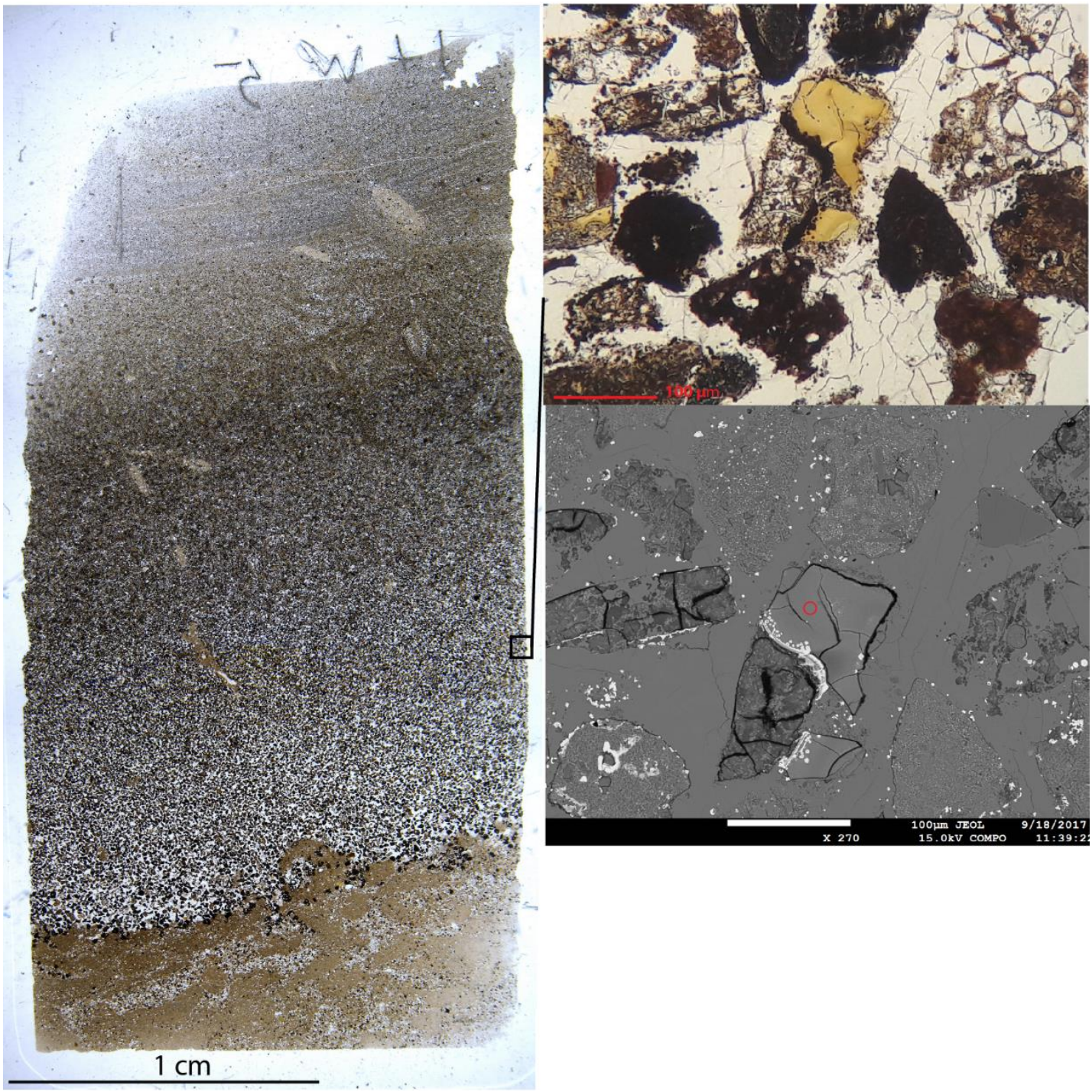

Figure 10.3.6: Analysis 5.7.

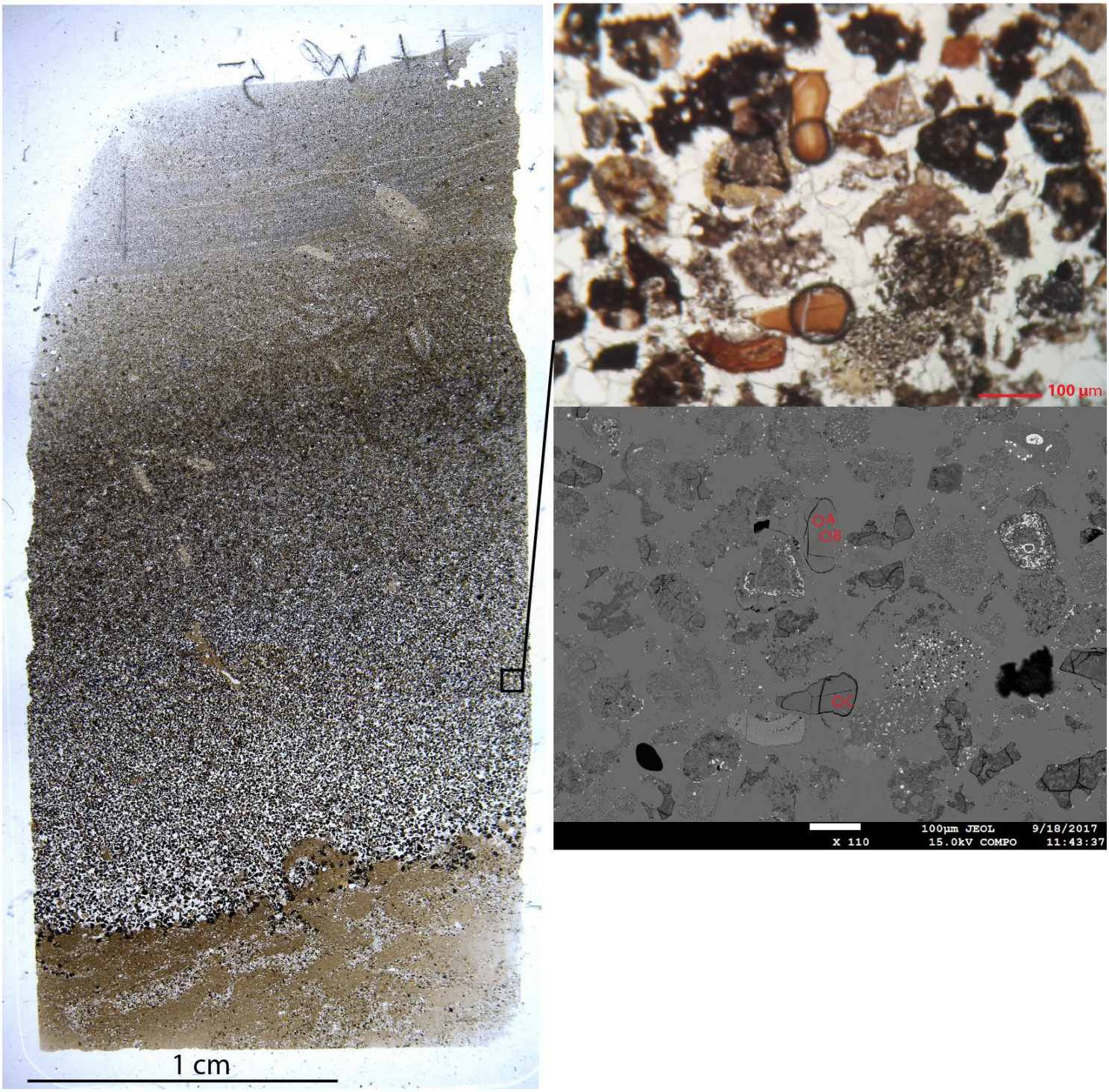

Figure 10.3.7: Analysis 5.8.

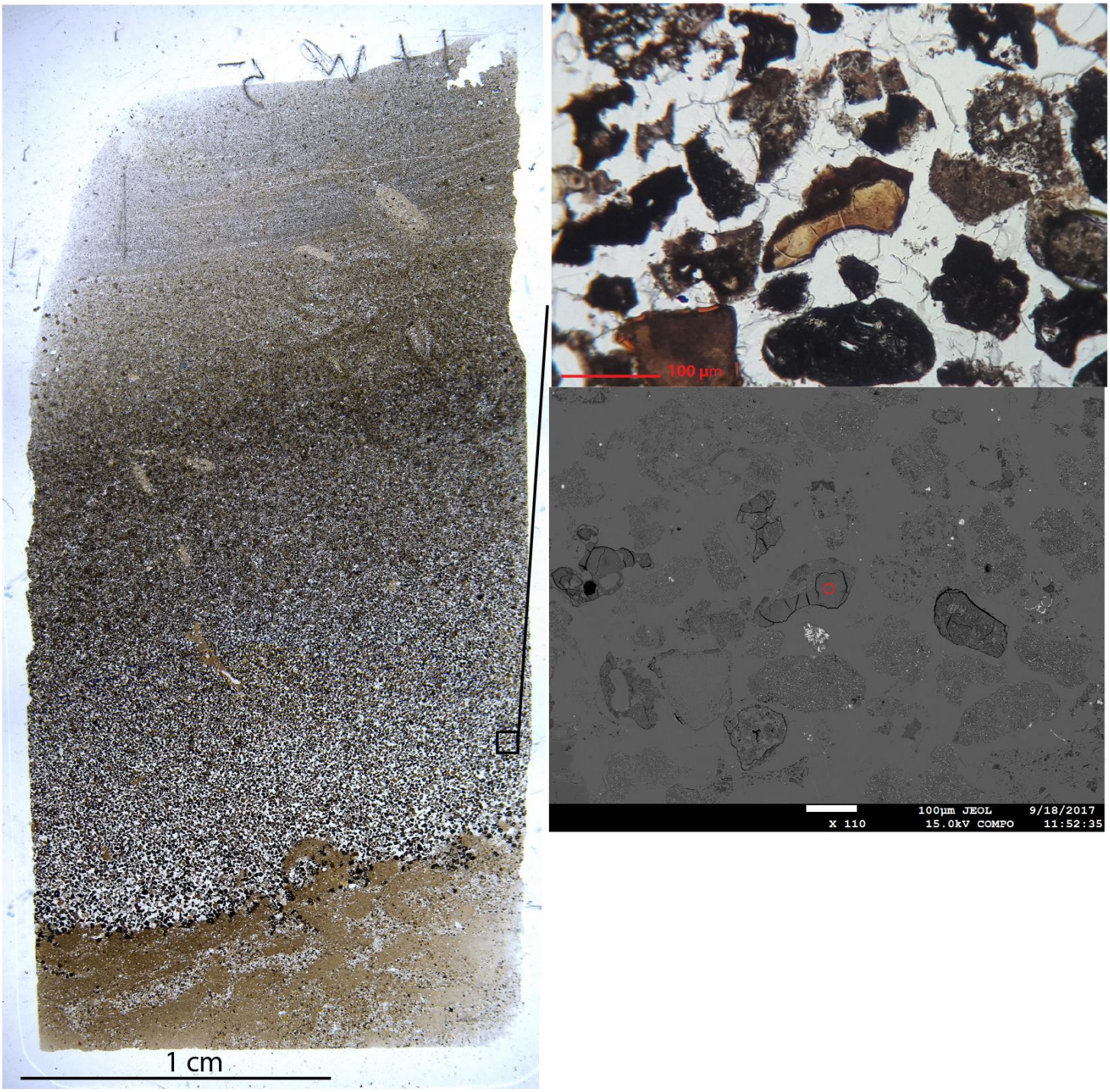

Figure 10.3.8: Analysis 5.9.

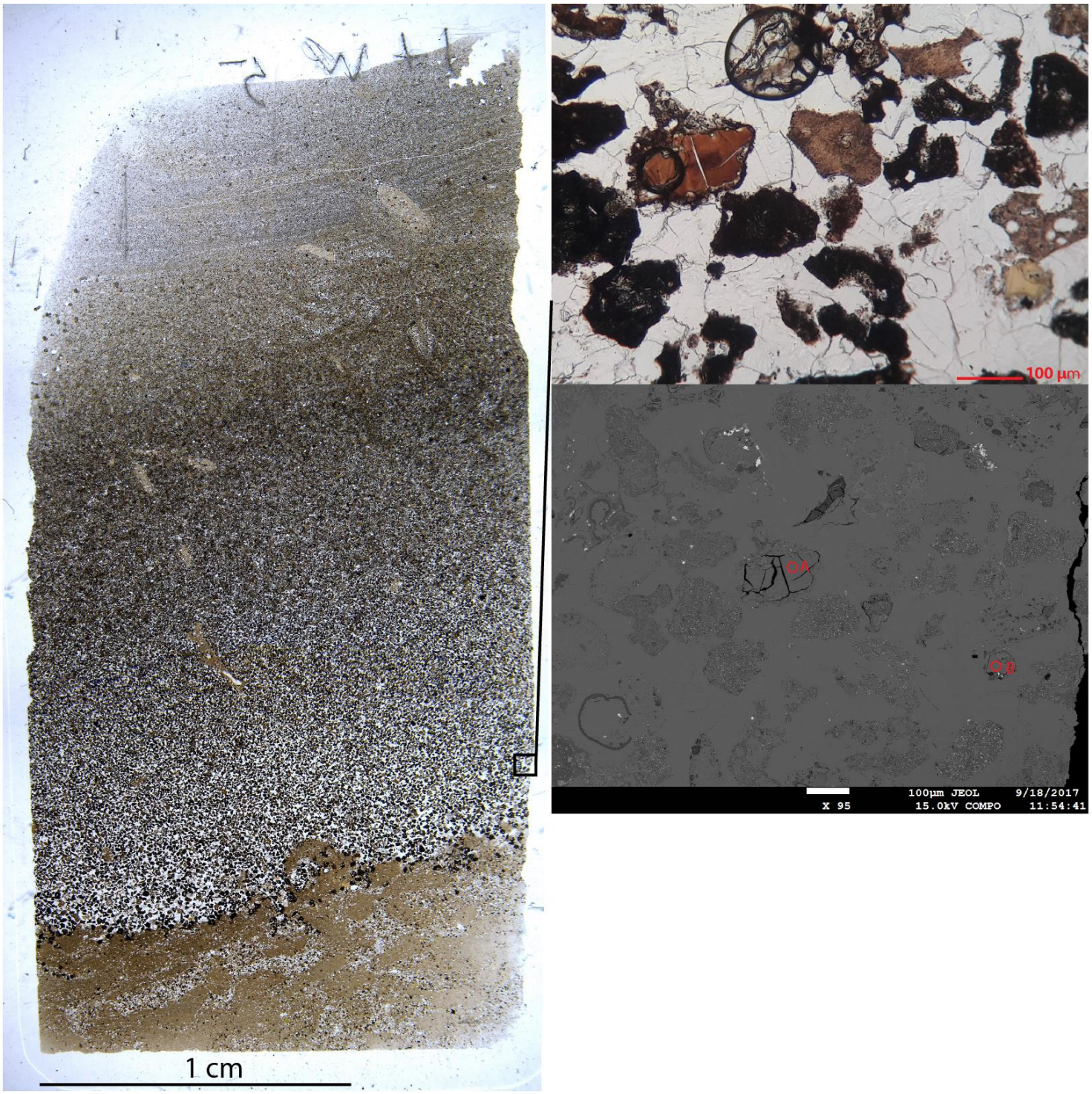

Figure 10.3.9: Analysis 5.10.

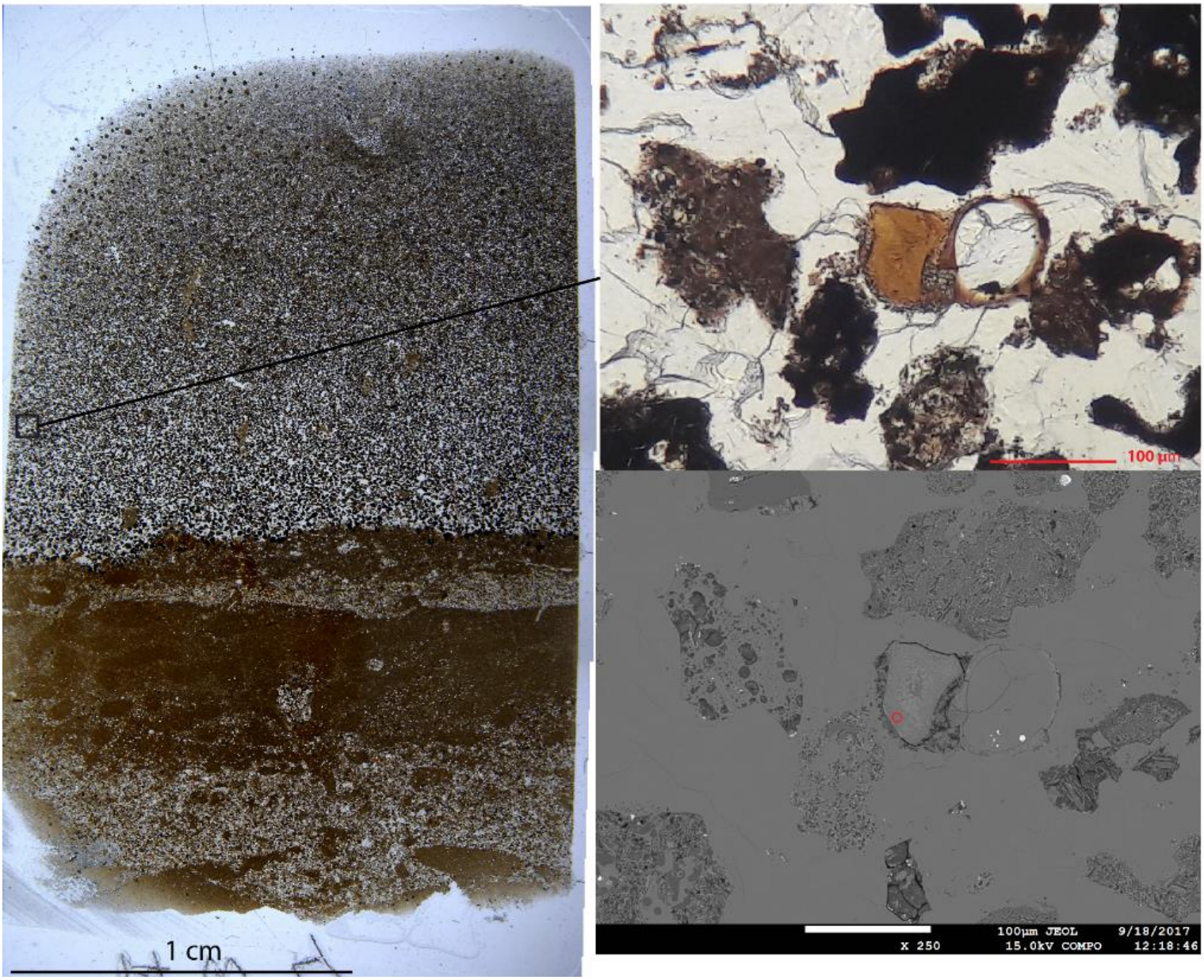

Figure 10.3.10: Analysis 4.1.

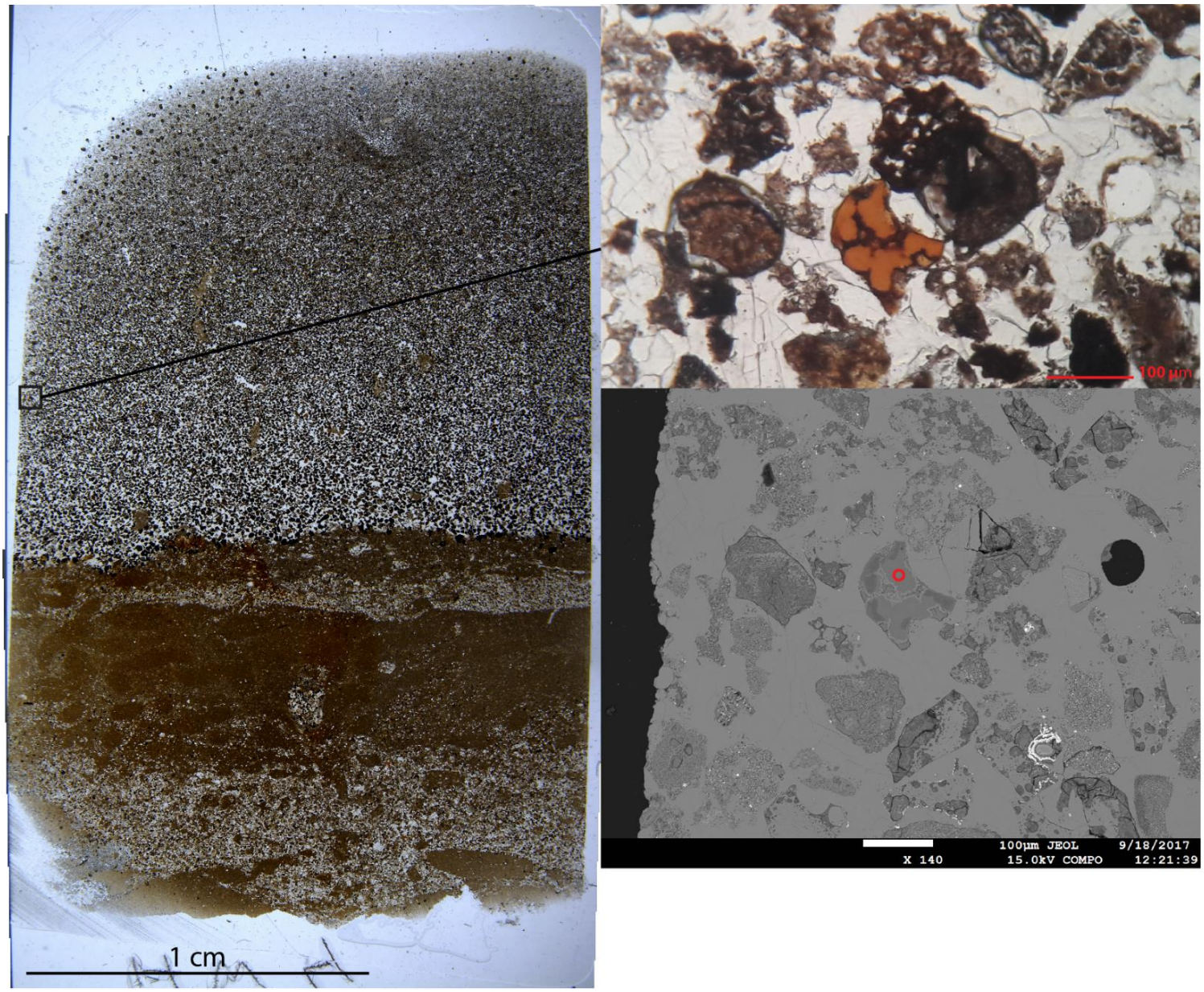

Figure 10.3.11: Analysis 4.2.

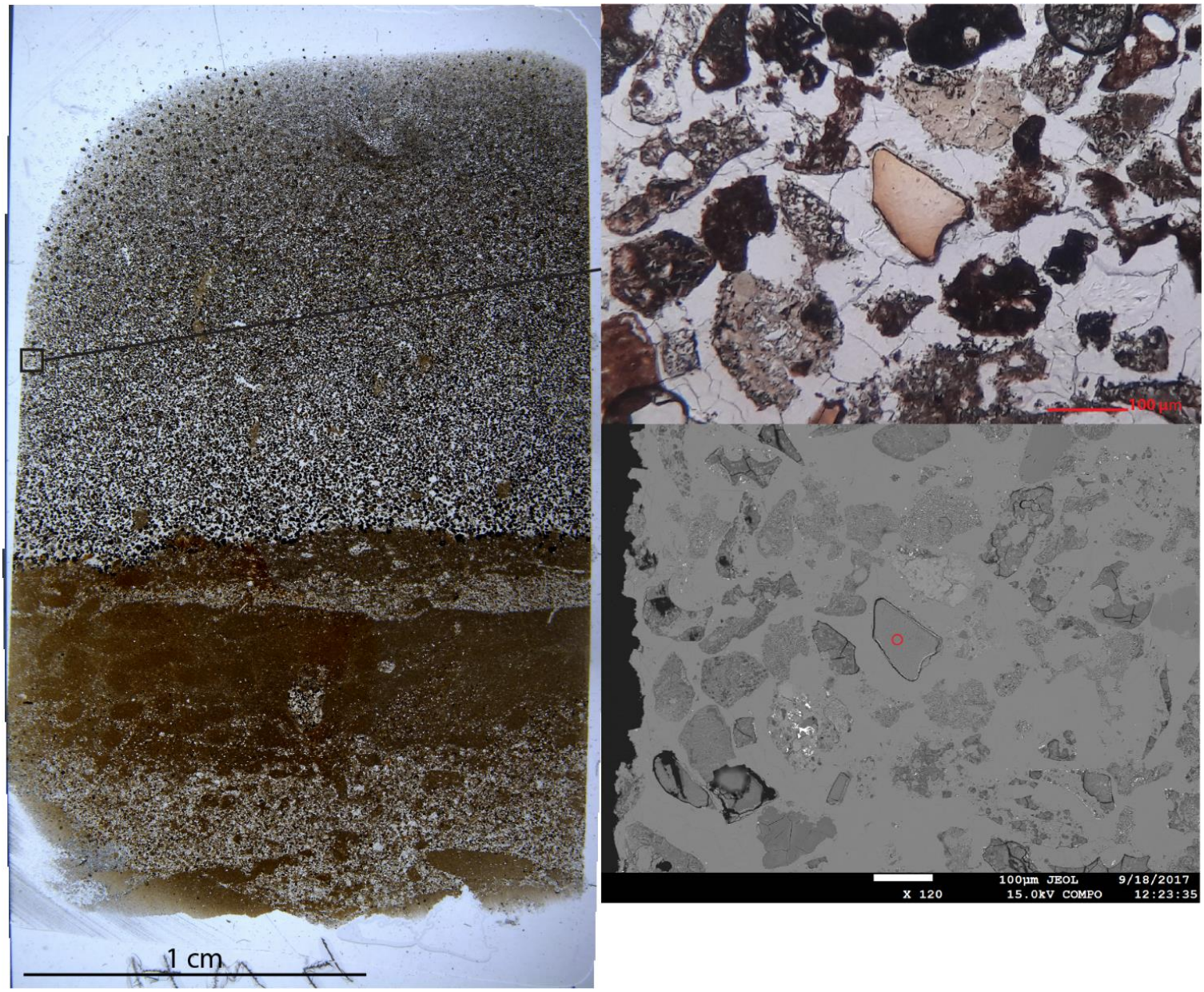

Figure 10.3.12: Analysis 4.3.

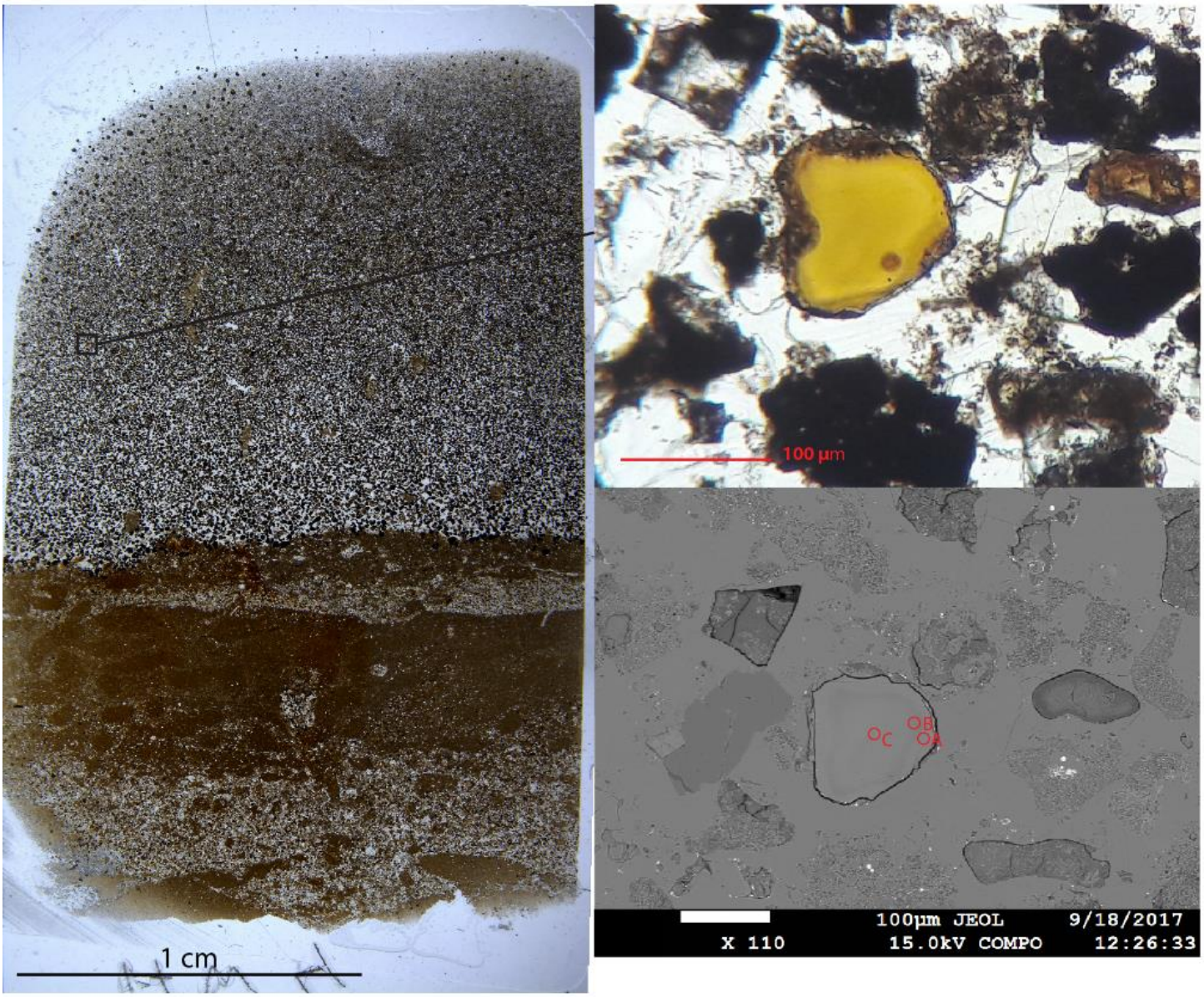

Figure 10.3.13: Analysis 4.4.

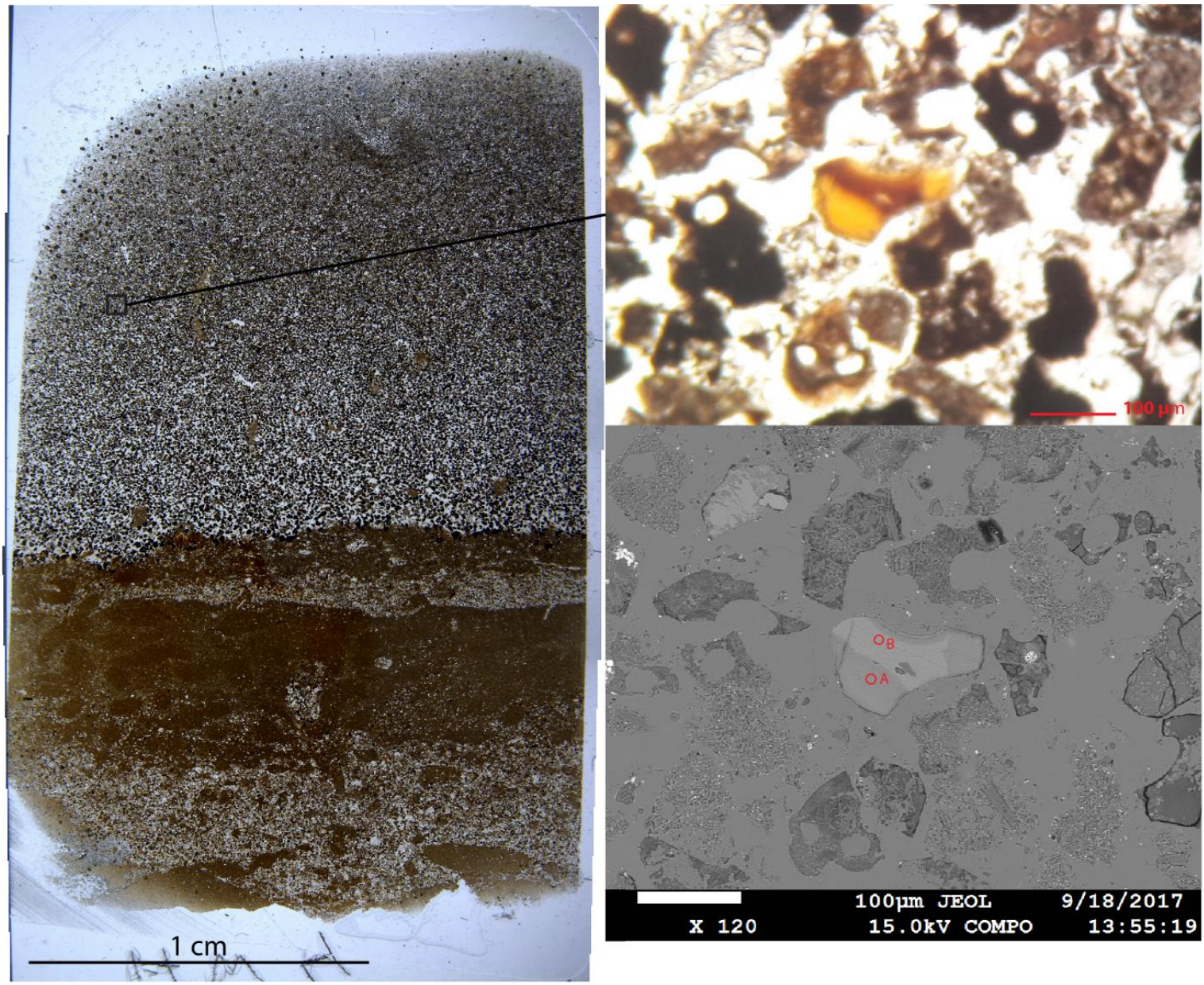

Figure 10.3.14: Analysis 4.5.

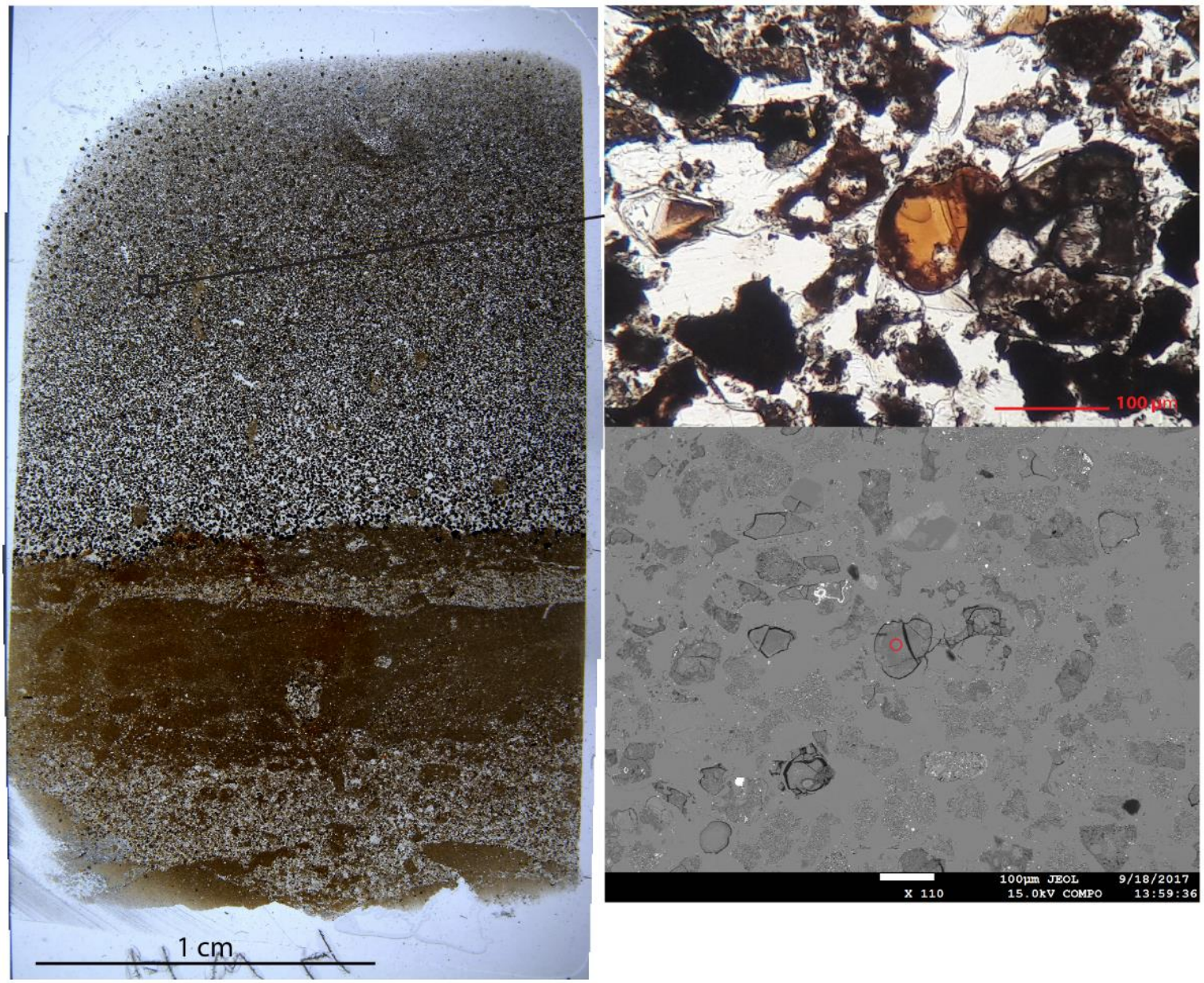

Figure 10.3.15: Analysis 4.6.

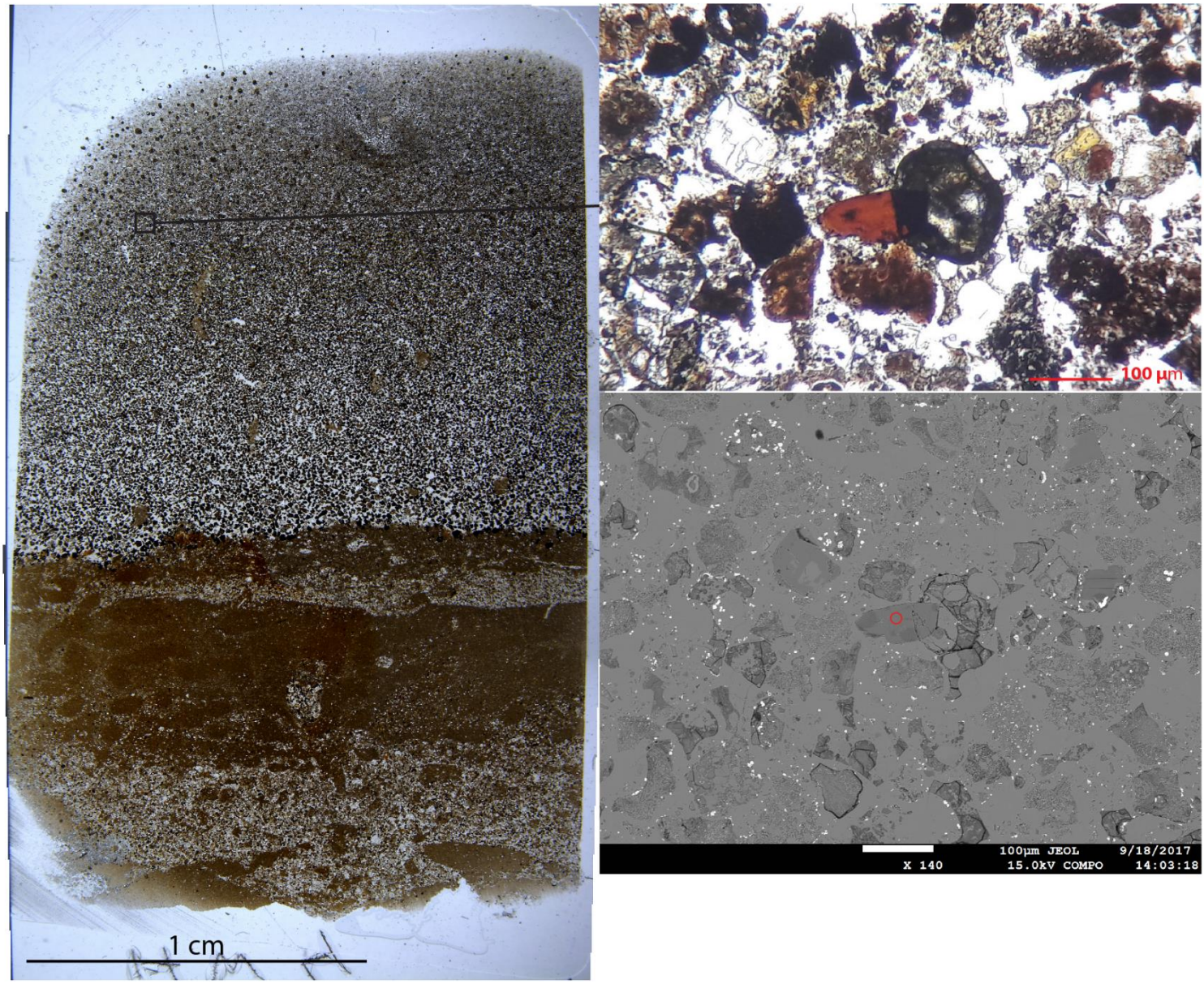

Figure 10.3.16: Analysis 4.7.

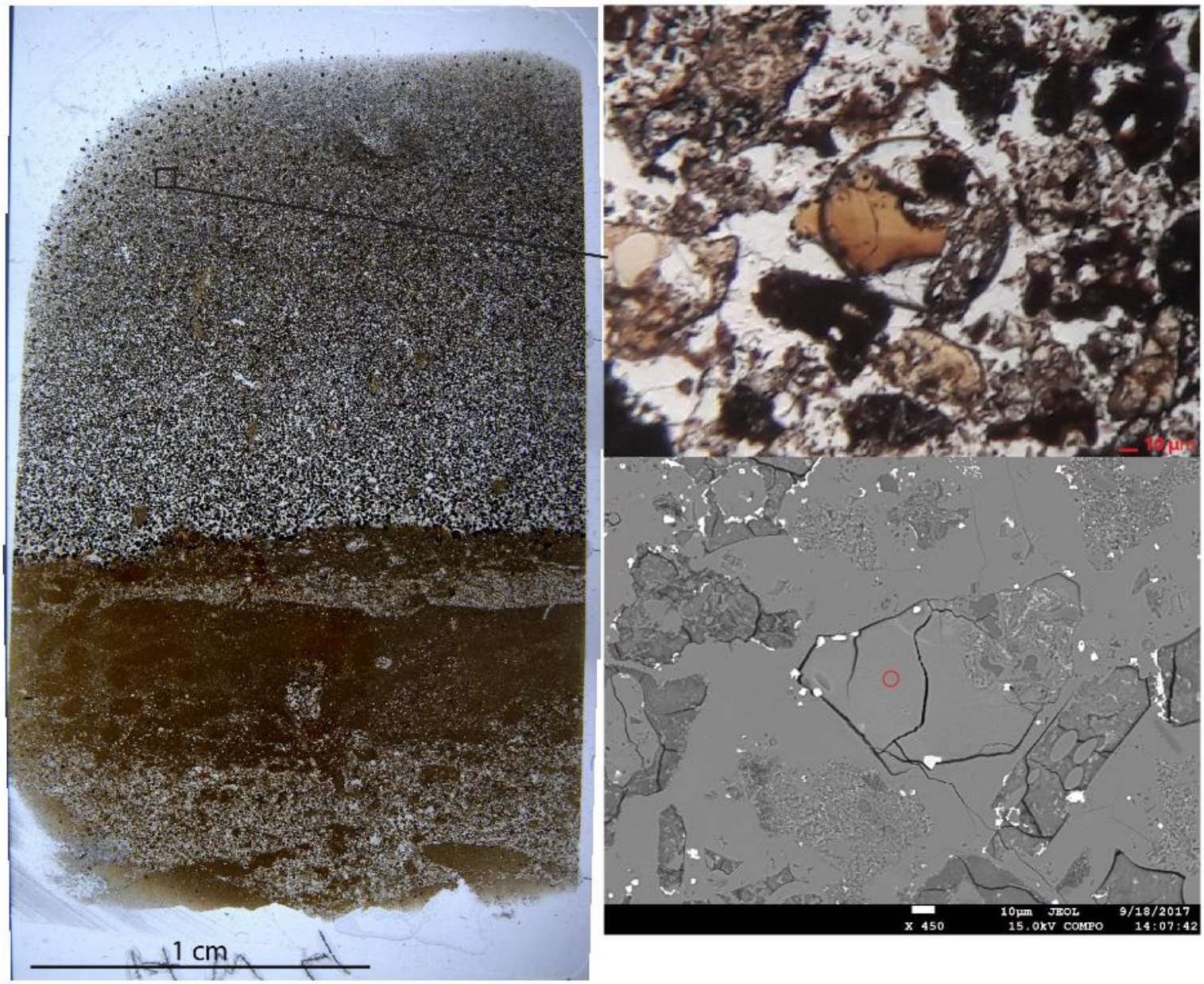

Figure 10.3.17: Analysis 4.8

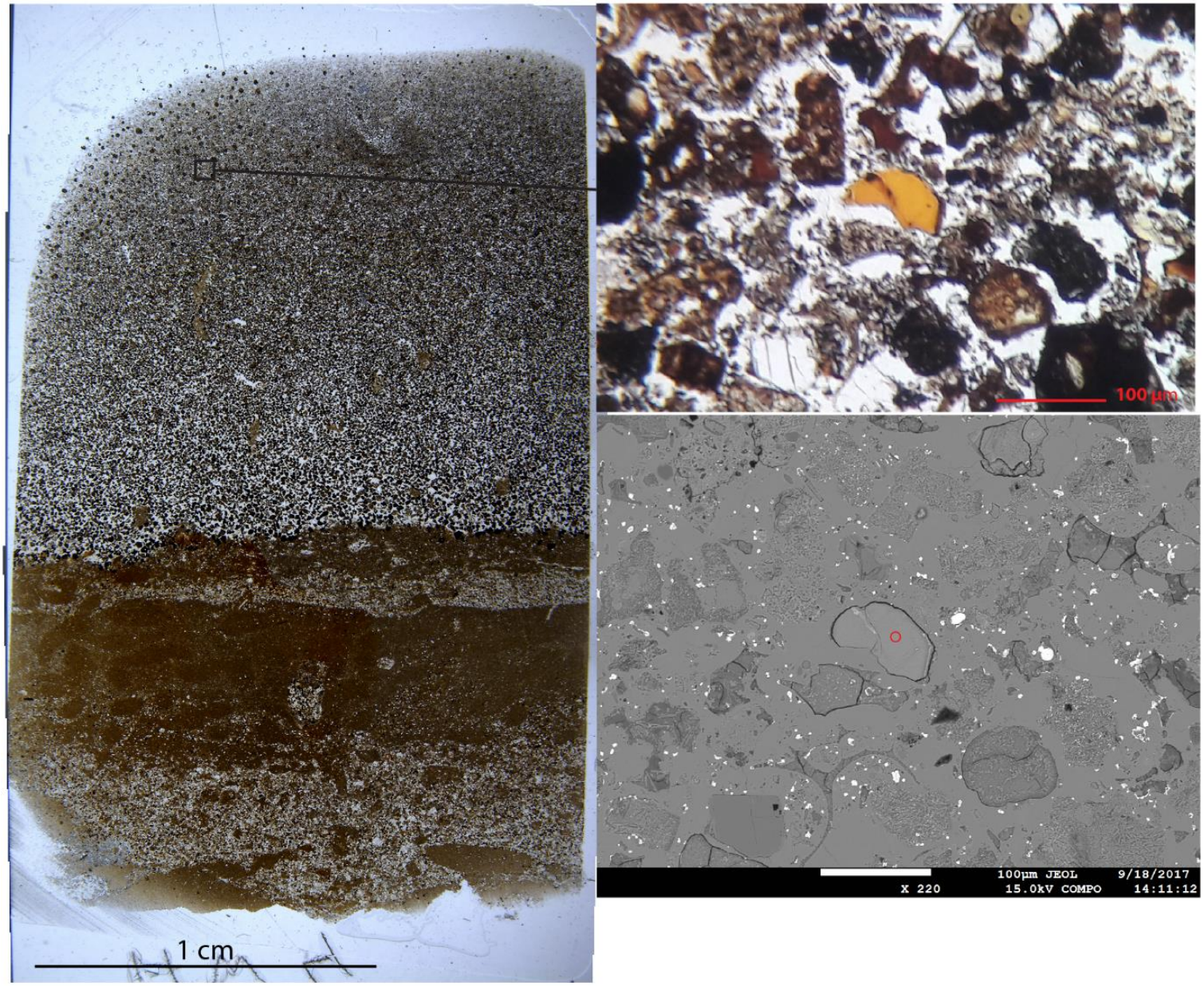

Figure 10.3.18: Analysis 4.9

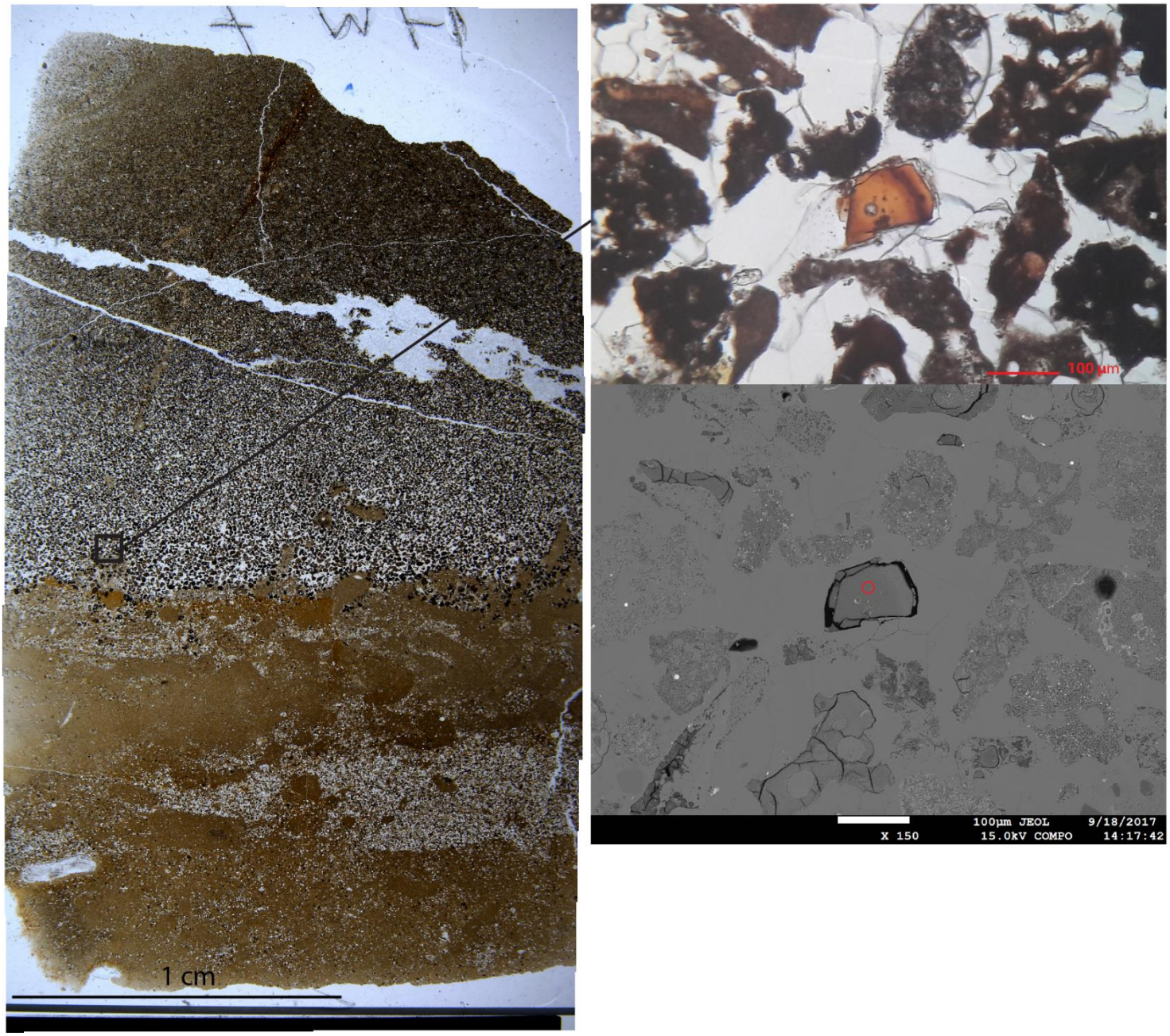

Figure 10.3.19: Analysis 7.1.

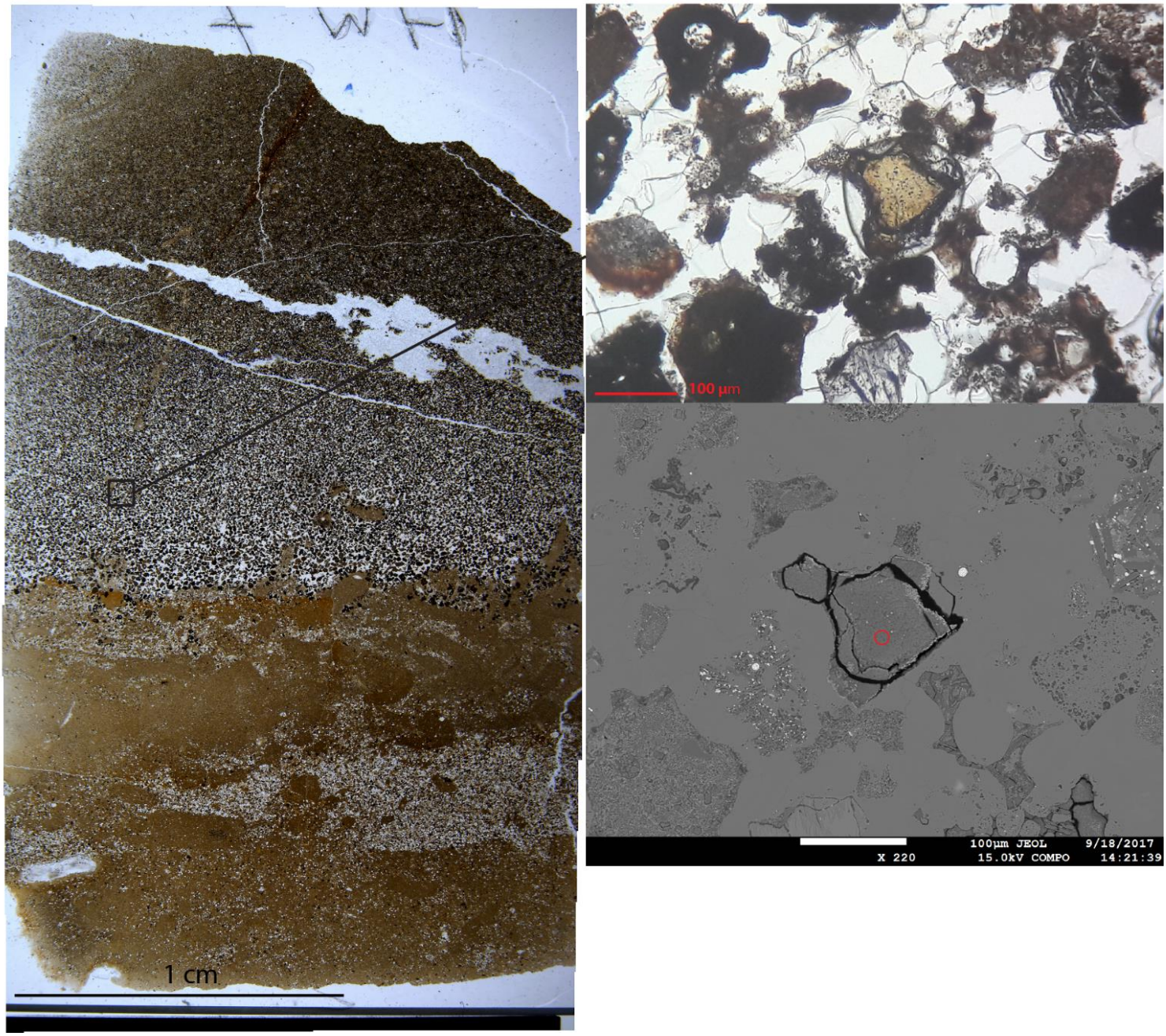

Figure 10.3.20: Analysis 7.2.

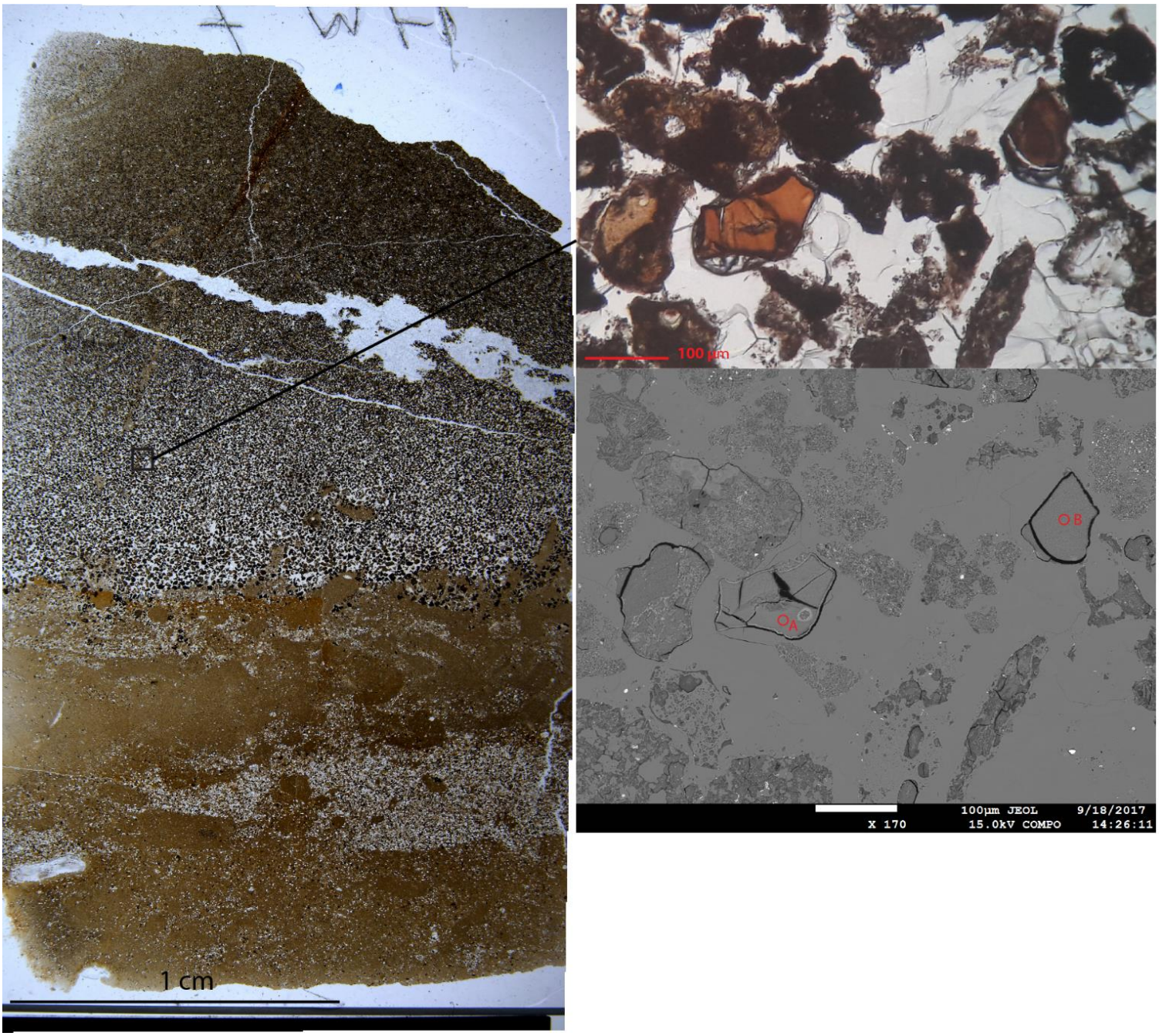

Figure 10.3.21: Analysis 7.3.

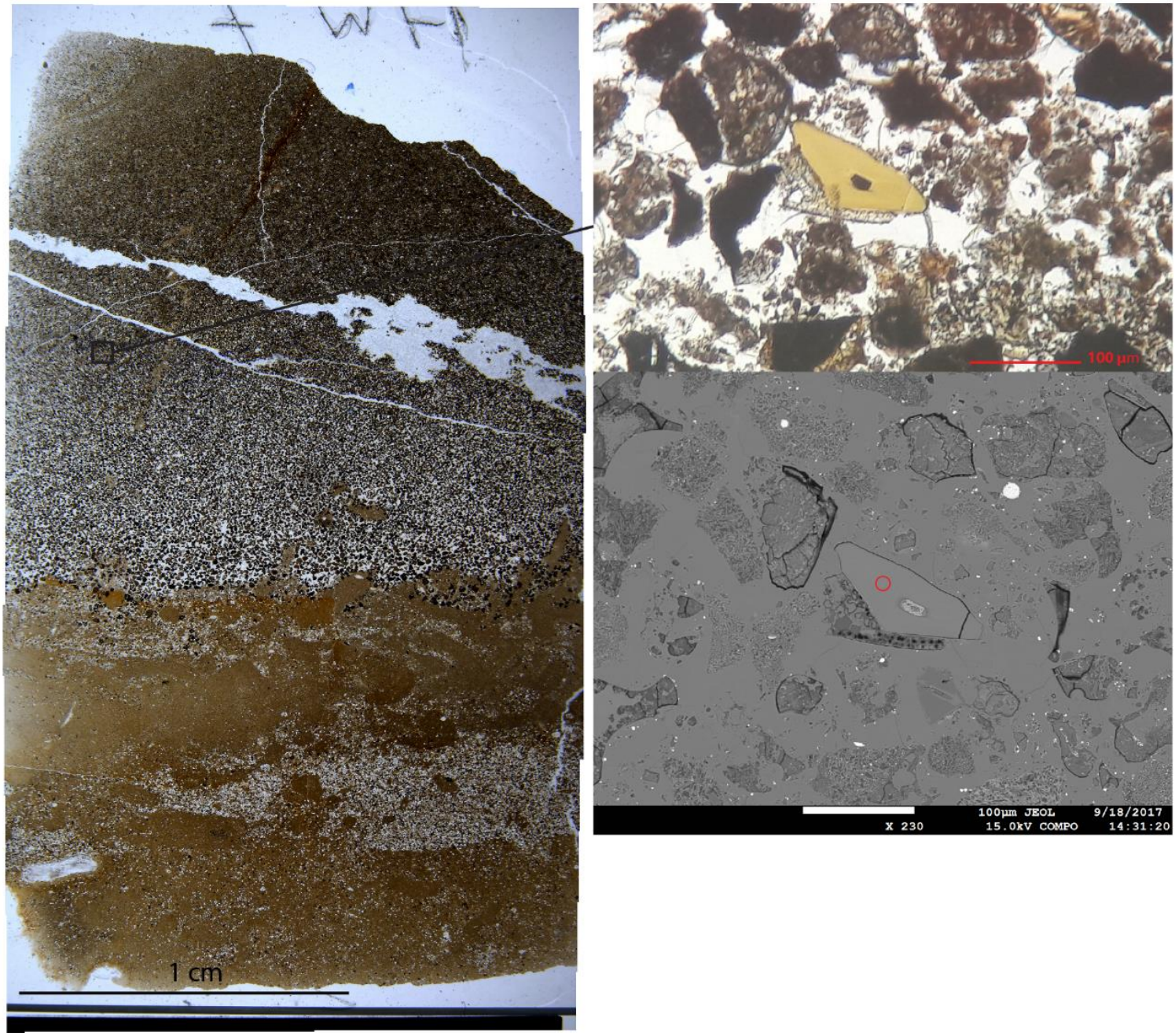

Figure 10.3.22: Analysis 7.4.

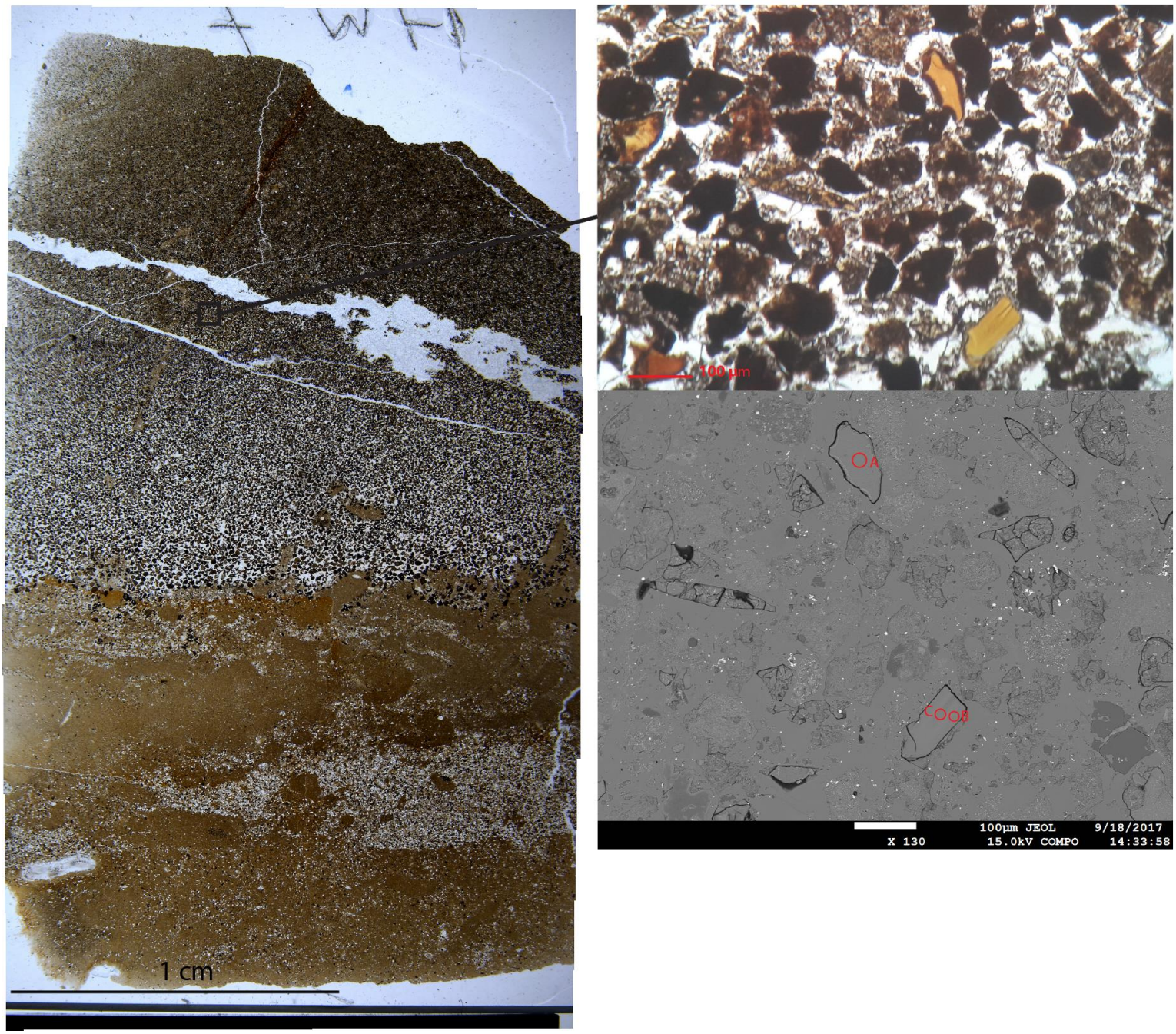

Figure 10.3.23: Analysis 7.5.

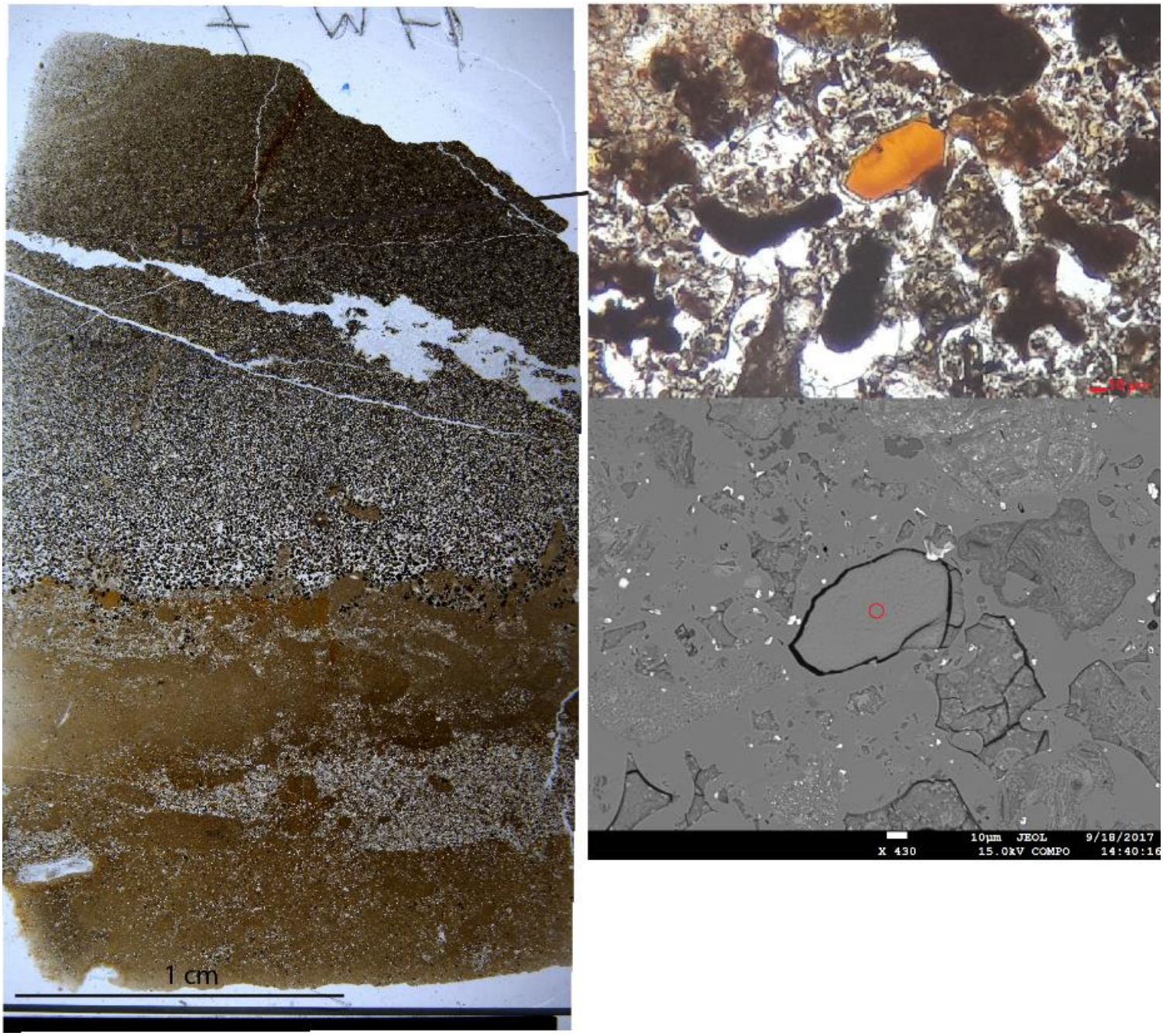

Figure 10.3.24: Analysis 7.6.

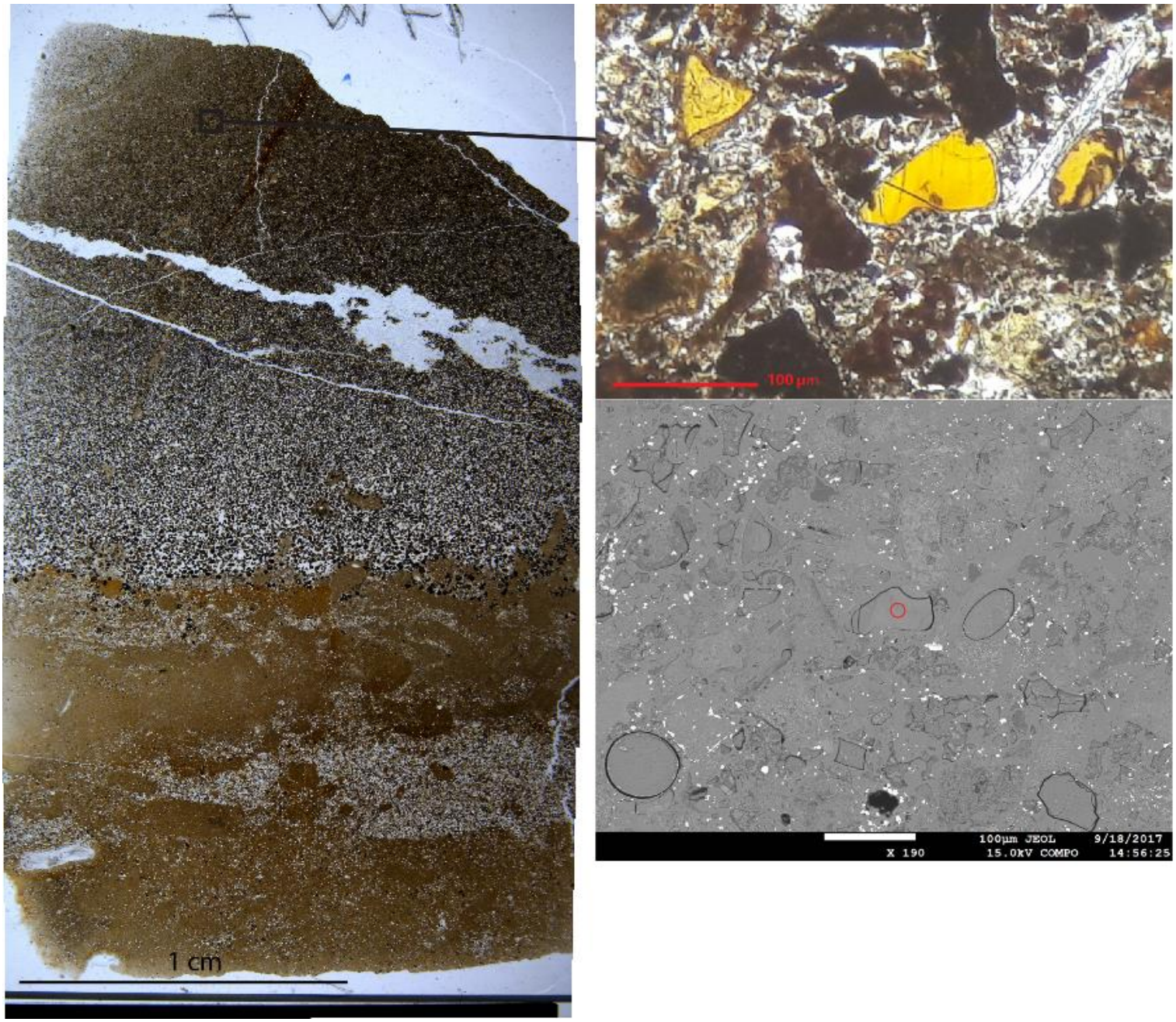

Figure 10.3.25: Analysis 7.7.

WT%	HW-S5.1	HW-S5.2	HW-S5.3	HW-S5.4A	HW-S5.4B	HW-S5.6A	HW-S5.6B	HW-S5.6C	HW-S5.6D	HW-S5.7	HW-S5.8A	HW-S5.8B	HW-S5.8C
SIO2	37.43	36.82	36.11	43.16	42.84	25.24	37.39	47.71	38.98	38.64	38.02	42.16	42.87
NA2O	0.15	0.12	0.16	3.36	3.18	0.34	0.18	4.13	0.18	0.12	0.08	0.09	0.05
P2O5	0.06	0.01	0.92	0.24	0.23	0.04	0.61	0.46	0.02	0.03	0.39	0.93	0.05
TIO2	9.57	2.82	1.61	2.82	2.78	10.32	1.03	2.94	0.73	1.01	2.45	1.57	4.78
CAO	2.30	2.08	3.06	3.75	3.69	1.31	2.61	4.87	1.68	2.02	2.74	3.52	2.24
K2O	0.19	0.25	0.83	3.47	3.23	0.26	1.47	3.37	1.55	1.07	0.33	0.37	0.36
MGO	2.88	3.08	5.05	0.11	0.21	1.66	3.84	0.05	6.59	4.74	2.79	2.79	2.81
AL2O3	17.48	17.13	14.92	16.11	15.97	13.88	14.23	17.91	13.31	15.50	19.41	19.57	21.07
FEO	15.75	26.16	25.86	10.56	11.60	18.69	26.69	7.74	24.95	25.91	23.07	19.59	15.94
MNO	0.08	0.09	0.16	0.03	0.02	0.05	0.14	0.00	0.20	0.15	0.15	0.10	0.12
VOLATILES	14.10	11.43	11.32	16.38	16.24	28.20	11.82	10.81	11.81	10.81	10.56	9.33	9.71
TOTAL	85.90	88.57	88.68	83.62	83.76	71.80	88.18	89.19	88.19	89.19	89.44	90.67	90.29

WT%	HW-S5.9	HW-S5.10A	HW-S5.10B	HW-S4.1	HW-S4.2	HW-S4.3	HW-S4.4A	HW-S4.4B	HW-S4.4C	HW-S4.5A	HW-S4.5B	HW-S4.6	HW-S4.7
SIO2	40.90	38.10	40.91	31.42	49.73	37.61	40.20	41.91	40.31	16.65	3.09	41.42	47.25
NA2O	0.10	0.24	0.23	0.27	3.06	0.13	0.11	0.11	0.13	0.52	0.67	0.24	3.62
P2O5	0.03	0.05	0.02	4.60	0.19	0.02	0.08	0.03	0.03	18.70	26.90	0.06	0.42
TIO2	1.37	6.62	0.52	1.33	2.14	3.04	2.36	0.69	1.06	2.14	7.84	2.37	3.15
CAO	2.22	2.18	2.40	8.65	3.89	2.01	2.21	2.46	2.20	29.57	41.41	1.99	4.20
K2O	0.36	0.44	1.12	0.26	4.16	0.34	0.55	0.73	0.85	0.53	0.04	0.28	3.97
MGO	2.74	2.06	4.33	5.62	0.05	2.83	5.37	4.19	3.99	1.26	0.17	2.08	0.04
AL2O3	22.14	20.60	16.02	11.84	17.74	19.04	15.27	16.52	16.42	7.13	1.66	25.89	17.28
FEO	19.11	19.94	23.85	21.89	5.10	19.30	22.68	22.90	24.16	11.56	4.91	16.37	7.23
MNO	0.09	0.13	0.11	0.22	0.10	0.30	0.19	0.19	0.17	0.18	0.17	0.20	0.11
VOLATILES	10.94	9.65	10.48	13.89	13.83	15.39	10.99	10.27	10.68	11.77	13.14	9.11	12.72
TOTAL	89.06	90.35	89.52	86.11	86.17	84.61	89.01	89.73	89.32	88.23	86.86	90.89	87.28

WT%	HW-S4.8	HW-S4.9	HW-S7.1	HW-S7.2	HW-S7.3A	HW-S7.3B	HW-S7.4	HW-S7.5A	HW-S7.5B	HW-S7.5C	HW-S7.6	HW-S7.7
SIO2	37.48	36.23	40.01	44.58	39.99	43.58	42.50	41.40	41.72	42.41	38.02	41.57
NA2O	0.31	0.12	0.26	0.14	0.20	0.12	0.39	0.09	0.13	0.16	0.12	0.24
P2O5	2.00	0.02	0.06	0.47	0.02	0.06	1.13	0.02	0.01	0.04	0.04	0.03
TIO2	3.94	1.32	4.08	1.32	3.63	4.81	1.57	1.04	1.84	1.70	4.15	1.48
CAO	4.81	1.97	2.12	3.09	2.39	2.40	3.47	2.63	2.40	2.61	2.54	2.45
K2O	1.25	0.58	0.30	0.27	0.32	0.73	3.02	0.33	0.67	1.35	0.88	1.61
MGO	3.44	5.99	1.31	2.34	2.40	3.56	4.49	3.44	5.11	3.88	4.57	4.25
AL2O3	14.85	13.94	27.68	25.63	20.79	19.69	13.16	17.23	15.80	16.15	13.94	13.88
FEO	21.55	28.71	14.58	13.13	20.80	15.81	20.07	23.02	22.02	21.05	25.08	25.26
MNO	0.16	0.27	0.16	0.12	0.14	0.11	0.20	0.12	0.13	0.13	0.22	0.17
VOLATILES	10.20	10.84	9.43	8.90	9.33	9.14	10.00	10.69	10.16	10.52	10.44	9.06
TOTAL	89.80	89.16	90.57	91.10	90.67	90.86	90.00	89.31	89.84	89.48	89.56	90.94

Table 10.3.1: Electron microprobe results.